MODELING DYNAMIC STALL OF SC-1095 AIRFOIL AT HIGH MACH NUMBERS

A Thesis
Presented To
The Academic Faculty

By

Brian Clark

In Partial Fulfillment
of the Requirements for the Degree
Master of Science in the
School of Aerospace Engineering

Georgia Institute of Technology

May 2010

MODELING DYNAMIC STALL OF SC-1095 AIRFOIL AT
HIGH MACH NUMBERS

Approved by:

Dr. Lakshmi Sankar
School of Aerospace Engineering
Georgia Institute of Technology

Dr. J.V.R. Prasad
School of Aerospace Engineering
Georgia Institute of Technology

Dr. Mark Costello
School of Aerospace Engineering
Georgia Institute of Technology

Date Approved: January 15, 2010

ACKNOWLEDGEMENTS

I would like to sincerely thank my advisor, Dr. Lakshmi Sankar. His patience and advice were invaluable to the completion of this work. I also owe a debt of gratitude to other graduate students working in the CFD lab that have assisted me over the course of my studies at Georgia Tech. Nischint Rajmohan and Jeremy Bain in particular have dedicated much of their time to assist me, and their help is greatly appreciated. Finally, I would like to acknowledge the emotional support and encouragement I have routinely received from friends and family.

TABLE OF CONTENTS

LIST OF TABLES

LIST OF FIGURES

NOMENCLATURE

A1	Leishman-Beddoes constant, 0.3
A2	Leishman-Beddoes constant, 0.7
A3	Leishman-Beddoes constant, 1.5
A4	Leishman-Beddoes constant, -0.5
A5	Leishman-Beddoes constant, 1.0
b1	Leishman-Beddoes constant, 0.14
b2	Leishman-Beddoes constant, 0.53
b3	Leishman-Beddoes constant, 0.25
b4	Leishman-Beddoes constant, 0.1
b5	Leishman-Beddoes constant, 0.5
c	Airfoil chord length, *ft*
C_X^c	Coefficient for circulatory component
C_X^{ai}	Coefficient for non-circulatory (impulsive) component due to pitch
C_X^{qi}	Coefficient for non-circulatory (impulsive) component due to pitch rate
C_C	Chord force coefficient
C_d	Drag force coefficient
C_{d0}	Skin friction drag coefficient
C_l	Lift force coefficient
C_m	Pitching moment coefficient about quarter-chord
C_{m0}	Zero-lift pitching moment

C_n Normal force coefficient

C_n' Lagged normal force coefficient

Cna Normal force curve slope, deg^{-1}

C_{n1} Critical normal force coefficient

DFD Chord force smoothing parameter

f Effective separation point from Kirchoff theory

k Reduced frequency

k_0 Center of pressure offset

k_1 Static pitching moment parameter (related to separation effects)

k_2 Static pitching moment parameter (related to shape of moment break)

m Separation point power in static moment curve fit, 2

M Mach number

n Current time index

S Non-dimensional distance traveled in semi-chords, 2Ut/c

St Strouhal number for vortex shedding, 0.19

S1 Kirchoff stall parameter for $\alpha<\alpha_1$

S2 Kirchoff stall parameter for $\alpha>\alpha_1$

t Time, *s*

T_f Time constant related to trailing edge separation

T_p Time constant related to leading edge separation

T_v Time constant related to dynamic stall lift from vortex convection

T_{vl} Time constant related to dynamic stall pitching moment from vortex convection

U	Freestream air velocity, *ft/s*
x	Distance from Airfoil Nose, *ft*
α	Airfoil angle of attack, *deg*
α_C	Oscillation cyclic angle of attack
α_m	Oscillation mean angle of attack
α_0	Zero-lift angle of attack
α_1	Angle of attack for f=0.7
β	Prandtl-Glauert compressibility factor, $\sqrt{1-M^2}$
η	Chord force recovery factor

SUMMARY

In this thesis, the Leishman-Beddoes method of determining airloads for an airfoil undergoing dynamic stall is studied over a range of Mach numbers. To validate the method for conditions where little experimental data is available, a computational fluid dynamics solver is utilized to provide airload predictions for comparison to the Leishman-Beddoes results.

It is found that even for high Mach numbers the Leishman-Beddoes method provides reliable predictions for lift coefficient. However, at the higher Mach numbers pitching moment is sometimes overpredicted at high angle of attack. This is seemingly due to an inability to accurately determine the center of pressure in the high speed unsteady flow environment.

CHAPTER 1: INTRODUCTION

Dynamic stall is a complicated, nonlinear problem in aerodynamics, and one that is important in helicopter performance, as it may greatly alter key design parameters such as lift and pitching moment. Airfoil oscillation leading to dynamic stall tends to delay onset of stall and increase lift compared to static airfoil performance, but also leads to spikes in pitching moment and increased torsional loads. As such, a rotor designer must be able to model dynamic stall to predict performance and produce a reliable rotor.[23]

Dynamic stall is characterized by the unsteady airloads resulting from flow separation, vortex formation, subsequent shedding, and finally flow reattachment. These nonlinear aerodynamic effects do not lend themselves to a closed form solution. Computational fluid dynamics (CFD) with a full Navier-Stokes solver tends to be the best tool to accurately predict performance of an airfoil undergoing dynamic stall. However, since it is highly computationally intensive, it remains suboptimal for extensive design and optimization.

Many semi-empirical models have been developed to model dynamic stall, but as they are based in part on experimental data, the fact that there is not much data for oscillating airfoils at high Mach numbers means that they have mostly been validated for lower Mach numbers, and as such their suitability for high Mach numbers is somewhat uncertain.

J.G. Leishman and T.S. Beddoes jointly developed a popular semi-empirical method of modeling dynamic stall that has proven to provide good estimates for lift, drag, and pitching moment of an airfoil undergoing dynamic stall with a very reasonable level of computational power. It is applicable to an airfoil in arbitrary motion, and has been extensively compared against data for oscillating and ramping airfoils, but again mostly for lower Mach numbers.

Since their method was first introduced, it has been refined by Leishman and others to account for sweep effects[10], trailing edge flaps[13], and other aerodynamic problems more complicated than the relatively simple 2-D flow over an airfoil. Additionally, it has been utilized in several comprehensive aerodynamic codes such as Rotorcraft Comprehensive Analysis System (RCAS) and the wind turbine analysis program Aerodyn.

Dynamic stall most frequently occurs in the inboard region of the retreating blade of a helicopter rotor in forward flight, as the airfoil is typically at a high angle of attack at this point. As such, the relative air speed to the airfoil in this region is often very low. The utility of studying dynamic stall models at high Mach numbers may then be called into question. However, the current research has been conducted for primarily three reasons; first, it is useful to know the practical limits and possible error of any model used as extensively as Leishman-Beddoes. Second, while less common, dynamic stall may occur on regions of a helicopter rotor other than inboard region of the retreating blade, and this will correspond to higher local Mach numbers. Finally, as the subsystems are used in very large

aerodynamic programs like RCAS and Aerodyn, the algorithms are frequently called by the main program when an airfoil is in a high Mach number flow. As such, understanding how the Leishman-Beddoes method's predictions compare to the flow physics is of value.

Other methods of determining airloads for an airfoil undergoing dynamic stall exist as well. Some of the early, simpler methods such as the Boeing-Vertol gamma method and Johnson method are not as heavily used today. However, the ONERA method, like the Leishman-Beddoes method, has undergone many refinements through the years and is frequently utilized in analysis codes. It is particularly popular for use in aeroelastic codes since its differential equation underpinnings make this application more straightforward.

Another promising method is the use of neural networks (NN) to provide aerodynamic load predictions. By training neural networks with data derived from CFD data, very good correlation between the neural network's predictions and CFD data for which the NN has not yet been trained has been achieved.[26] Since a NN uses a fraction of the computing power of a CFD simulation, this approach is computationally efficient; a small number of CFD simulations may be performed for training purposes, and then future analysis may subsequently be performed by the NN for design and optimization. However, as there are no physical underpinnings for the NN, the output will be only as good as the CFD data. Figure 1 from Reference [26] displays the potential of NN to the application of modeling dynamic stall.

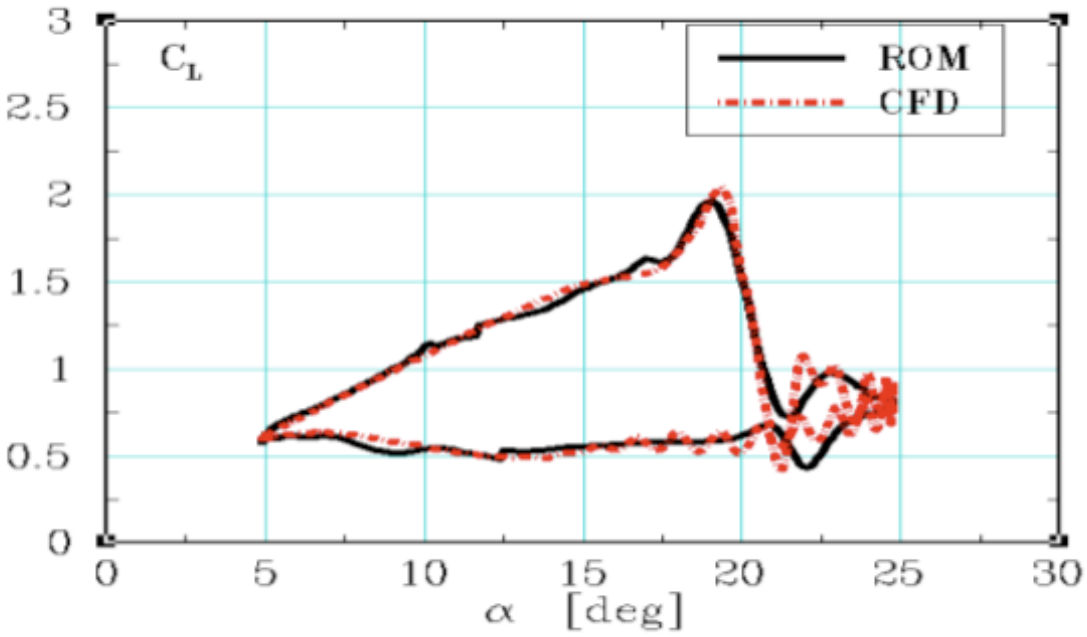

Figure 1: Comparison of CFD and NN Reduced Order Model (ROM)[26]

Similar to the indicial formulation of the Leishman-Beddoes method, the Rational Function Approximation (RFA) approach has been utilized for the computation of unsteady aerodynamics common to rotorcraft. RFA is a time-domain state-space method that uses a Laplace domain representation of aerodynamics. A Reduced Order Model (ROM) is developed using oscillatory CFD data which is transformed into the time domain to achieve a computationally efficient state-space model.[27] This method has been used by Friedmann, Smith, et al in Reference [27] to achieve accurate predictions of aerodynamics of a helicopter rotor with a trailing edge flap.

CHAPTER 2: RESEARCH OBJECTIVES

In this thesis, the applicability of the Leishman-Beddoes dynamic stall model to airfoils operating at high freestream Mach numbers is studied. The ability of the model to predict the lift, drag, and pitching moments at high Mach numbers is assessd using test data and CFD based hysteresis loops. An attempt is also made to evaluate the assumptions and curve fits in the model with the aid of CFD simulations.

Flow dynamics around a Sikorsky SC-1095 airfoil are computed using OVERFLOW to obtain detailed 2-D CFD performance data for a pitching airfoil in a steady flow. The airfoil's movement is modeled as

$$\alpha = \alpha_m + \alpha_C \sin\left(\frac{kMa}{b} t\right)$$

The test matrix developed is given in Table 1.

Table 1: Test Matrix

Mach Number	Airfoil Parameters	# cases
0.3, 0.4	α_m =[15, 10, 5, 0, -6]	45
	α_C =[10, 5, 2.5]	
	k=[0.03, 0.05, 0.10]	
0.5, 0.6	α_m =[7, 3, 0, -3]	24
	α_C =[4, 2]	
	k=[0.03, 0.05, 0.10]	
0.7	α_m =[5, 2, 0, -2]	24
	α_C =[2, 1]	
	k=[0.03, 0.05, 0.10]	

The test matrix was formed to cover a wide range of Mach numbers and also correspond to frequently used values of angle of attack and reduced frequency in experiments. This will allow comparisons to experimental data for validation, such as from McAlister, Pucci, McCroskey, and Carr[5].

Additionally, a program has been written using the Leishman-Beddoes method of modeling dynamic stall to evaluate loads for the test cases above for comparison to the CFD results. By comparing the Leishman-Beddoes results to the CFD results that have been validated against experimental data, the ability of Leishman-Beddoes to accurately capture the effects of the flow phenomena may be assessed across the range of parameters detailed in Table 1.

In this study, a 2-D airfoil is studied in a constant velocity flow field. For an actual operating helicopter there will be 3-D aerodynamic effects such as sweep effects and if the helicopter is in forward flight or in maneuvers there may be massive variation in local flow velocity. While the studies here are restricted to unswept airfoils in a constant velocity flow, the present approach may be extended to include sweep effects as well.

CHAPTER 3: ANATOMY OF DYNAMIC STALL

For a helicopter in forward flight, it is common for the cyclical motion of the airfoil angle of attack (AoA) to range from well below static stall AoA to above dynamic stall AoA.[9] To accurately model rotor loads throughout this process, we must model attached flow, the formation and subsequent shedding of a strong leading edge vortex, fully separated flow, and finally flow reattachment.

Dynamic stall differs from static stall primarily in the formation of the concentrated vorticity at the leading edge and the subsequent shedding of this vortex. This causes additional lift above that possible with a static case and a large pressure wave across the top of the airfoil.[9] A diagram showing some of the key physical phenomena of dynamic stall and their effect on normal force and pitching moment is shown in Figure 2, taken from Reference [9].

The onset of stall occurs at a significantly higher critical AoA for a rapidly oscillating airfoil, but this dynamic stall then tends to be much more severe and persistent than static stall.[4] Because of the oscillatory nature of a helicopter rotor, there may be significant hysteresis in the loads and thus any solution will be highly time dependent.

As an airfoil begins at a low angle of attack and pitches upward, its behavior may be modeled well using linear thin airfoil theory. At a point above where stall would occur on a static airfoil, flow reversals begin to occur in the boundary layer. Depending on the geometry of the airfoil, these reversals may either begin at the trailing edge and move forward towards the leading edge, or it

may form rapidly near the leading edge just downstream of the suction peak[4]. During this flow regime the lift achieved exceeds that which would be possible for a static airfoil.

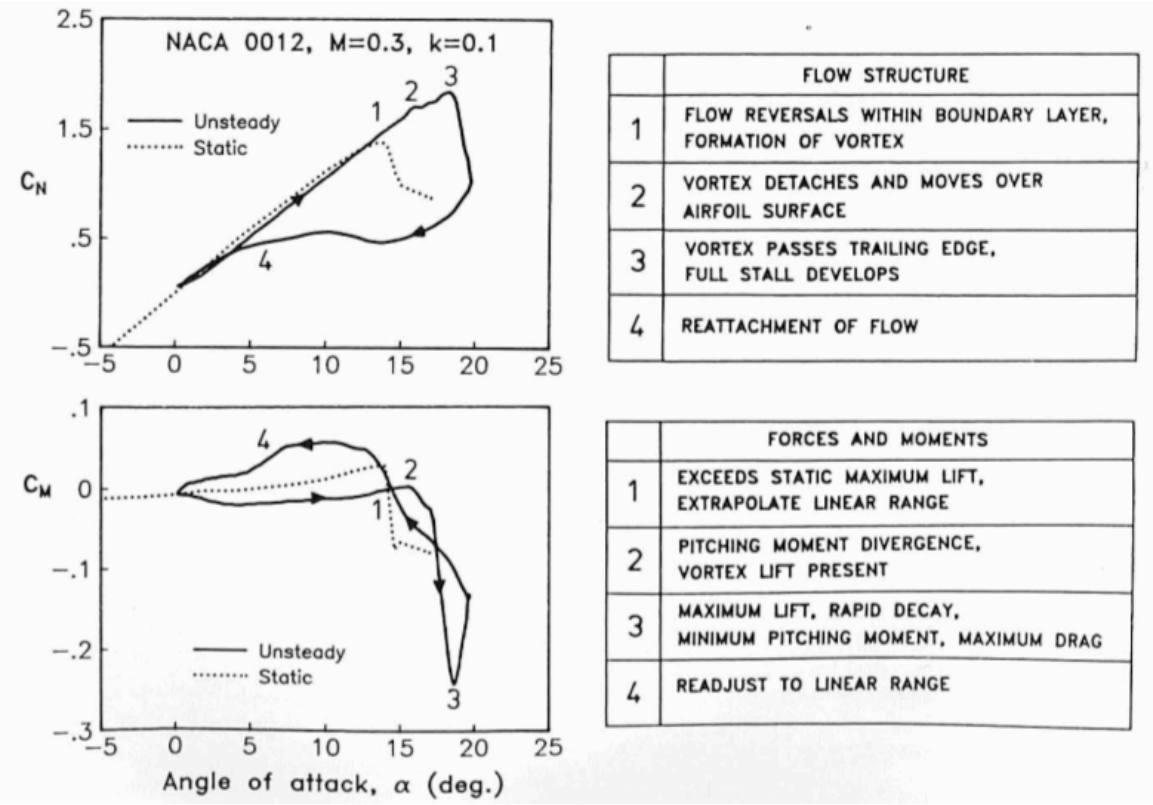

Figure 2: The Effect of Dynamic Stall on NACA 0012 Airfoil[9]

At this point, a vortex begins to form at the leading edge and spread rearward at a speed just under one half of the freestream velocity[4]. This period corresponds to point 2 in Figure 2 and correlates to a small increase in lift and a rapid change in pitching moment.

The vortex will then be shed and travel downstream across the airfoil. Lift decreases rapidly while pitching moment peaks. As the vortex moves away from

the airfoil, full stall is achieved as the flow is fully separated. As the airfoil pitches back downward flow reattachment will be achieved, but typically at an angle of attack below that corresponding to static stall due to unsteady flow[12].

CHAPTER 4: LEISHMAN-BEDDOES MODEL

Leishman-Beddoes consists of an attached flow model for linear airloads, and a separated flow model and a dynamic stall model for nonlinear airloads. The outputs for the attached flow subsystem are used as the inputs for the separated flow model, and the outputs from that subsystem are in turn used as inputs for the dynamic stall vortex shedding model. The attached flow model may be solved independently of the other subsystems, while the separated flow model and dynamic stall subsystems interact through adjustments to appropriate time constants.

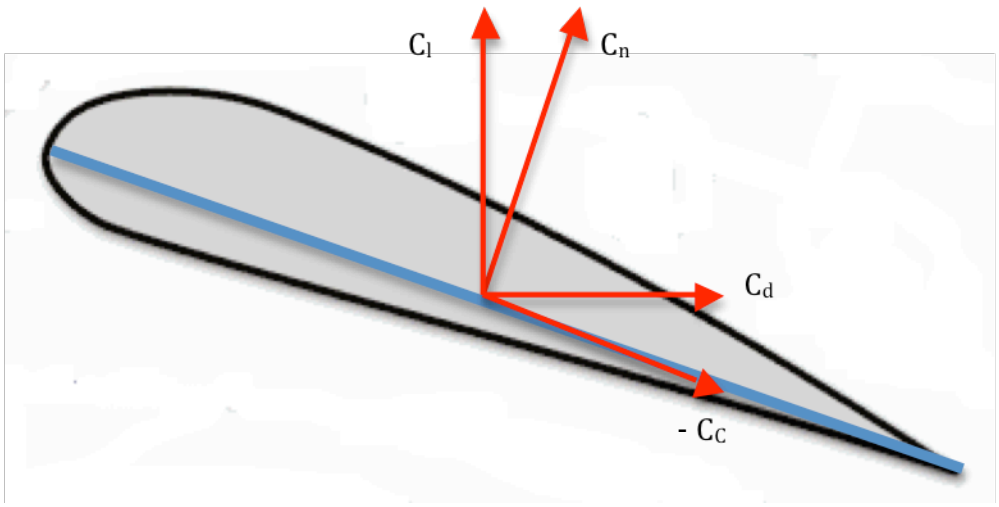

Figure 3: Forces Acting on Airfoil

Attached Flow Model

In the attached flow subsystem, indicial response functions for a step increase in the angle of attack are used to determine loads using Duhamel's

integral. These indicial response functions are composed of a circulatory and non-circulatory component.

For the circulatory component of the chord normal force, the force is put into terms of an effective angle of attack and an empirically determined normal force curve slope, Cna.

$$C_n^c = \mathrm{Cna} * \alpha_{\mathrm{tot}} \tag{1}$$

α_{tot} takes into account the effects of pitch and rate of change of pitch:

$$\alpha_{\mathrm{tot}} = \alpha_{\mathrm{eff}} + \frac{\dot{\alpha}_{eff} * c}{2 * U} \tag{2}$$

where

$$\alpha_{eff} = \alpha - X1 - X2 \tag{3}$$

$$\dot{\alpha}_{eff} = \dot{\alpha} - X3 - X4 \tag{4}$$

and the deficiency functions X1, X2, X3, and X4 are given by

$$X1_{(n)} = X1_{(n-1)} * \exp\left(-b1\beta^2\Delta S\right) + A1 * \Delta\alpha * \exp\left(\frac{-b1\beta^2\Delta S}{2}\right) \tag{5}$$

$$X2_{(n)} = X2_{(n-1)} * \exp\left(-b2\beta^2\Delta S\right) + A2 * \Delta\alpha * \exp\left(\frac{-b2\beta^2\Delta S}{2}\right) \tag{6}$$

$$X3_{(n)} = X3_{(n-1)} * \exp\left(-b1\beta^2\Delta S\right) + A1 * \Delta\dot{\alpha} * \exp\left(\frac{-b1\beta^2\Delta S}{2}\right) \quad (7)$$

$$X4_{(n)} = X4_{(n-1)} * \exp(-b2\beta^2\Delta S) + A2 * \Delta\dot{\alpha} * \exp\left(\frac{-b2\beta^2\Delta S}{2}\right) \quad (8)$$

In the program, the following calculations are made:

$$\Delta\alpha = \alpha_{(n)} - \alpha_{(n-1)} \quad (9)$$

$$\dot{\alpha} = \frac{\Delta\alpha}{\Delta t} \quad (10)$$

$$\Delta\dot{\alpha} = \dot{\alpha}_{(n)} - \dot{\alpha}_{(n-1)} \quad (11)$$

ΔS is the distance traveled in semi-chords and is given by

$$\Delta S = \frac{2 * U * \Delta t}{c} \quad (12)$$

and β is the Prandtl-Glauert factor, given by

$$\beta = \sqrt{1 - M^2} \quad (13)$$

The non-circulatory component is further broken up into a component due to angle of attack, C_n^{ai} and a component due to pitch rate, C_n^{qi}.

$$C_n^{ai} = \left(\frac{4 * ka * Ti}{M}\right) * (Ka - Ka') \tag{14}$$

$$C_n^{qi} = \left(\frac{-kq * Ti}{M}\right) * (Kq - Kq') \tag{15}$$

ka and kq are Mach number dependent constants, and have been reduced by 25% from the theoretical values based on correlation with experimental data by Leishman and Beddoes (1989).

$$ka = \frac{0.75}{1 - M + \pi * \beta * M^2 * (A1 * b1 + A2 * b2)} \tag{16}$$

$$kq = \frac{0.75}{1 - M + 2 * \pi * \beta * M^2 * (A1 * b1 + A2 * b2)} \tag{17}$$

Ti is the non-circulatory time constant, given by c/U. Ka, Ka', Kq, and Kq' are then given by

$$Ka = \frac{\Delta\alpha}{\Delta t} \tag{18}$$

$$Ka'_{(n)} = Ka'_{(n-1)} * \exp\left(\frac{-\Delta t}{ka * Ti}\right) + (Ka_{(n)} - Ka_{(n-1)}) * \exp\left(\frac{-\Delta t}{2 * ka * Ti}\right) \tag{19}$$

$$Kq = \frac{c * \Delta\dot{\alpha}}{\Delta t * U} \tag{20}$$

$$Kq'_{(n)} = Kq'_{(n-1)} * \exp\left(\frac{-\Delta t}{kq * Ti}\right) + (Kq_{(n)} - Kq_{(n-1)}) * \exp\left(\frac{-\Delta t}{2 * kq * Ti}\right) \tag{21}$$

The normal force coefficient for potential flow may then be determined using

$$C_{n,pot} = C_n^c + C_n^{ai} + C_n^{qi} \tag{22}$$

The method for determining the pitching moment is similar. The non-circulatory components are given by

$$C_m^{ai} = -kam * Ti * \left(A3 * b3 * (Ka - Ka'')\right) + \left(\frac{A4 * b4}{M}\right) * (Ka - Ka''') \tag{23}$$

$$C_m^{qi} = \frac{-7 * kqm * Ti * (Kq - Kq'')}{12 * M} \tag{24}$$

Like ka and kq, kam and kqm are Mach number dependent constants reduced to match experimental data, but here they are reduced 20%.

$$kam = 0.8 * \frac{(A3 * b4 + A4 * b3)}{\left(b3 * b4 * (1 - M)\right)} \tag{25}$$

$$kqm = 0.8 * \frac{7}{15 * (1 - M) + 3 * \pi * \beta * M^2 * b5} \tag{26}$$

Ka'', Ka''', and Kq'' are given by

$$Ka''_{(n)} = Ka''_{(n-1)} * \exp\left(\frac{-\Delta t}{b3 * kam * Ti}\right) + (Ka_{(n)} - Ka_{(n-1)}) * \exp\left(\frac{-\Delta t}{2 * b3 * kam * Ti}\right) \tag{27}$$

$$Ka'''_{(n)} = Ka'''_{(n-1)} * \exp\left(\frac{-\Delta t}{b4 * kam * Ti}\right) + (Ka_{(n)} - Ka_{(n-1)}) * \exp\left(\frac{-\Delta t}{2 * b4 * kam * Ti}\right) \quad (28)$$

$$Kq''_{(n)} = Kq''_{(n-1)} * \exp\left(\frac{-\Delta t}{kqm * Ti}\right) + (Kq_{(n)} - Kq_{(n-1)}) * \exp\left(\frac{-\Delta t}{2 * kqm * Ti}\right) \quad (29)$$

The chord force may be determined using the effective angle of attack determined earlier and two empirically derived constants; Cna, defined earlier, and η, the suction recovery factor. The drag force may then be determined for a given angle of attack using the chord normal force, chord force, and empirically determined skin friction drag coefficient, C_{d0}.

$$C_C = \eta * Cna * \tan(\alpha_{eff}) \approx \eta * Cna * \alpha_{eff}^2 \quad (30)$$

$$C_d = C_n \sin(\alpha) - C_C \cos(\alpha) + C_{d0} \quad (31)$$

Separated Flow Model

A trailing edge separation model based on Kirchoff theory is used in Leishman-Beddoes. The onset of the separated flow model is triggered by a critical normal force coefficient, C_{n1}. This coefficient is empirically derived and is based on either a shock reversal or leading edge criterion. A delay is built into C_n for comparison to C_{n1}.

$$C_n' = C_{n,pot} - Dp \quad (32)$$

where Dp is a deficiency function given by

$$Dp_{(n)} = Dp_{(n-1)} * \exp\left(\frac{-\Delta S}{Tp}\right) + (C_{n}^{c}{}_{(n)} - C_{n}^{c}{}_{(n-1)}) * \exp\left(\frac{-\Delta S}{2 * Tp}\right) \quad (33)$$

In this subsystem, calculation for the normal force is identical to the linear attached flow subsystem, except that the circulatory component is scaled by an effective separation point. The actual separation point over the airfoil is unknown, so first an effective separation point is determined by inverting eqn. (34) and solving for the separation point, f, at each angle of attack.

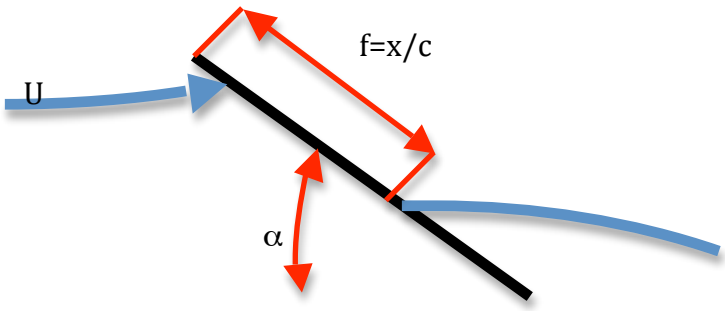

Figure 4: Diagram Showing Flow Separation on an Airfoil

$$C_{n} = Cna * \left(\frac{1+\sqrt{f}}{2}\right)^{2} \alpha \quad (34)$$

A curve fit is then performed for calculation of the effective separation point within the program using

$$f = \begin{cases} 1 - 0.3 * \exp\left(\dfrac{\left(|\alpha| - \alpha 1\right)}{S1}\right), & |\alpha| \le \alpha 1 \\ 0.04 + 0.66 * \exp\left(\dfrac{\left(\alpha 1 - |\alpha|\right)}{S2}\right), & |\alpha| > \alpha 1 \end{cases} \tag{35}$$

To model the hysteresis evident in oscillatory pitch data under quasi-static conditions, an offset is used,

$$\alpha 1_{(n)} = \alpha 1 - \Delta\alpha 1 * (1 - f_{(n-1)})^{0.25} \tag{36}$$

Another effective angle of attack is determined for the unsteady pressure response for use in Kirchoff theory which accounts for the delay built into C_n'.

$$\alpha_f = \frac{C_n'}{Cna} \tag{37}$$

This effective angle of attack is then used in eqn. (35), yielding

$$f' = \begin{cases} 1 - 0.3 * \exp\left(\dfrac{\left(|\alpha_f| - \alpha 1\right)}{S1}\right), & |\alpha_f| \le \alpha 1 \\ 0.04 + 0.66 * \exp\left(\dfrac{\left(\alpha 1 - |\alpha_f|\right)}{S2}\right), & |\alpha_f| > \alpha 1 \end{cases} \tag{38}$$

To model the unsteady boundary layer response, a lag is applied to f' using a deficiency function Df, yielding f''.

$$f'' = f' - Df \tag{39}$$

$$Df_{(n)} = Df_{(n-1)} * \exp\left(\frac{-\Delta S}{Tf}\right) + (f'_{(n)} - f'_{(n-1)}) * \exp\left(\frac{-\Delta S}{2 * Tf}\right) \tag{40}$$

Finally, the normal force coefficient including separation effects is given by

$$C_n^f = Cna * 0.25 * \left(1 + \sqrt{f''}\right)^2 * \alpha_{tot} + C_n^{ai} + C_n^{qi} \tag{41}$$

To determine the pitching moment, a few more steps are required first. Reattachment is handled differently than separation for pitching moment, so if the angle of attack is increasing (Ka>0) the previous method of determining f' is used. However, for decreasing angle of attack where flow may be reattaching, first a quasi-steady reattachment point is defined,

$$f_{qs} = \begin{cases} 1 - 0.3 * \exp\left(\frac{(\alpha - \alpha 0 - \alpha 1)}{S1}\right), & \alpha \le \alpha 1 \\ 0.04 + 0.66 * \exp\left(\frac{(\alpha 1 - \alpha + \alpha 0)}{S2}\right), & \alpha > \alpha 1 \end{cases} \tag{42}$$

The lagged reattachment separation point is then given by

$$f_r' = f_r - Dfr \tag{43}$$

where

$$Dfr_{(n)} = Dfr_{(n-1)} * \exp\left(\frac{-\Delta S}{Tf}\right) + (fr_{(n)} - fr_{(n-1)}) * \exp\left(\frac{-\Delta S}{2 * Tf}\right) \tag{44}$$

In the program, fr is defined as the appropriate separation point (based either on f or fqs) using appropriate logic. The equation for pitching moment including separation effects is then universally applicable and is given by

$$C_m^f = \left(k0 + k1 * (1 - fr') + k2 * \sin(\pi * fr'^m)\right) * C_n^f + C_m^{ai} + C_m^{qi} + C_{m0} - \frac{\pi * c}{8 * U * \beta} * (\dot{\alpha} - X5) \tag{45}$$

where X5 is another deficiency function, given by

$$X5_{(n)} = X5_{(n-1)} * \exp(-b5 * \beta^2 * \Delta S) + A5 * \Delta\dot{\alpha} * \exp\left(\frac{-b5 * \beta^2 * \Delta S}{2}\right) \tag{46}$$

The chord force including the effects of separated flow is then given by

$$C_C^f = \eta * Cna * \alpha^2 \sqrt{f} \tag{47}$$

Drag force is calculated as in eqn. (31).

Dynamic Stall Model with Vortex Shedding

The dynamic stall model uses the solution from the second subsystem and adds another factor to account for vortex effects for both normal force and pitching moment.

For the chord normal force, this additional factor is a function of the circulatory normal force from the first subsystem and separation point from the second subsystem. First, an increment for vortex lift is defined

$$C_v = C_n^c * (1 - Kn) \tag{48}$$

where

$$Kn = 0.25 * \left(1 + \sqrt{f''}\right)^2 \tag{49}$$

The accumulated vortex lift is modeled as exponentially decaying, giving rise to an equation for vortex lift.

$$C_{n(n)}^v = C_{n(n-1)}^v * \exp\left(\frac{-\Delta S}{Tv}\right) + (C_{v(n)} - C_{v(n-1)}) * \exp\left(\frac{-\Delta S}{2 * Tv}\right) \tag{50}$$

The vortex lift is only incremented while the vortex is over the airfoil; that is, once the vortex has passed the tail of the airfoil, eqn. (50) is reduced to

$$C^{v}_{n(n)} = C^{v}_{n(n-1)} * \exp\left(\frac{-\Delta S}{Tv}\right) \tag{51}$$

This is monitored using a dimensionless vortex passage time, τ_v. τ_v is defined as being 0 at the moment of vortex detachment (when C_n' first exceeds Cn1) and is equal to T_{vl} at the point the vortex reaches the airfoil tail.

To determine the center of pressure of the vortex lift, eqn. (52) is used, which has been scaled by a factor of 0.20 determined through experience.

$$CPv = -0.20 * \left(1 - \cos\left(\frac{\pi * \tau_v}{Tvl}\right)\right) \tag{52}$$

The pitching moment due to vortex shedding may then be given by

$$C^{v}_{m} = CPv * C^{v}_{n} \tag{53}$$

After the initial vortex has shed, additional vortices may form and subsequently shed as well. This has empirically been found to correspond to a Strouhal number of St=0.19, and as such an additional vortex shedding time constant is modeled as

$$Tsh = \frac{2 * (1 - f'')}{St} \tag{54}$$

Total normal force and pitching moment coefficients may then be obtained for the Leishman-Beddoes method.

$$C_n = C_n^f + C_n^v \tag{55}$$

$$C_m = C_m^f + C_m^v \tag{56}$$

The chord force is modeled as

$$C_C = \begin{cases} \eta * Cna * \alpha_{tot}^2 * \sqrt{f''}, & C_n' < Cn1 \\ \eta * Cna * \alpha_{tot}^2 * f'', & C_n' > Cn1 \end{cases} \tag{57}$$

To avoid discontinuities in the calculation of chord force, eqn. (57) is modified to the following form:

$$C_C = \eta * Cna * \alpha_{tot}^2 * \sqrt{f''} * \left(f''\right)^{0.5*DFD*(C_n'-Cn1)} \tag{58}$$

Here, DFD is a chord force smoothing parameter and the quantity DFD*(C_n'-Cn1) ranges between 0 and 1.

Drag and lift coefficients may then be easily computed.

$$C_d = C_n * \sin(\alpha) - C_C * \cos(\alpha) + C_{d0} \tag{59}$$

$$C_l = C_n * \cos(\alpha) + C_C * \sin(\alpha) \quad (60)$$

Subsystem Interaction

In the interest of simplicity, to avoid additional equations and empirical constants, the Leishman-Beddoes method utilizes progressive adjustments to two of the time constants, T_v and T_f. Depending on whether the flow is attached, unattached or whether there is a vortex over the airfoil or not, values of the time constants are modified to cause the varying aerodynamic effects to occur faster or more slowly. The attached flow model may be solved for the entire oscillation on its own, but the other two subsystems must be calculated one after the other at each iteration so that the correct time constant may be used in each subsystem.

In total, there are 18 empirically determined coefficients, summarized in Table 2.

Table 2: Empirical Parameters Used in Leishman-Beddoes Method

Parameter	**Description**	**Source**
C_{n_α}	Normal force curve slope	Static data
α_0	Zero lift AoA	Static data
α_1	Kirchoff stall angle parameter	Static data
$\Delta\alpha_1$	Static lift hysteresis parameter	Static data
S_1	Kirchoff static stall parameter, $\alpha<\alpha_1$	Static data
S_2	Kirchoff static stall parameter, $\alpha>\alpha_1$	Static data
k_0	Center of pressure offset	Static data
k_1	Separation effects on center of pressure parameter	Static data
k_2	Moment break at stall parameter	Static data
C_{m0}	Zero lift pitching moment coefficient	Static data
C_{d0}	Skin friction drag coefficient	Static data
η	Suction recovery factor	Static data
DF_D	Chordwise force smoothing factor	Static data
C_{n1}	Critical normal force for leading edge separation	Static data
T_P	Leading edge separation time constant	Dynamic data
T_f	Trailing edge separation time constant	Dynamic data
T_v	Dynamic stall lift due to vortex convection time constant	Dynamic stall data
T_{vl}	Dynamic stall moment due to vortex convection time constant	Dynamic stall data

CHAPTER 5: VALIDATION OF THE LEISHMAN-BEDDOES MODEL

To ensure that the Leishman-Beddoes method has been correctly implemented here, results from Reference [10] have been superimposed on results derived from the current implementation of the Leishman-Beddoes method (displayed in red in the images). Results from this paper were chosen because the parameters used in the model were included, which allowed assessment of the model without any questions of how much the discrepancy is due to differences in source data. All of these results are for a NACA 0012 airfoil in an M=0.4 flow. The dotted line in the plots is for a different sweep angle and may be ignored. Cases of an airfoil undergoing dynamic stall were used as this requires accurate computation of all subsystems.

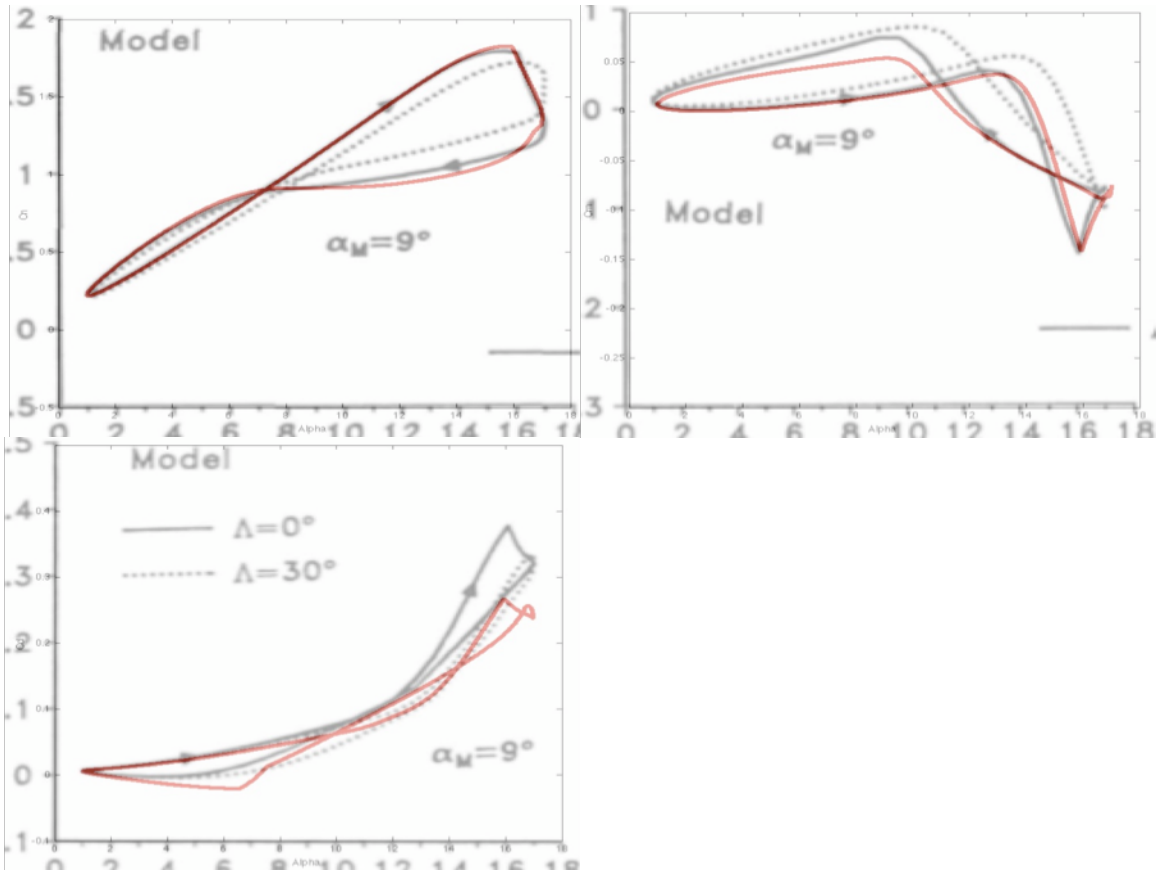

Figure 5: Leishman-Beddoes Results, k=.075, α_m=9, α_C=8

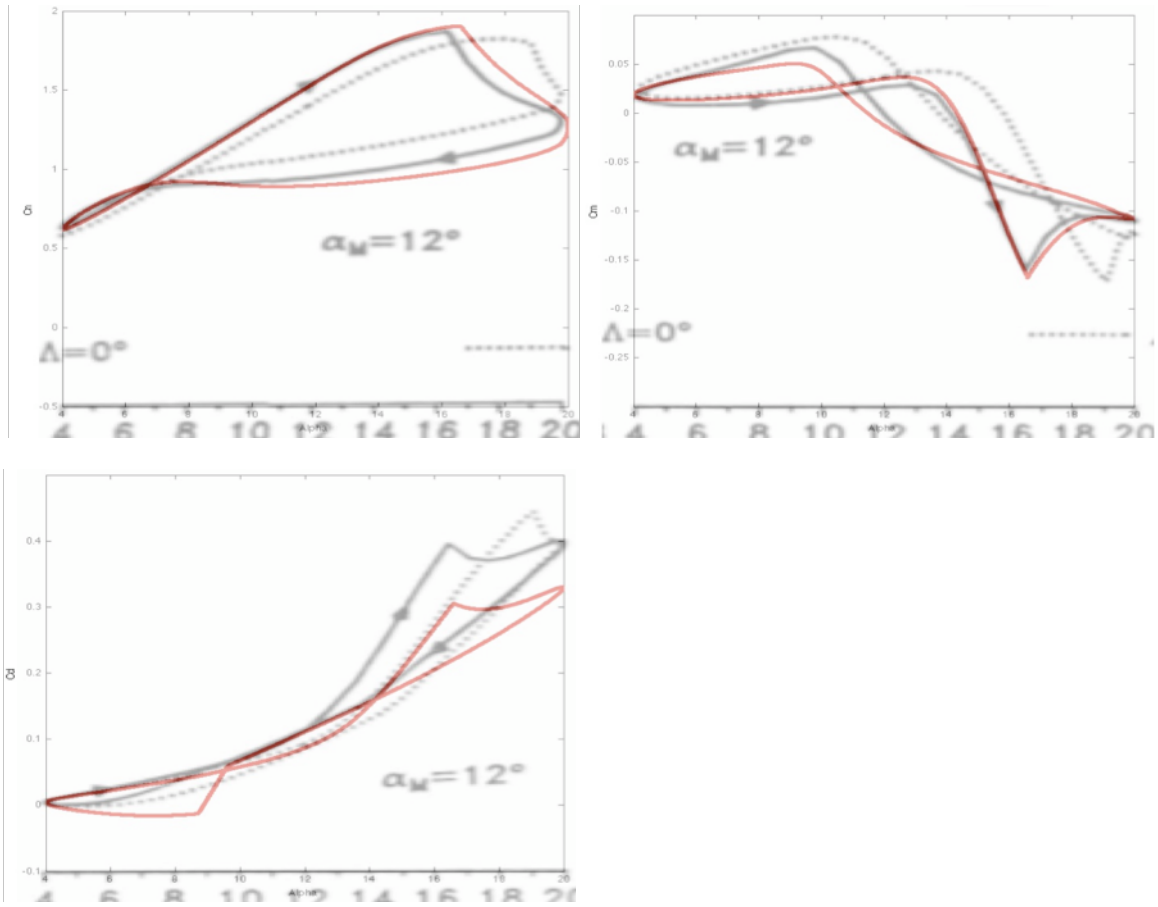

Figure 6: Leishman-Beddoes Results, k=.075, α_m=12, α_C=8

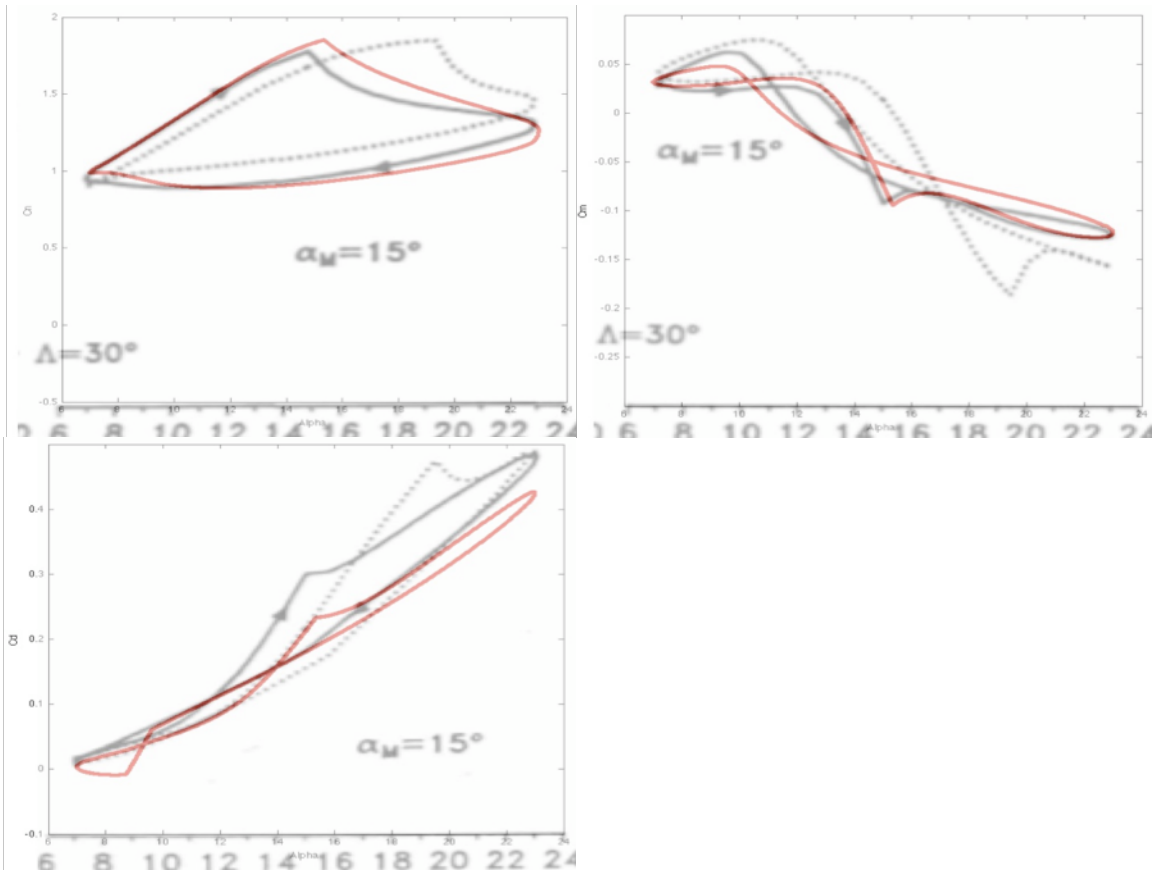

Figure 7: Leishman-Beddoes Results, k=.075, α_m=15, α_C=8

There is excellent correlation with the normal force coefficient. Pitching moment differs slightly on the downstroke. This is very likely due to a small difference in time constant modifications. Strategies for time constant modifications differ in some different papers, and the strategy used in Reference [10] is not described.

The peak drag for the current implementation of the Leishman Beddoes method lags below that for the published result. The reason for this discrepancy was not found, but peak drag force has been matched well with other published results, as shown in Figure 8, based on results from Reference [9].

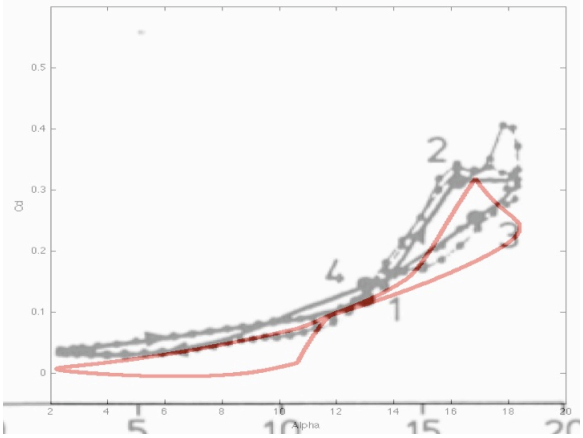

Figure 8: Drag Coefficient, M=0.4, k=.075, α_m=10.3, α_C=8.1

CHAPTER 6: DESCRIPTION AND VALIDATION OF THE CFD TOOLS

The CFD code utilized in this work is the one developed by Bain, et al and described in Reference [24]. It utilizes the Kinetic-Eddy Simulation (KES) turbulence model in NASA's OVERset grid FLOW (OVERFLOW) CFD code and is a Navier-Stokes solver.

KES is a hybrid of the Reynolds Averaged Navier-Stokes (RANS) and Large Eddy Simulation (LES) turbulence models. The RANS model has relatively low computational costs, but has been found to produce poor results for detached flow, even with fine grid spacing. LES directly computes the large scale turbulent eddies and then models the smaller structures. It has produced more accurate results than RANS, but at greater computational cost. KES is a method of attempting to capture benefits of LES inside of a RANS code, and researchers have found that it produces good results for the type of 2-D dynamic stall flows considered in this work. [24]

OVERFLOW is a time marching implicit Navier-Stokes code that has been developed for 3-D but is easily applicable to 2-D problems. It utilizes overset or Chimera grids to allow for modeling various flow phenomena as efficiently as possible.[25] However, in this case where a 2-D pitching airfoil without any slats or flaps in a viscous flow is considered, a carefully crafted C-grid with clustering near the airfoil provides a good computational space for the flow solution.

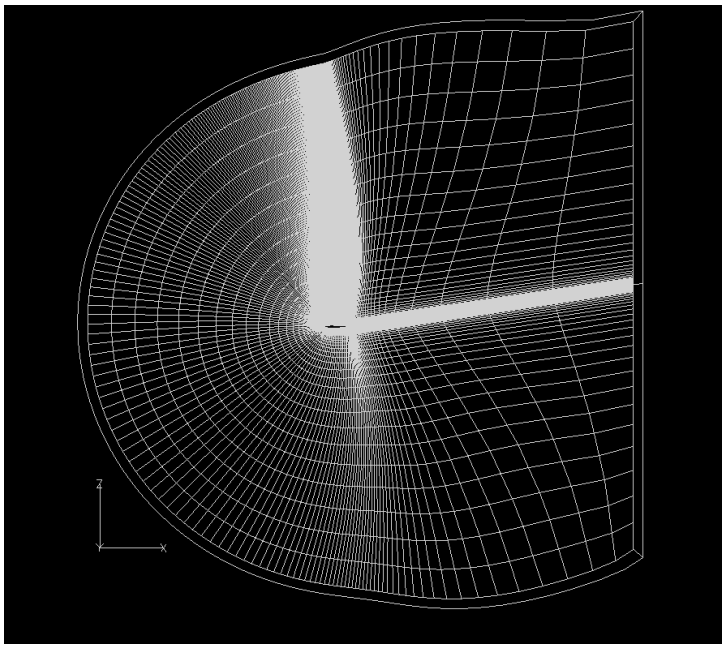

Figure 9: CFD Computational Grid

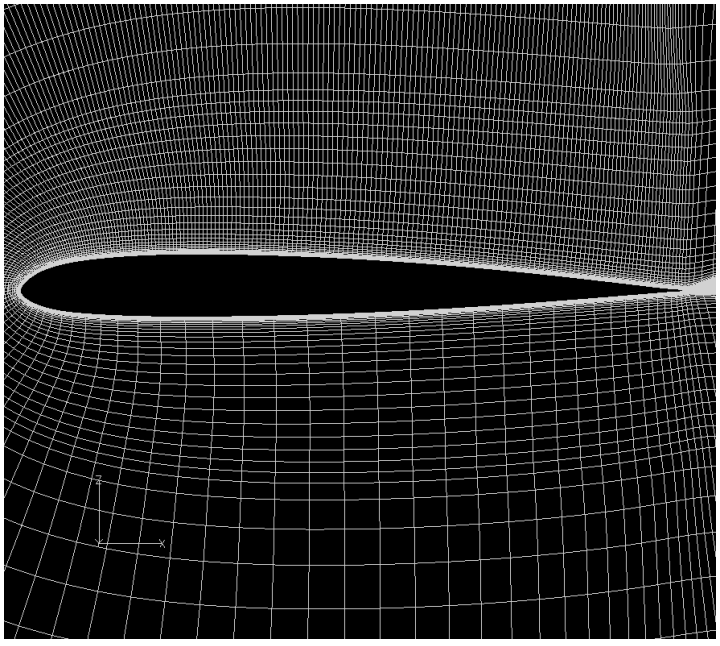

Figure 10: Close-up of Grid Around Airfoil

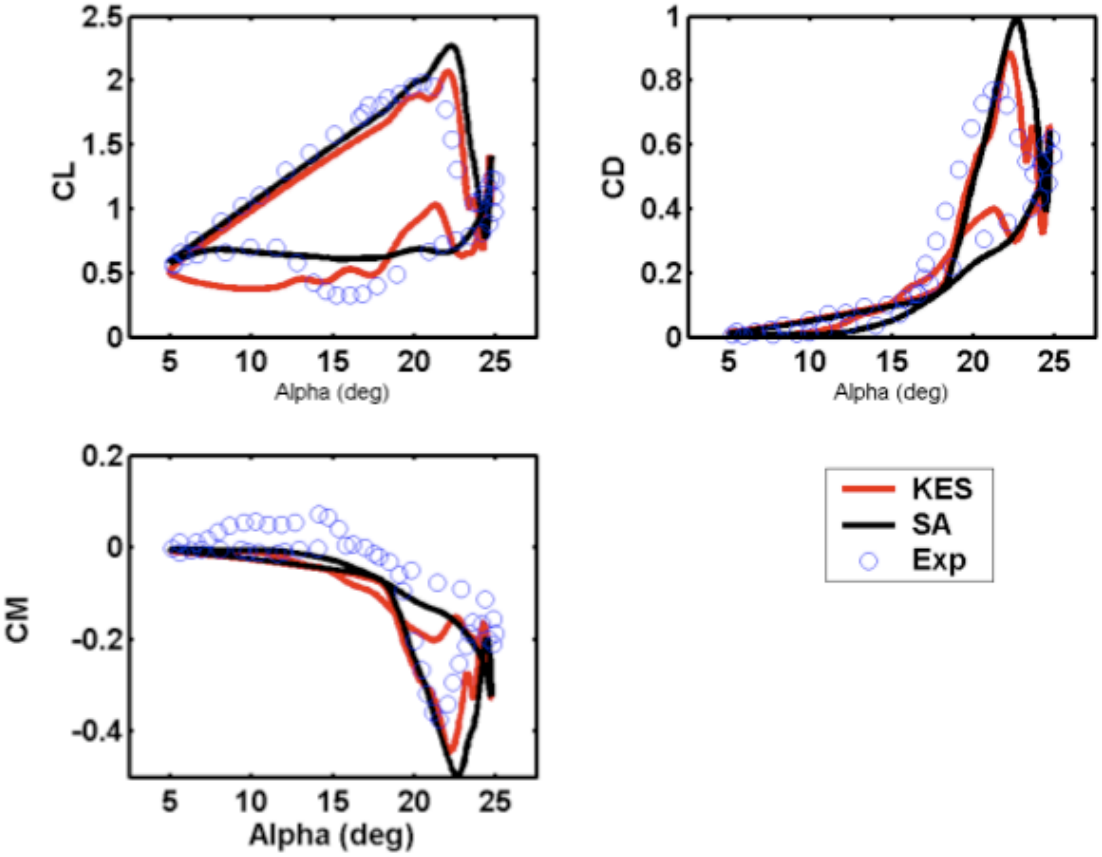

Figure 11: Predicted and Observed Airloads Using KES Model[24]

Figure 11 from Reference [24] shows a case of an airfoil undergoing dynamic stall, with the KES model compared to experimental data and the Spalart-Allmaras (SA) turbulence model. Here, the Mach number is 0.3, reduced frequency is 0.1, mean AoA is 15 degrees, and cyclic AoA is 10 degrees. The KES model is shown to provide better estimates than the SA model and fairly good representation of the experimental data, although peak pitching moment and peak drag are both slightly overpredicted.

CFD results were also compared to data available from the McCroskey, et al paper. In the following figures, the blue line represents the OVERFLOW results while the black line superimposed over the plot is from the McCroskey paper.

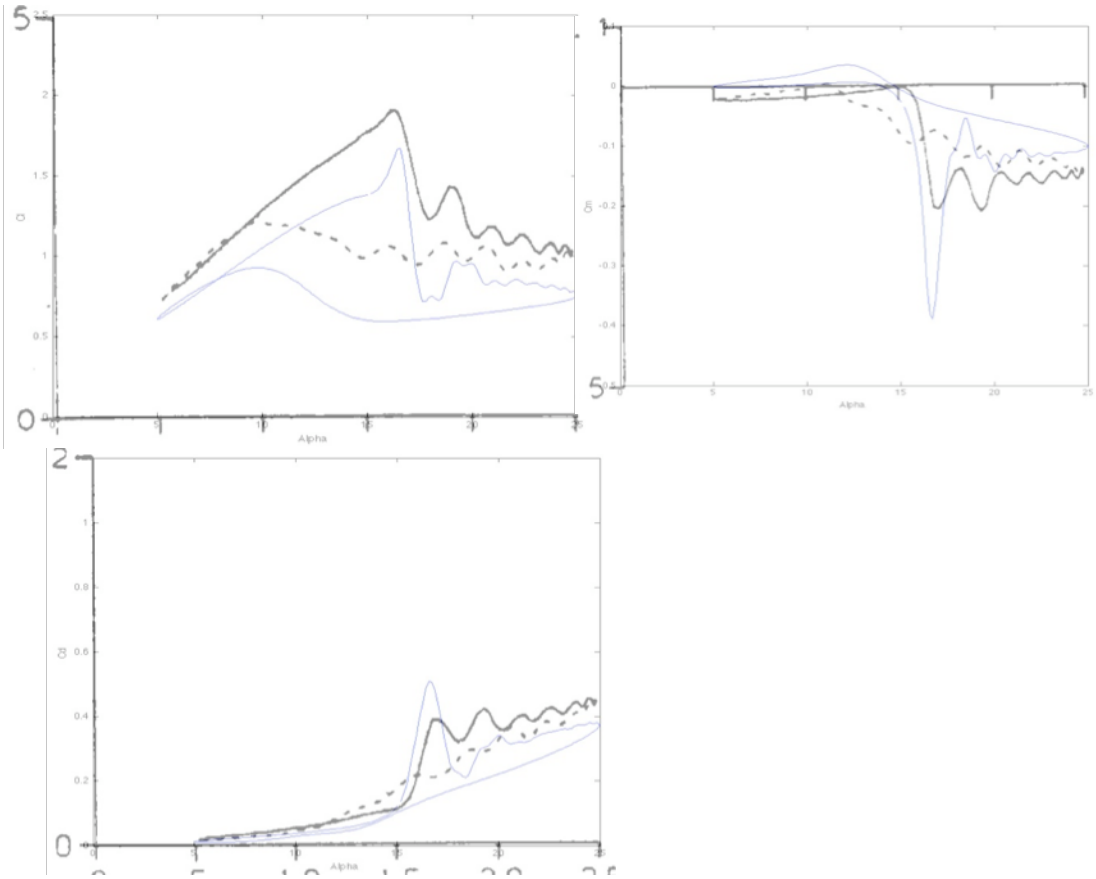

Figure 12: Comparison of CFD Results and Exp Data, M=0.3, k=.03, α_m=15, α_C=10

The experimental data displayed here has been shown to have strong wind tunnel effects, as discussed in Reference [21] and have been described to have limited utility. The CFD data corresponds fairly well to the estimated approximate 10% overprediction inherent in the C_l values from the McCroskey paper.

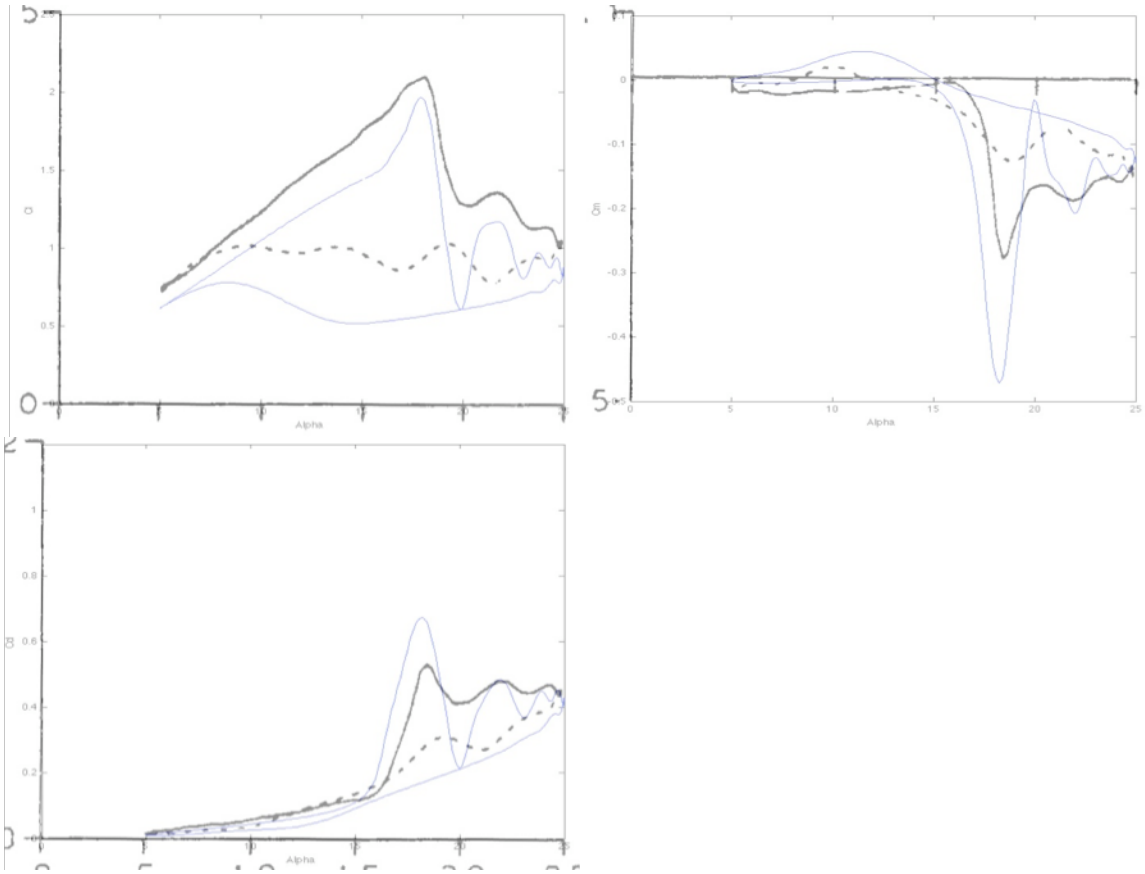

Figure 13: Comparison of CFD Results and Exp Data, M=0.3, k=.05, α_m=15, α_C=10

Additionally, experimental data was compared to CFD and Leishman-Beddoes results, as shown in Figure 14. This was performed to demonstrate that CFD results more closely approximate experimental data than the base Leishman-Beddoes results, and as such modifying Leishman-Beddoes results to more closely match CFD should have the effect of improving the predictions of the Leishman-Beddoes program. The conditions for Figure 14 were M=0.3, k=.1, α_m=10, α_C=10. As can be seen, for areas where predictions from Leishman-Beddoes and OVERFLOW have significant differences, the CFD results typically

are as close or closer to experimental results than Leishman-Beddoes. The one exception seems to be the downstroke of the lift coefficient plot, where OVERFLOW predicts lower lift than both Leishman-Beddoes and experimental data.

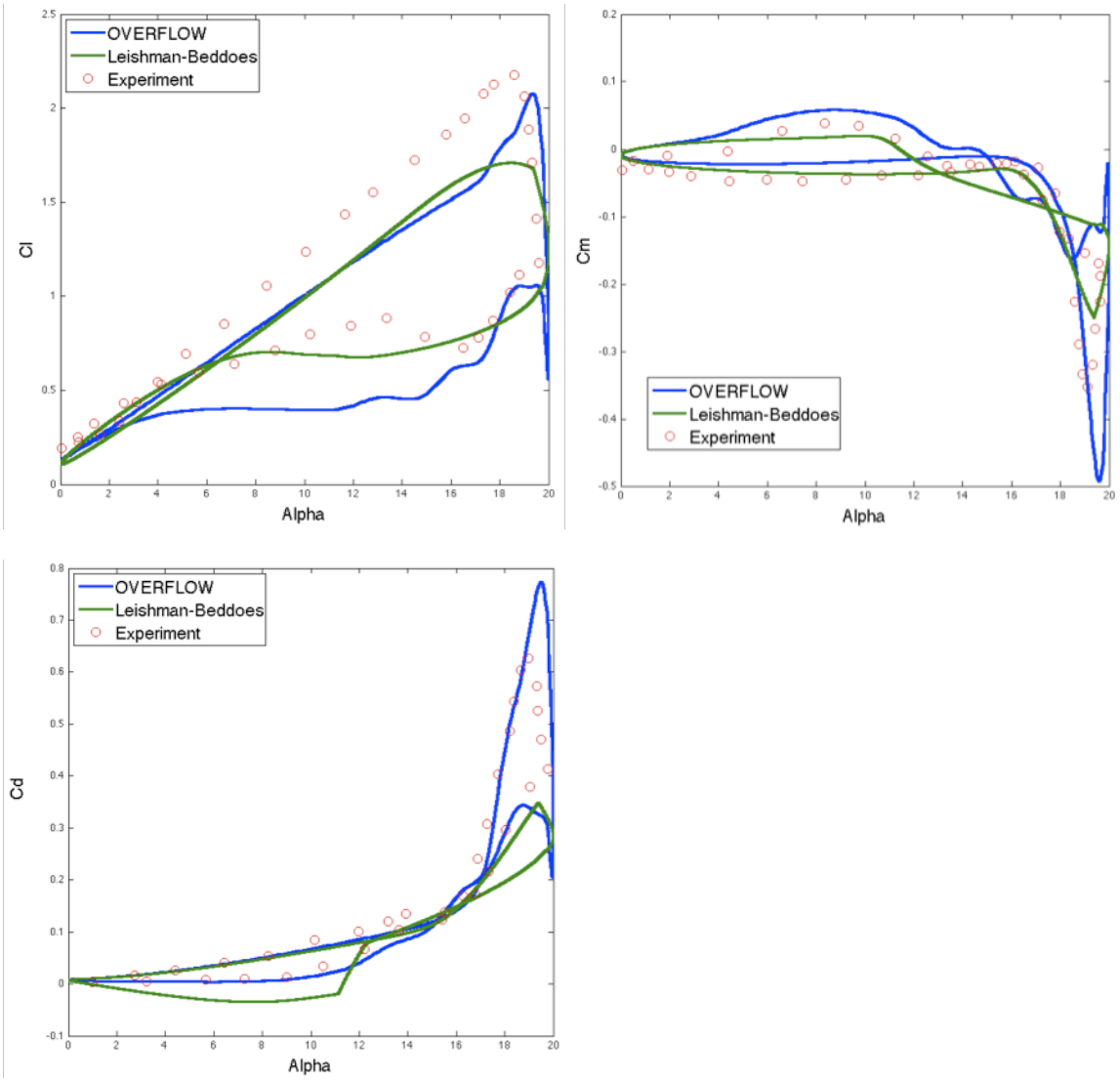

Figure 14: Comparison of Experimental, CFD, and Leishman-Beddoes Results

Jeremy Bain has run a CFD simulation with wind tunnel walls included[28] to see if this accounts for all of the variation between experiment and OVERFLOW results, displayed in the following figure.

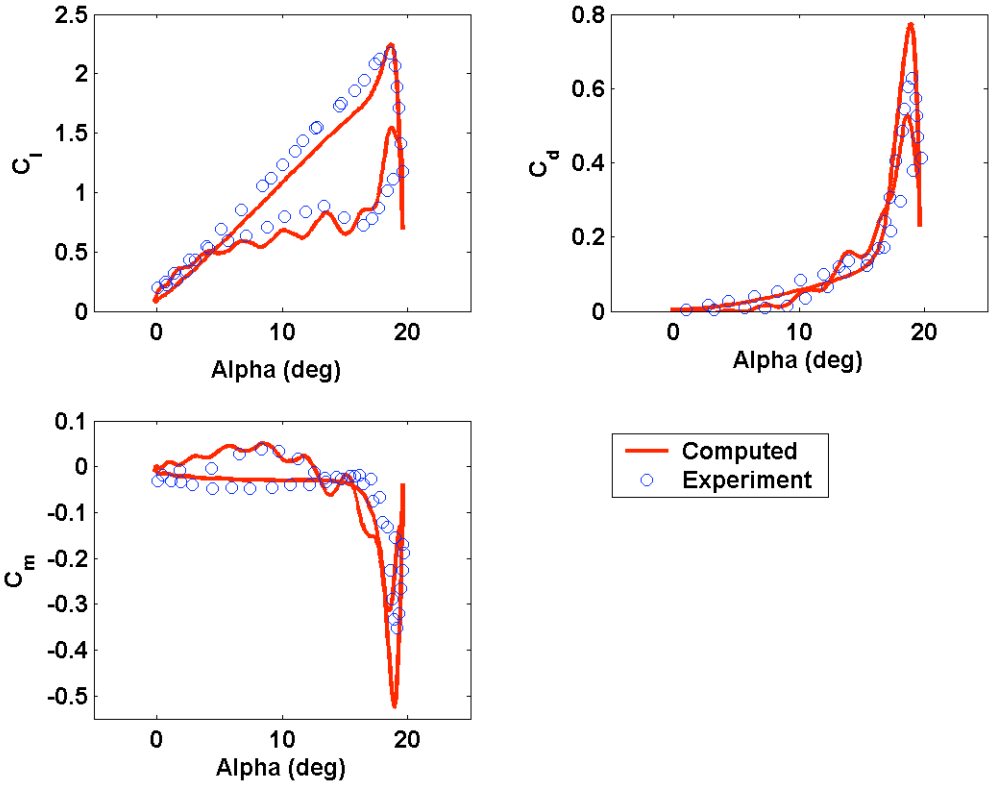

Figure 15: OVERFLOW Results Including Windtunnel Walls[28]

This appears to account for the discrepancy in the lift coefficient, although there is still some overshoot in pitching moment and drag. Given these results, the CFD predictions for lift are taken to be very reliable, but the possibility of some amount of error in peak pitching moment and drag must be kept in mind.

CHAPTER 7: ASSESSMENT OF THE LEISHMAN-BEDDOES MODEL

In this section, a cross section of results are included to provide the reader with an idea of how well the base Leishman-Beddoes predictions compare with CFD results for a range of Mach numbers and flow conditions (attached, separated, and deep dynamic stall).

To quantify the difference between CFD and Leishman-Beddoes, a root mean squared (RMS) error was defined. This error is displayed below, with lift coefficient used as an example.

$$\text{RMS error, } C_l = \sqrt{\frac{\sum_n \left(C_{l,\text{CFD}} - C_{l,\text{L-B}}\right)^2}{n}} \tag{61}$$

Here, n refers not to the time index, but rather the number of sample points used to calculate the RMS error. The standard output for the CFD code provided 400 data points per oscillation at equal time steps, and so this was chosen as the value for n.

The results in this section are based on the parameters derived using the methods discussed in Appendix A without referring to dynamic test data. For many of the cases this yields unsatisfactory results. Modifications to these constants as well as modifications to the model at large are discussed in the following section, “Modifications to the Model and Discussion”.

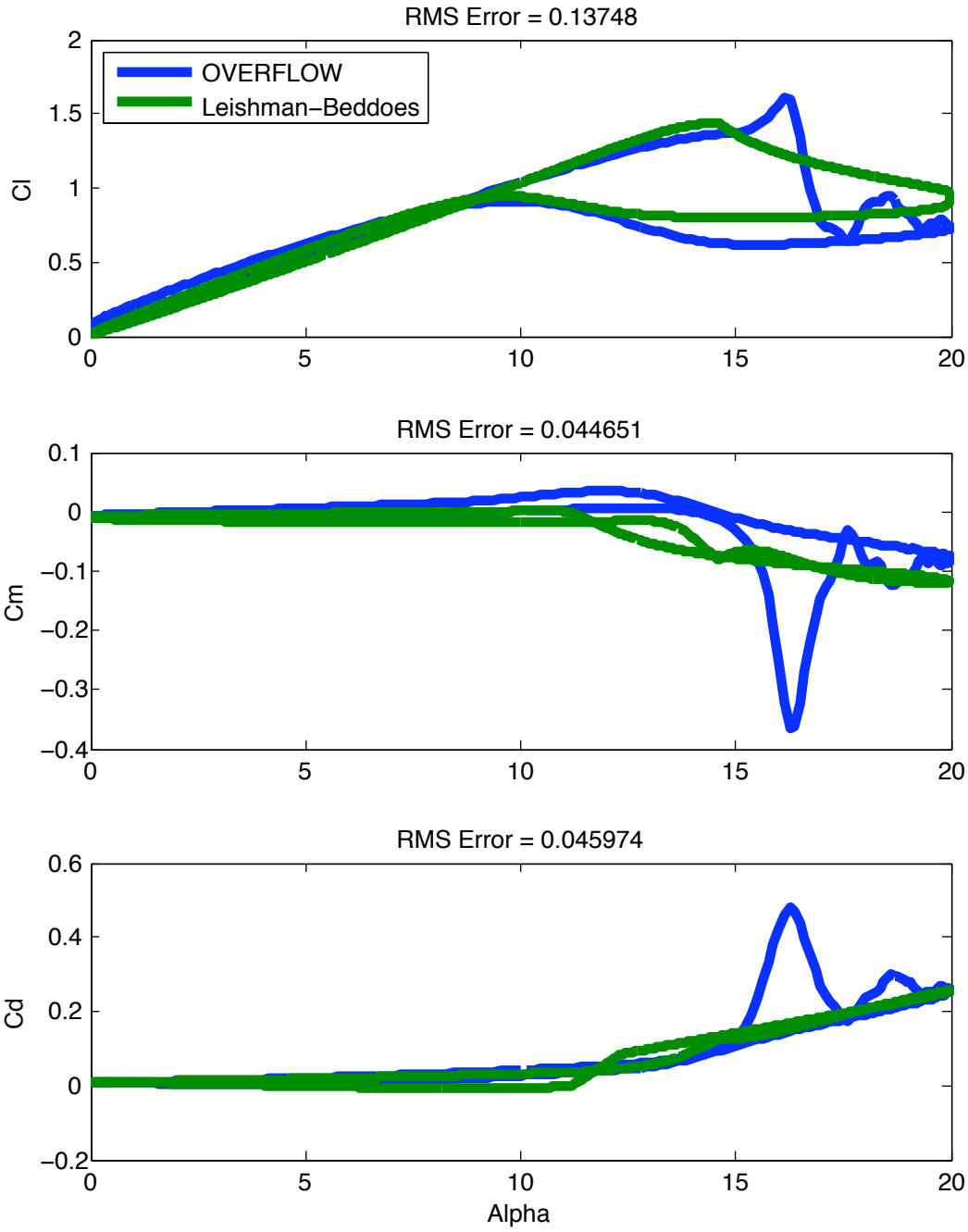

Figure 16: M=0.3, α_m=10, α_c=10, k=0.03

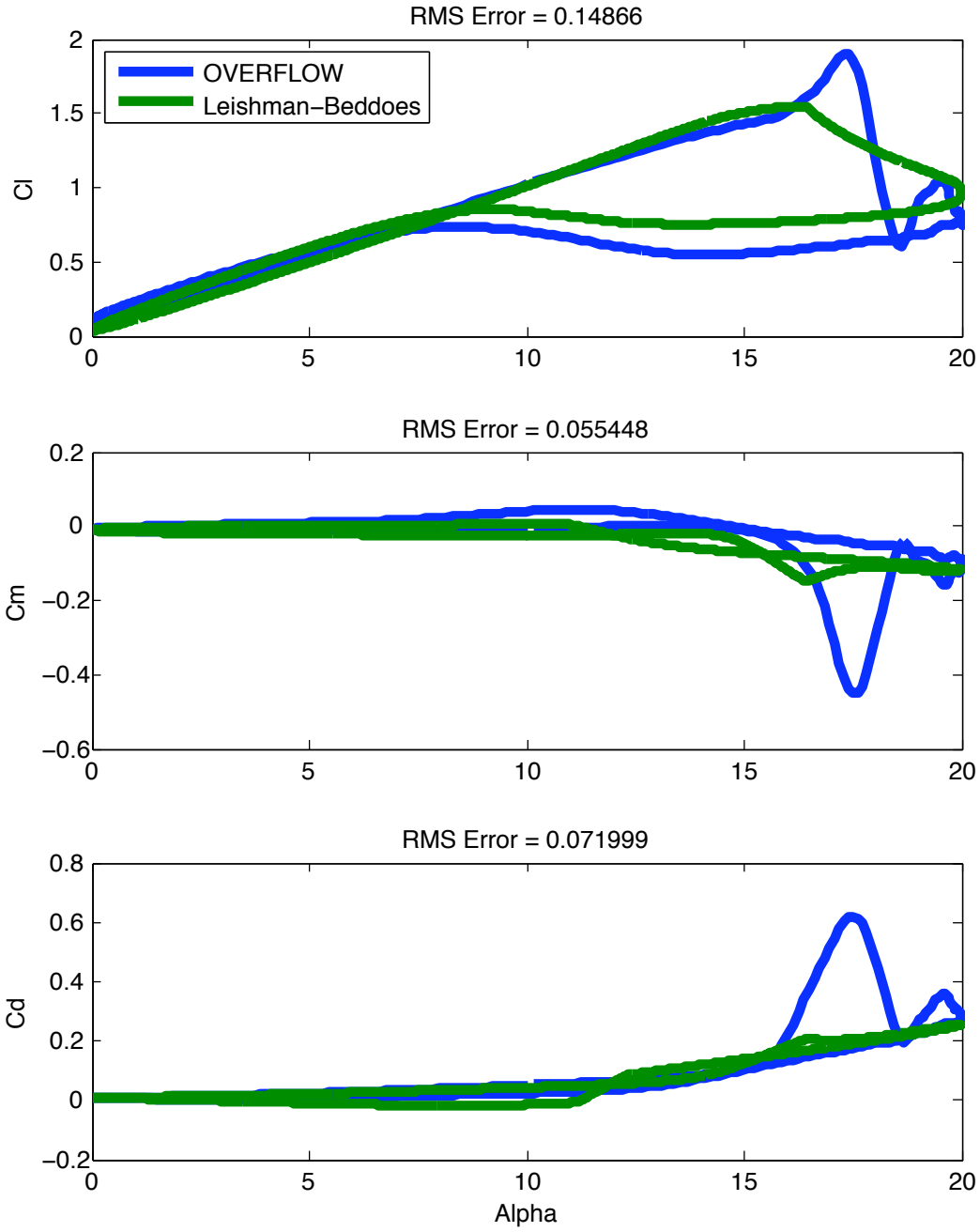

Figure 17: M=0.3, α_m=10, α_c=10, k=0.05

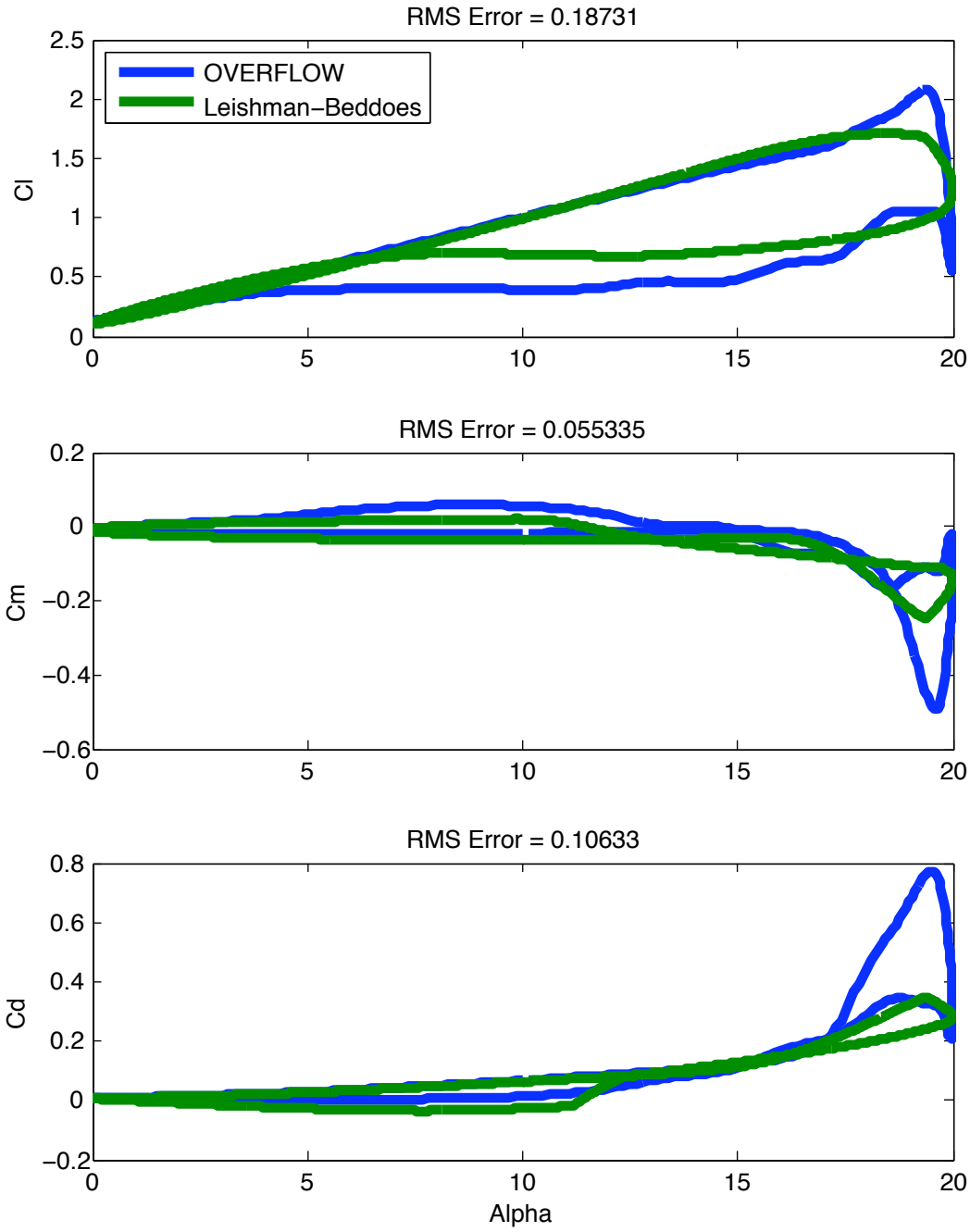

Figure 18: M=0.3, α_m=10, α_c=10, k=0.1

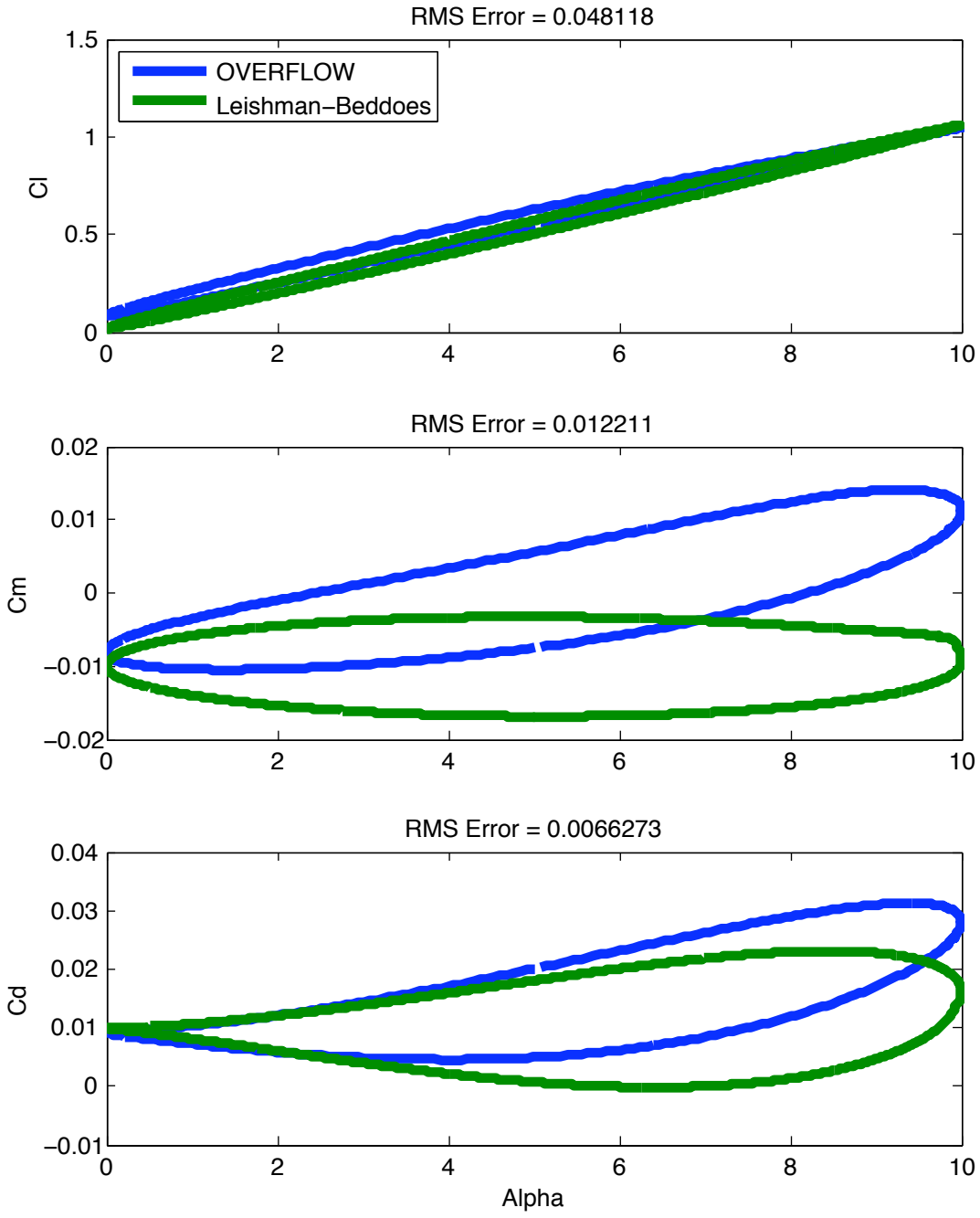

Figure 19: M=0.3, α_m=5, α_c=5, k=0.05

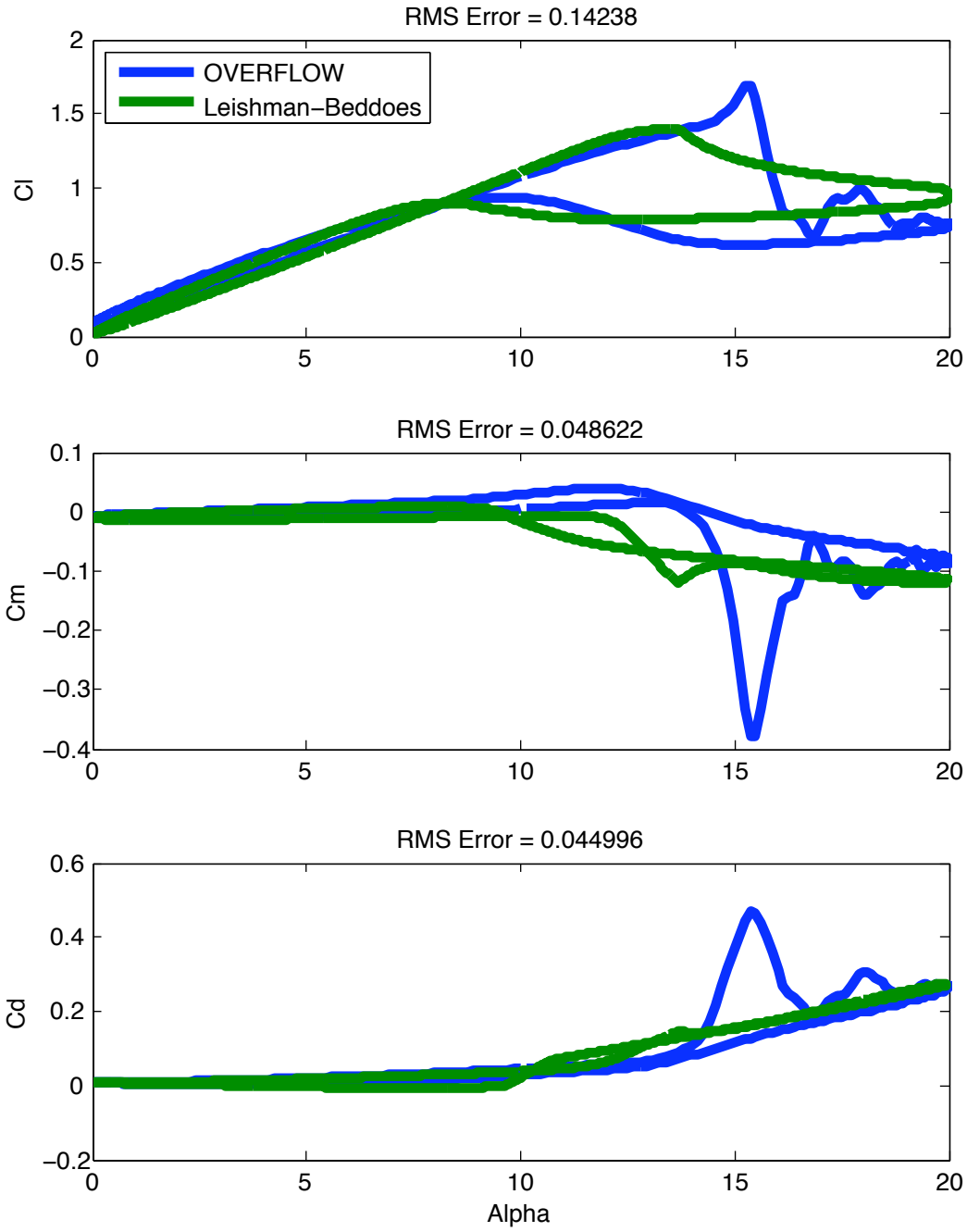

Figure 20: M=0.4, α_m=10, α_c=10, k=0.03

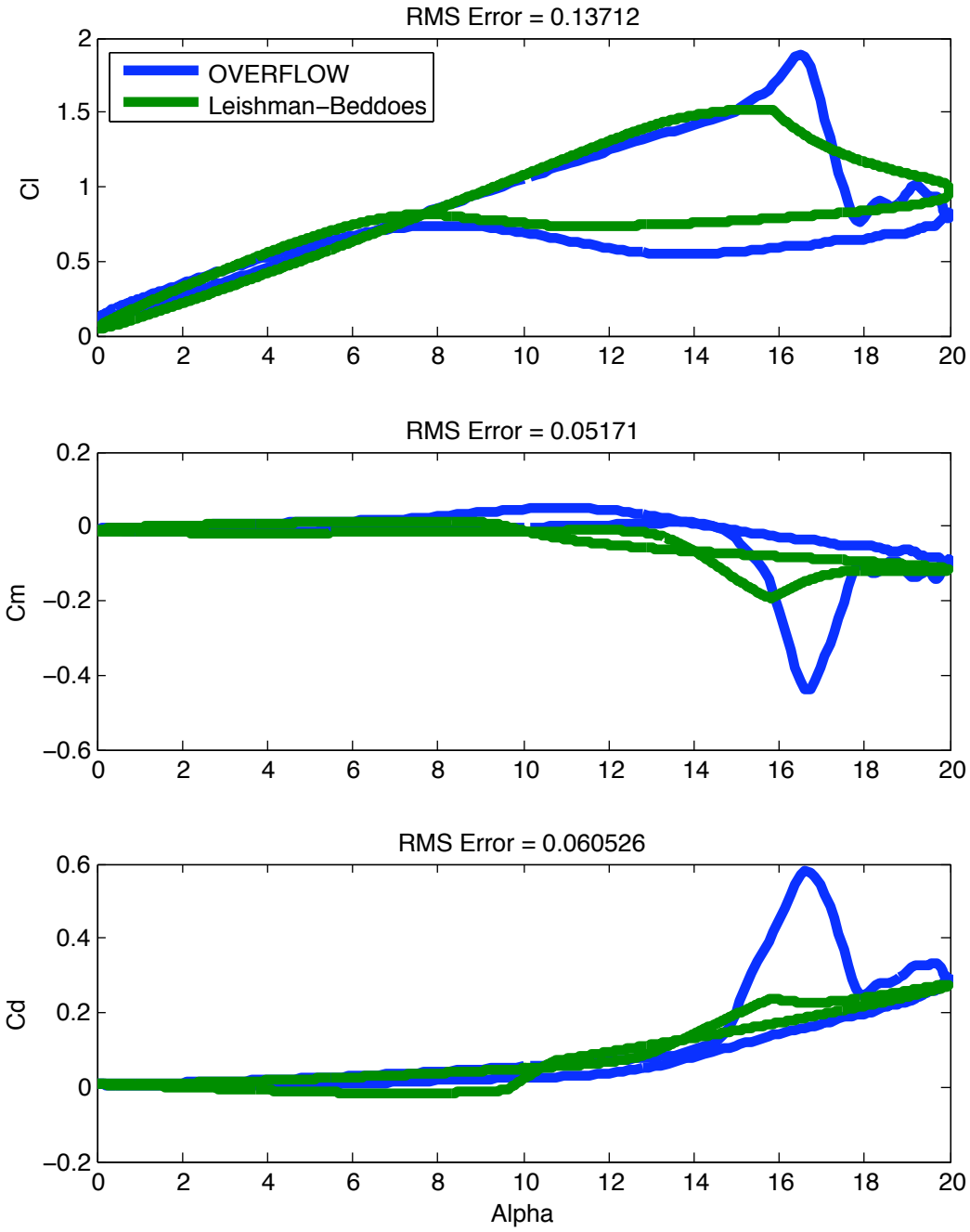

Figure 21: M=0.4, α_m=10, α_c=10, k=0.05

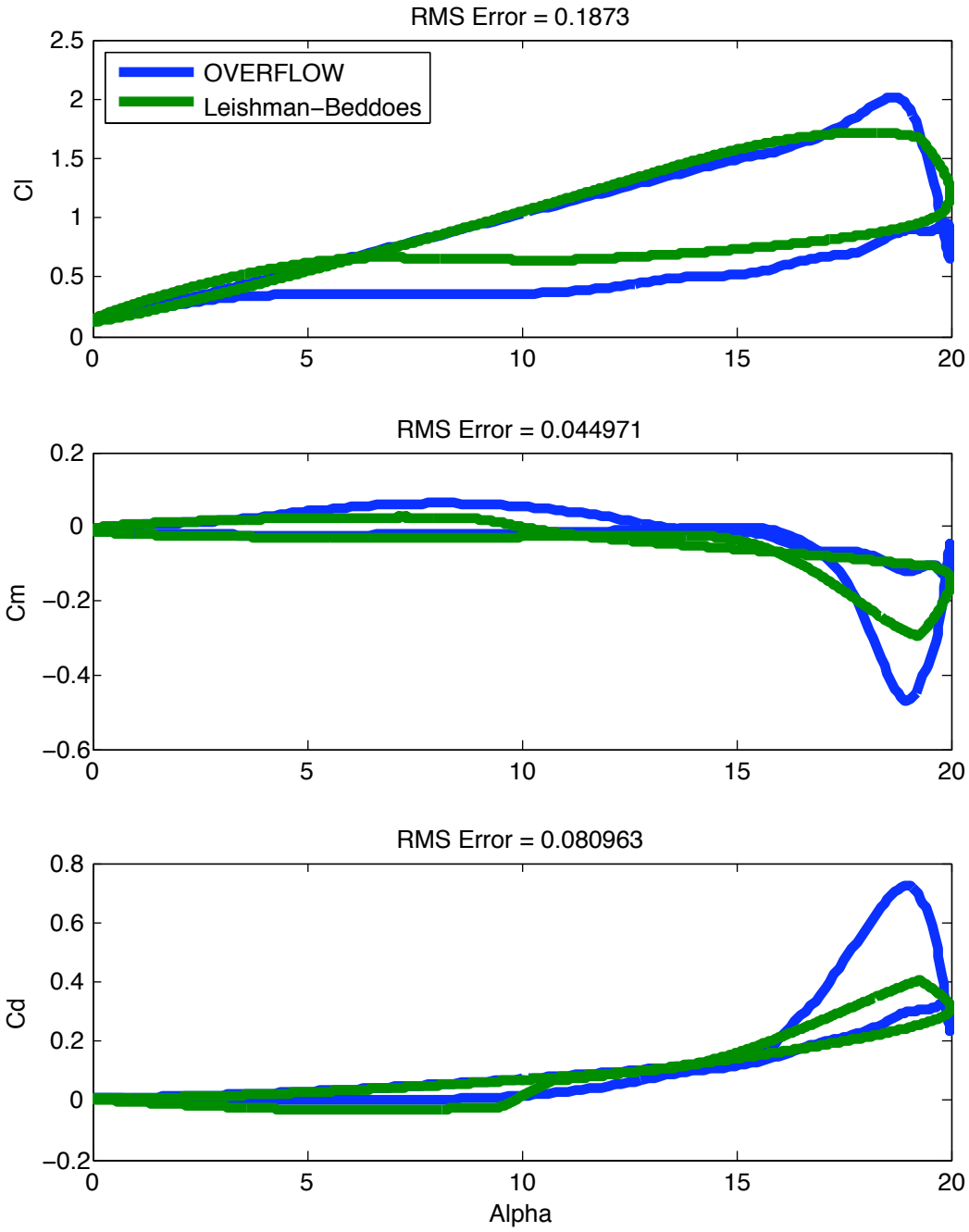

Figure 22: M=0.4, α_m=10, α_c=10, k=0.1

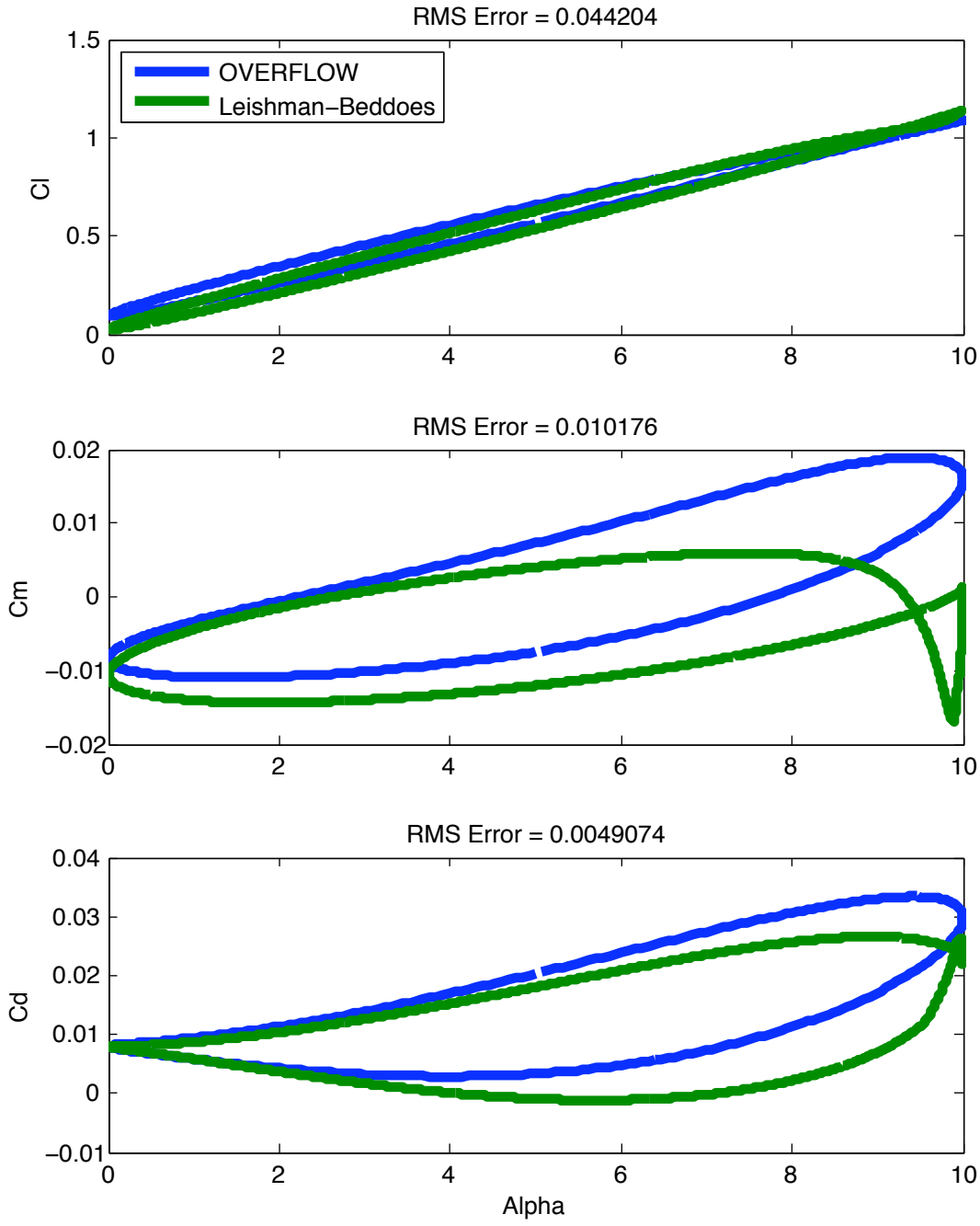

Figure 23: M=0.4, α_m=5, α_c=5, k=0.5

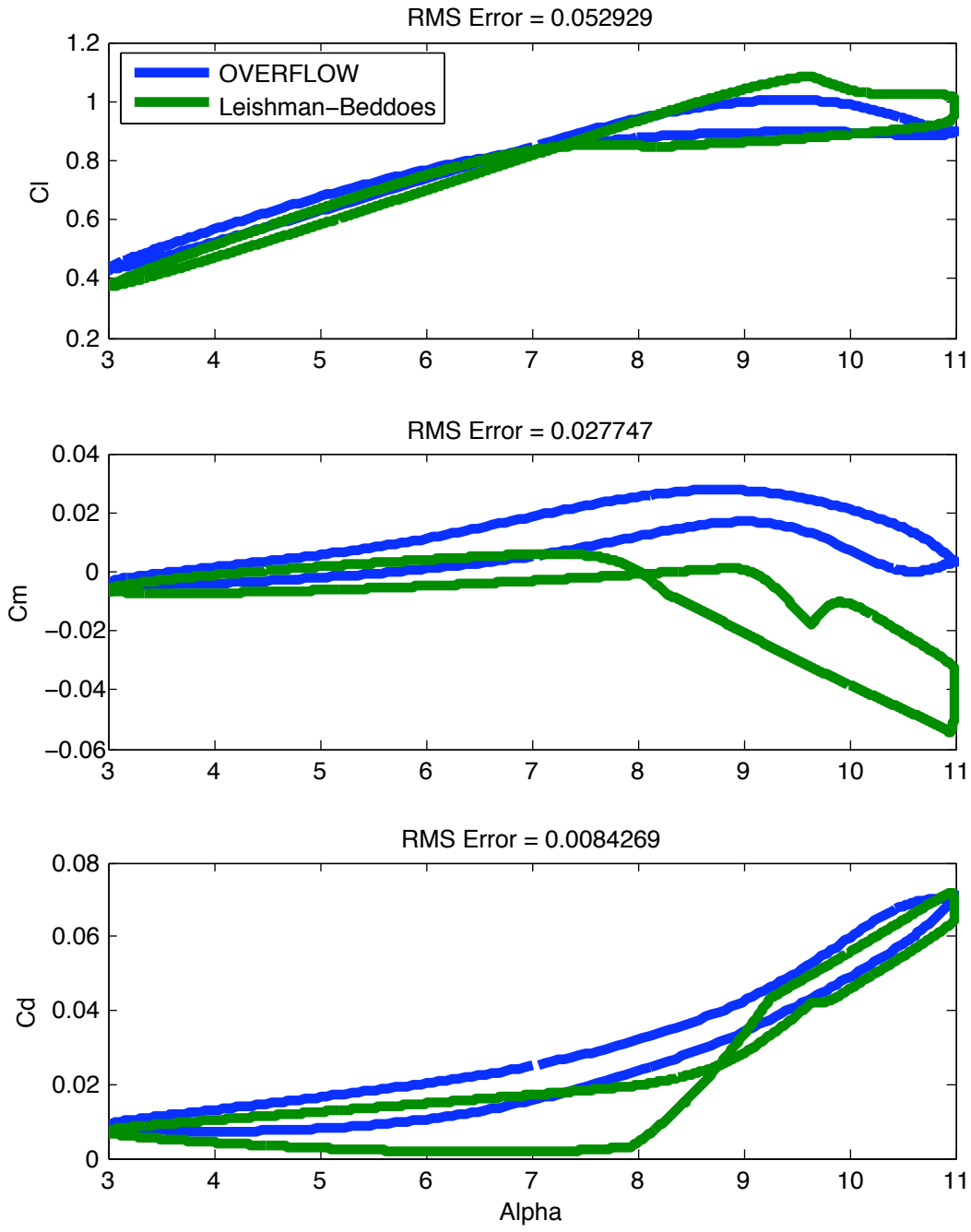

Figure 24: M=0.5, α_m=7, α_c=4, k=0.03

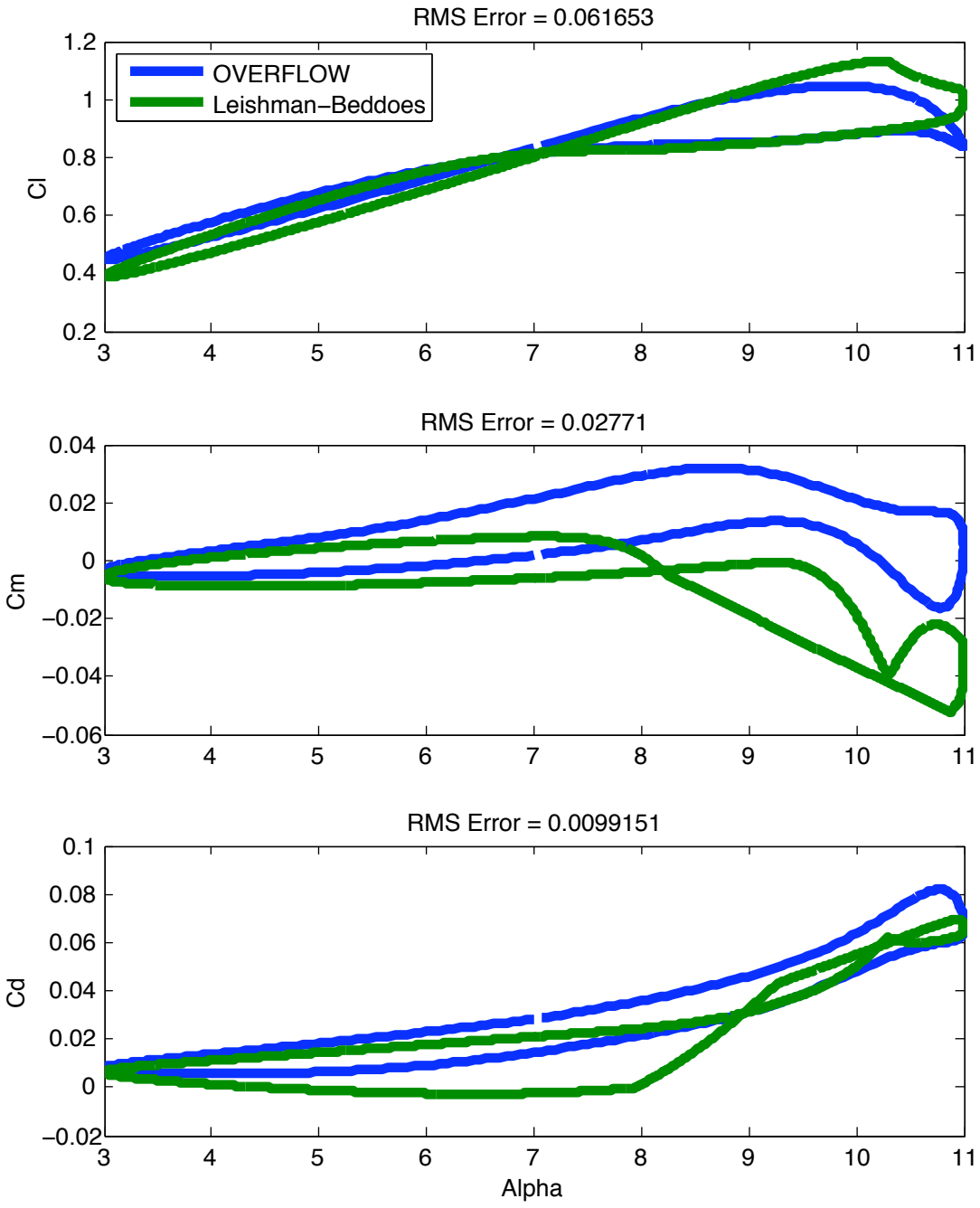

Figure 25: M=0.5, α_m=7, α_c=4, k=0.05

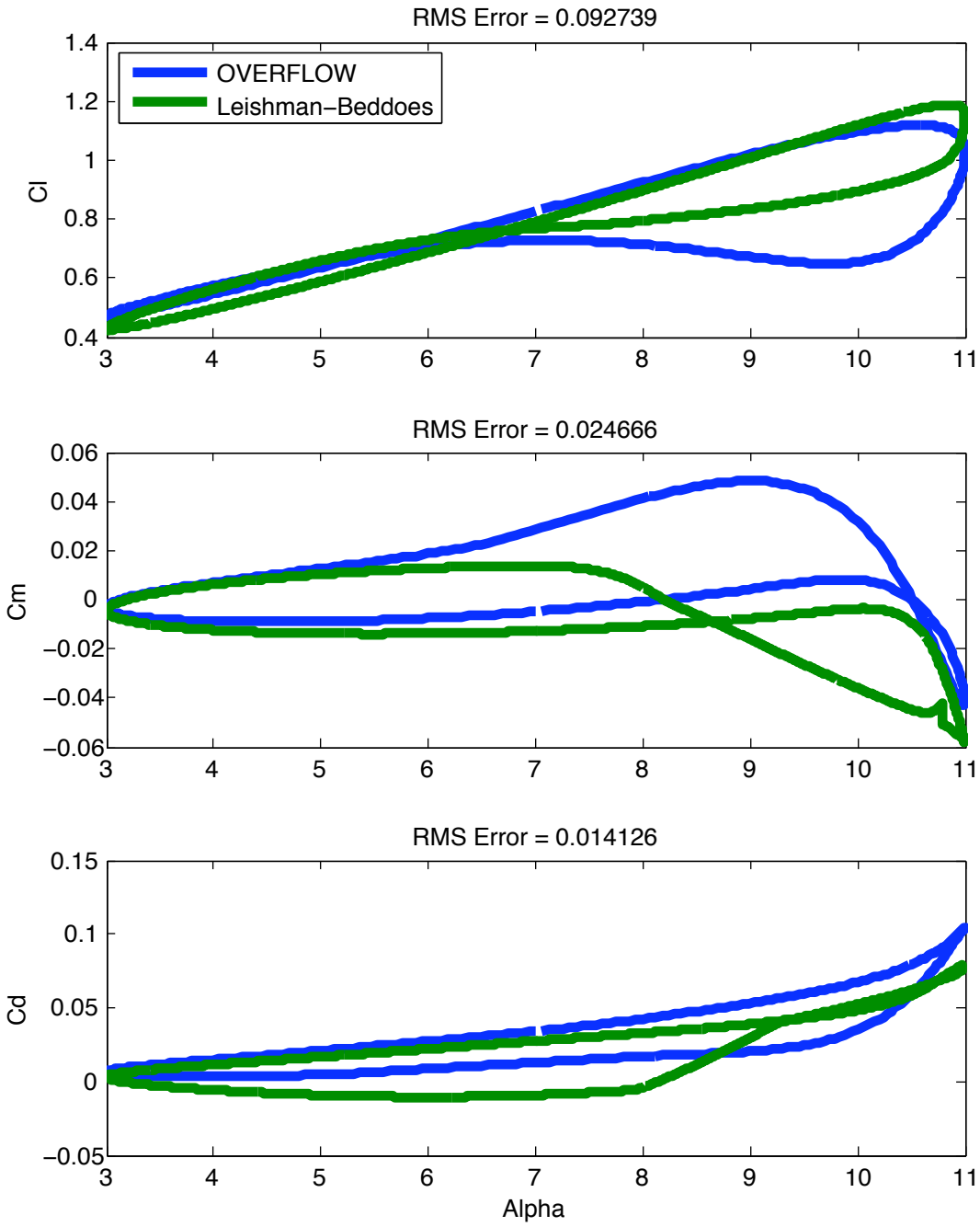

Figure 26: M=0.5, α_m=7, α_c=4, k=0.1

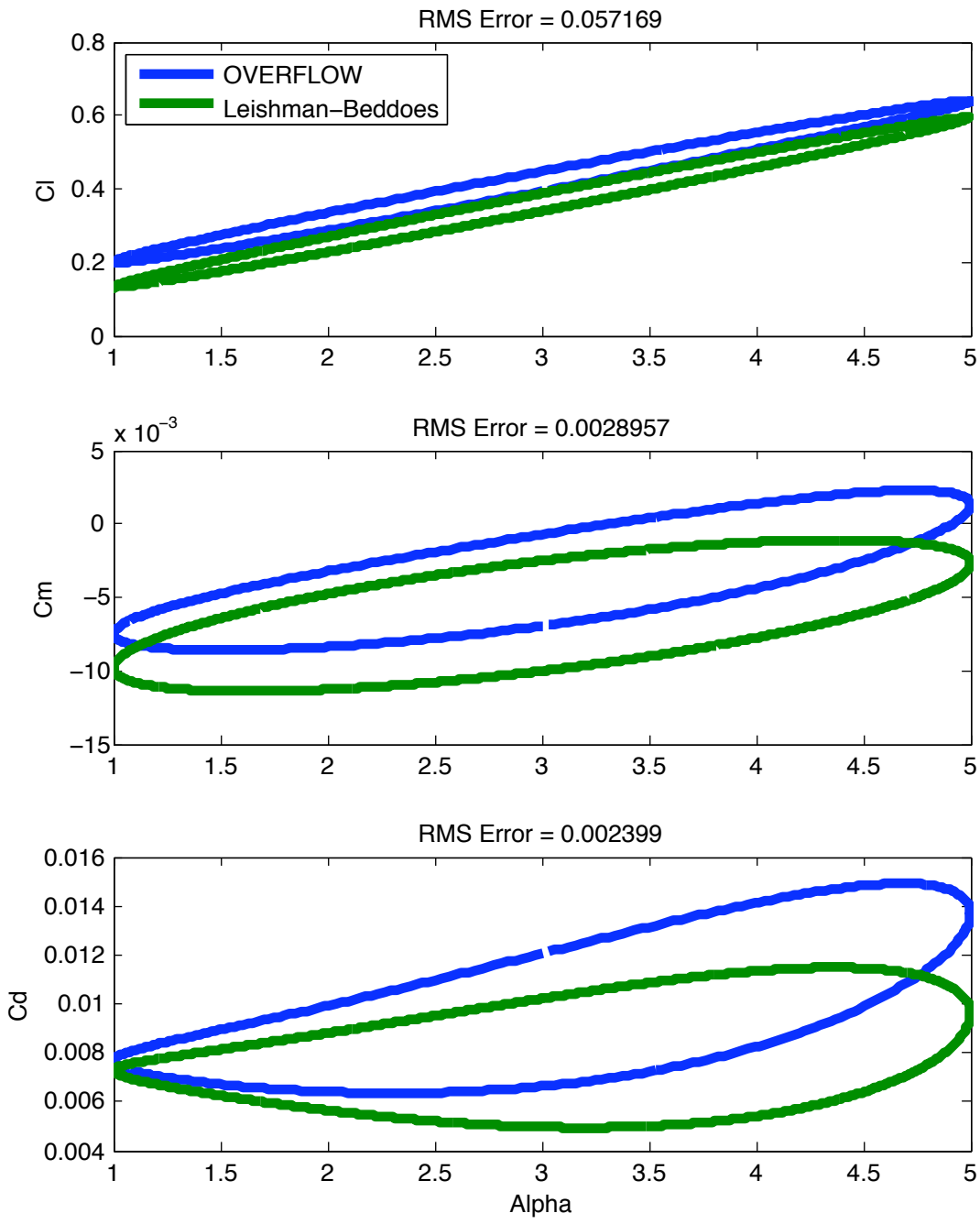

Figure 27: M=0.5, α_m=3, α_c=2, k=0.05

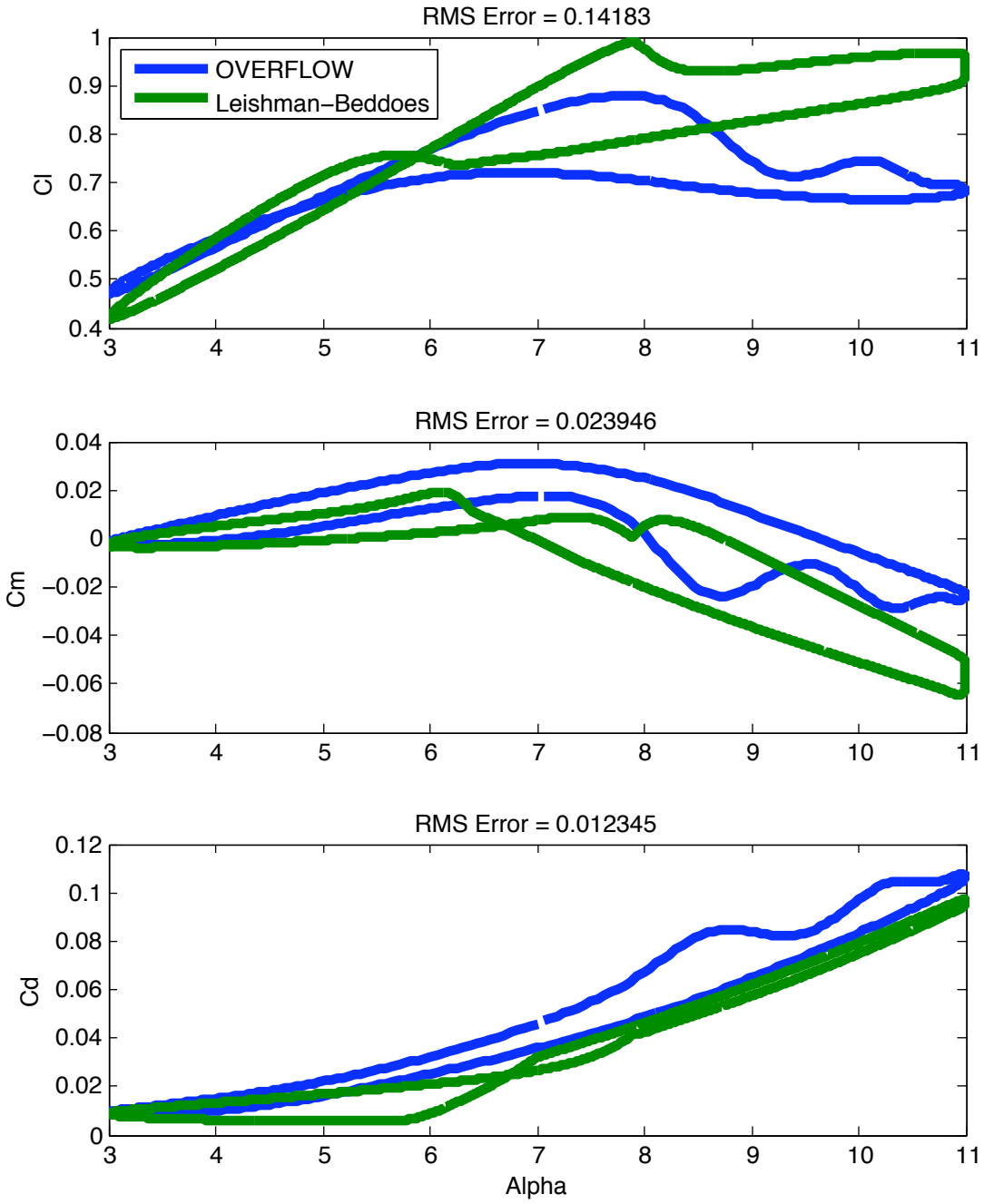

Figure 28: M=0.6, α_m=7, α_c=4, k=0.03

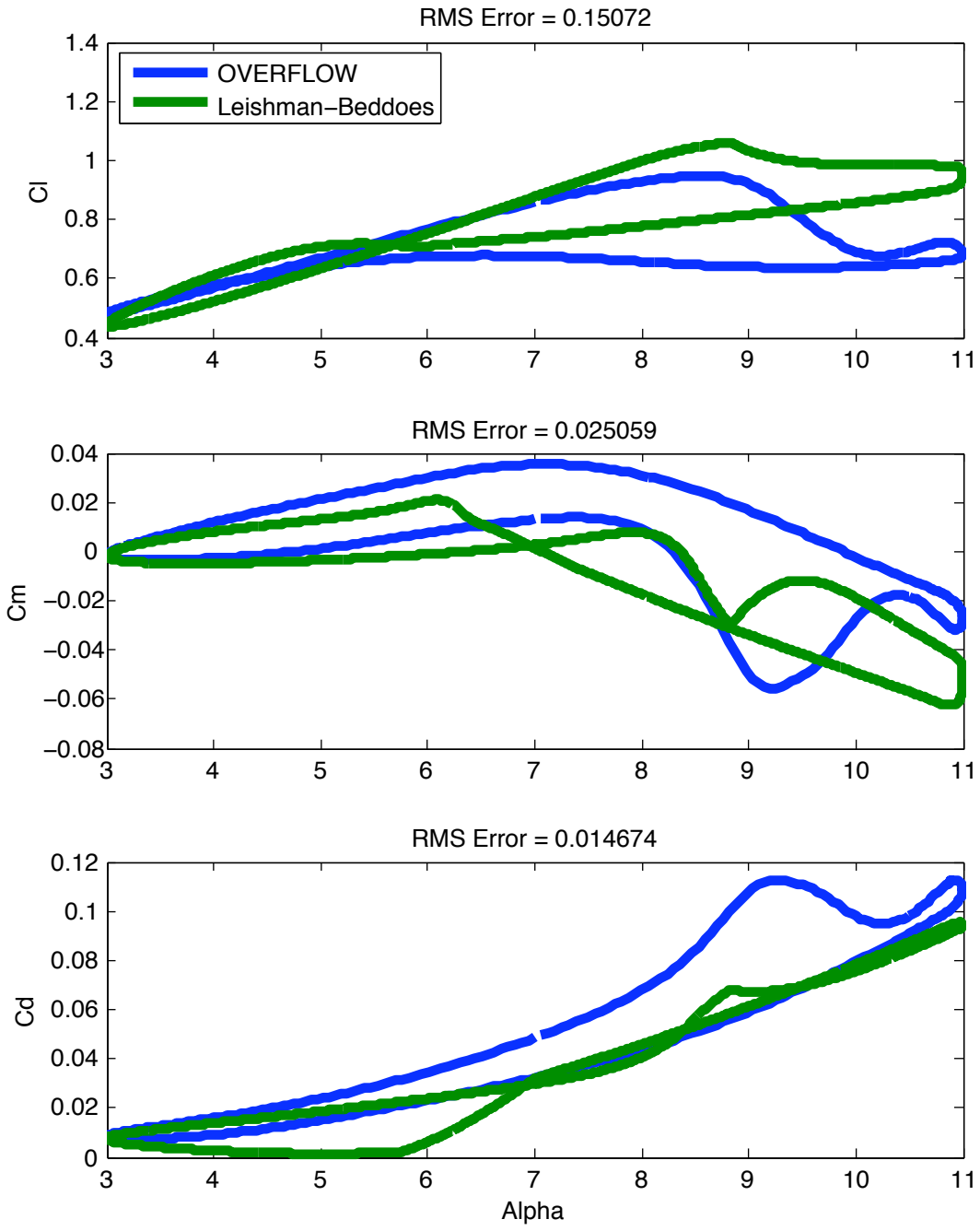

Figure 29: M=0.6, α_m=7, α_c=4, k=0.05

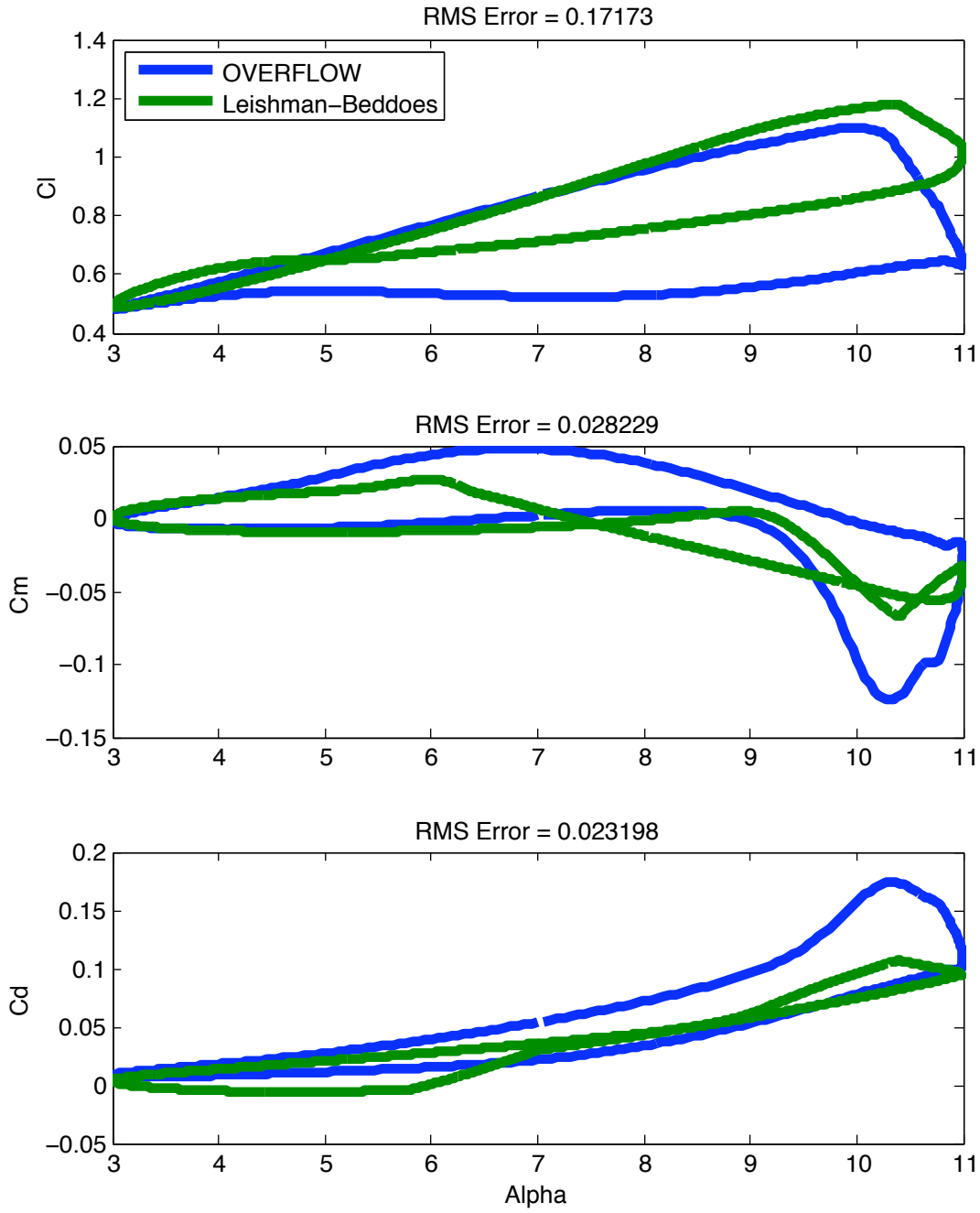

Figure 30: M=0.6, α_m=7, α_c=4, k=0.1

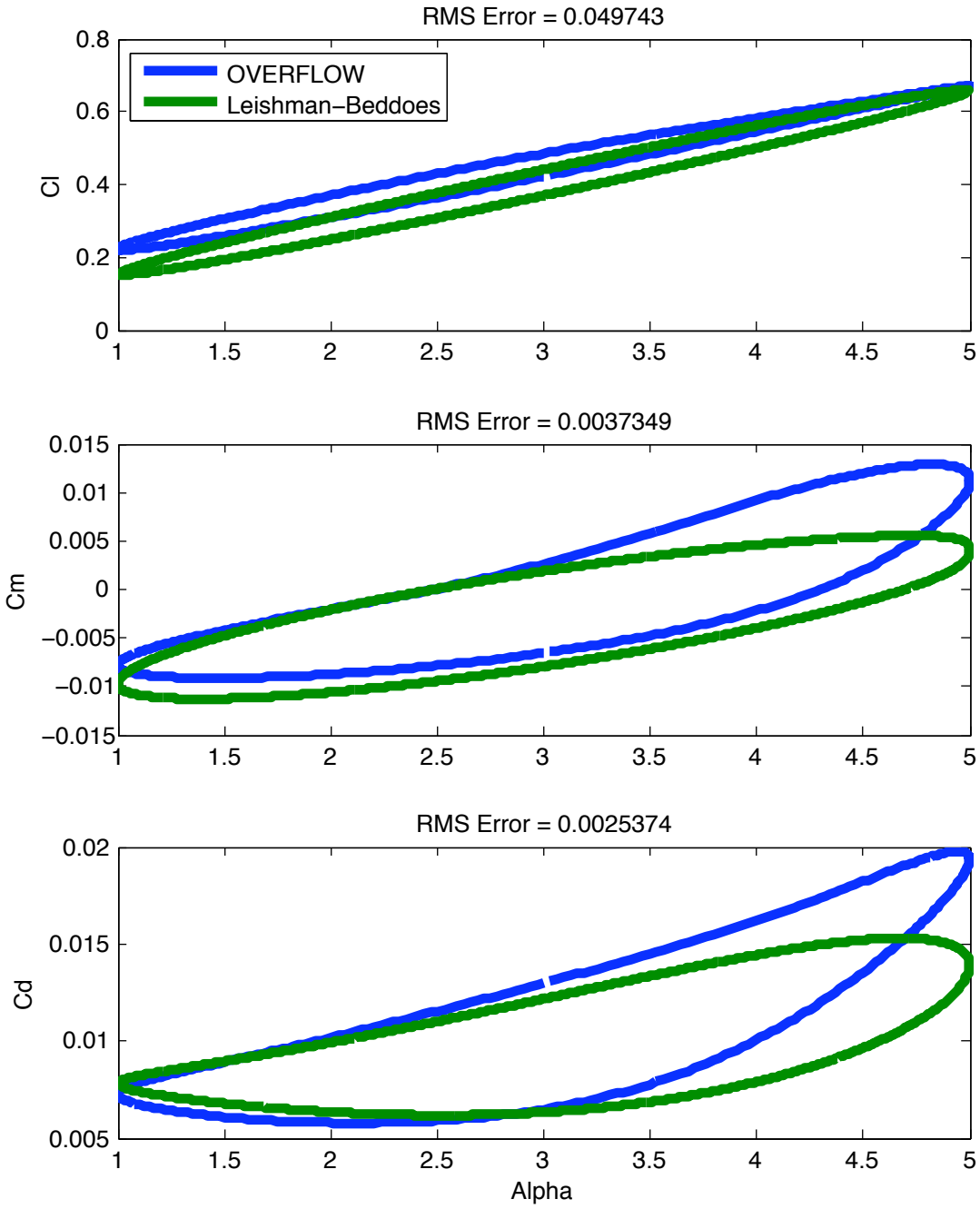

Figure 31: M=0.6, α_m=3, α_c=2, k=0.05

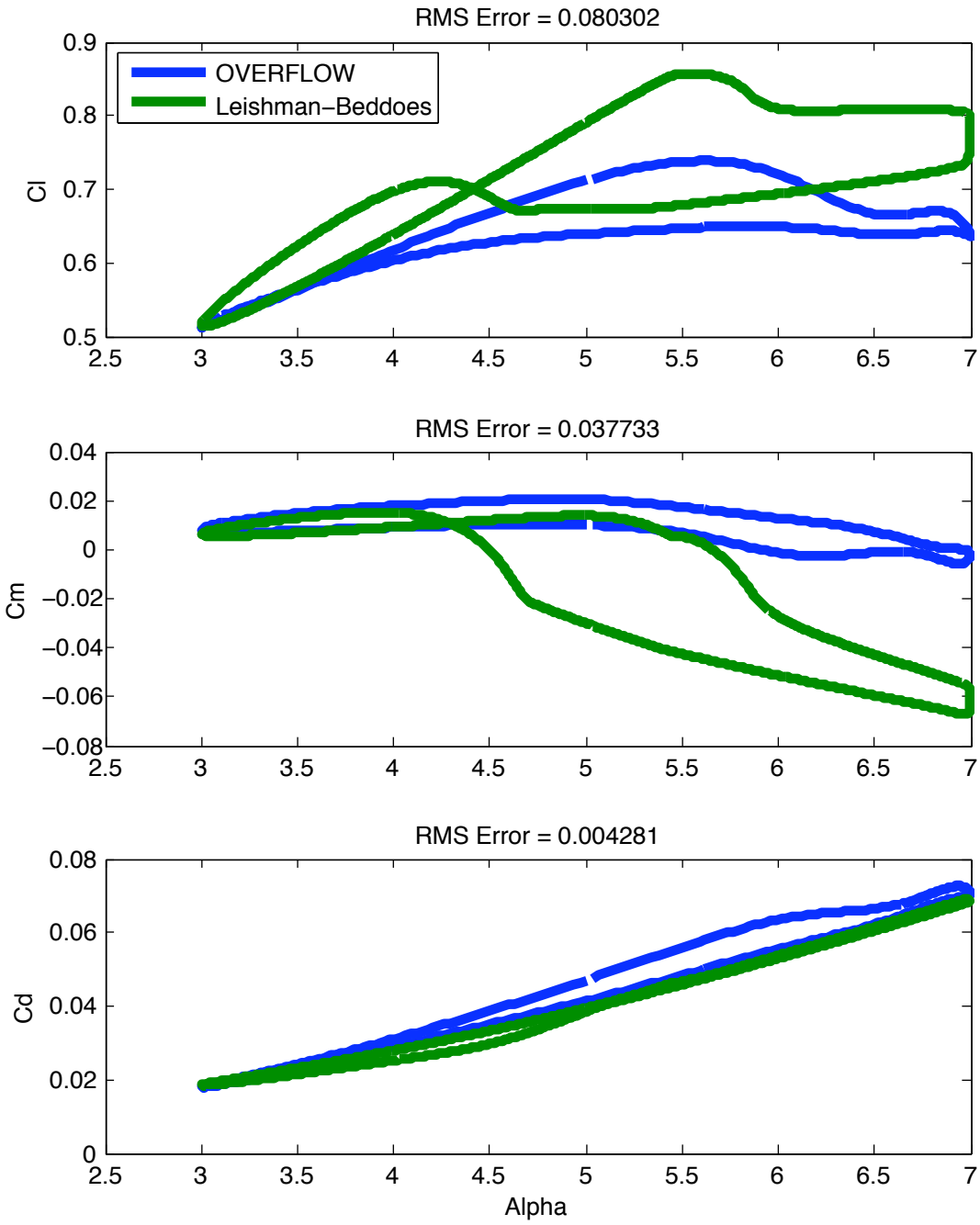

Figure 32: M=0.7, α_m=5, α_c=2, k=0.03

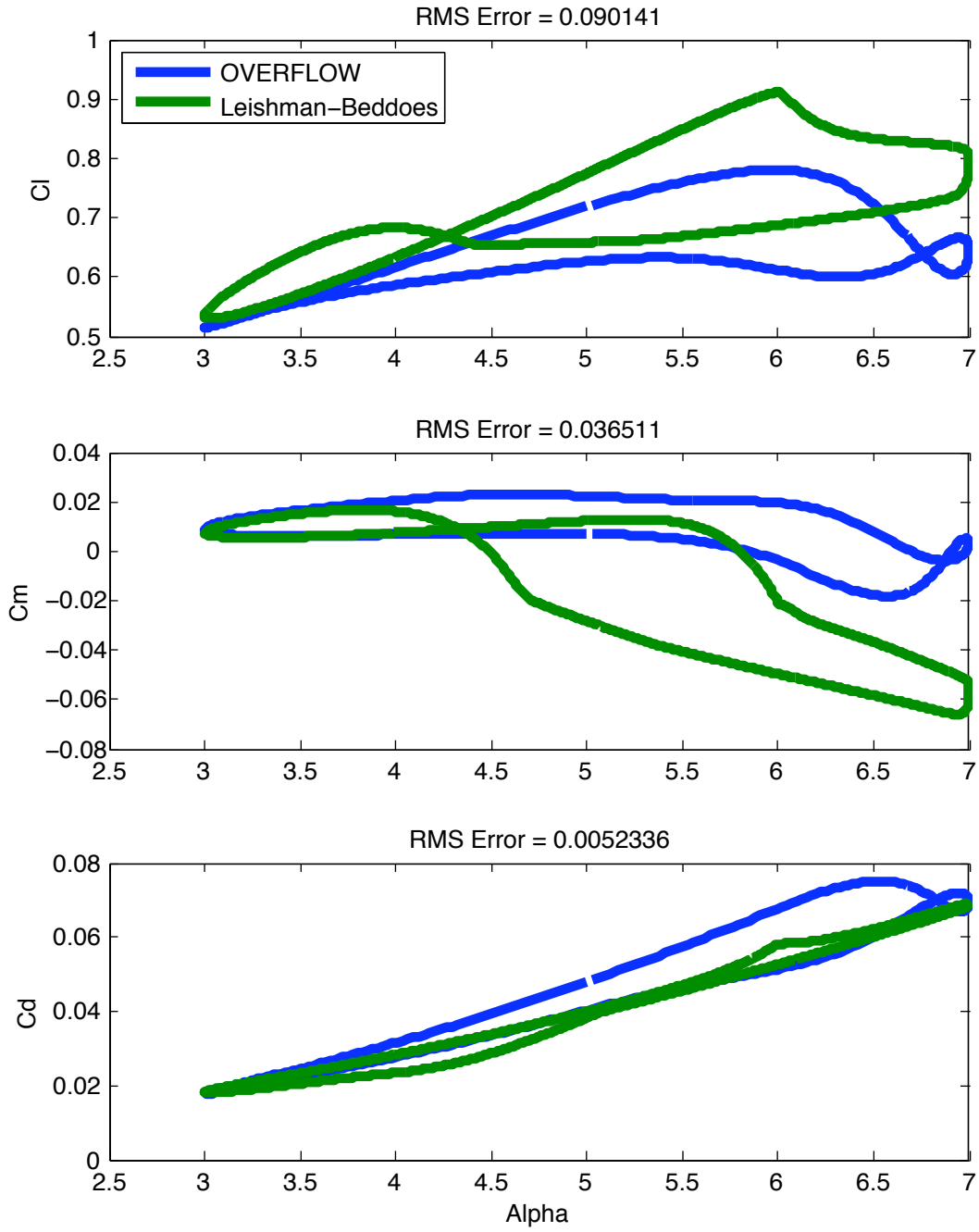

Figure 33: M=0.7, α_m=5, α_c=2, k=0.05

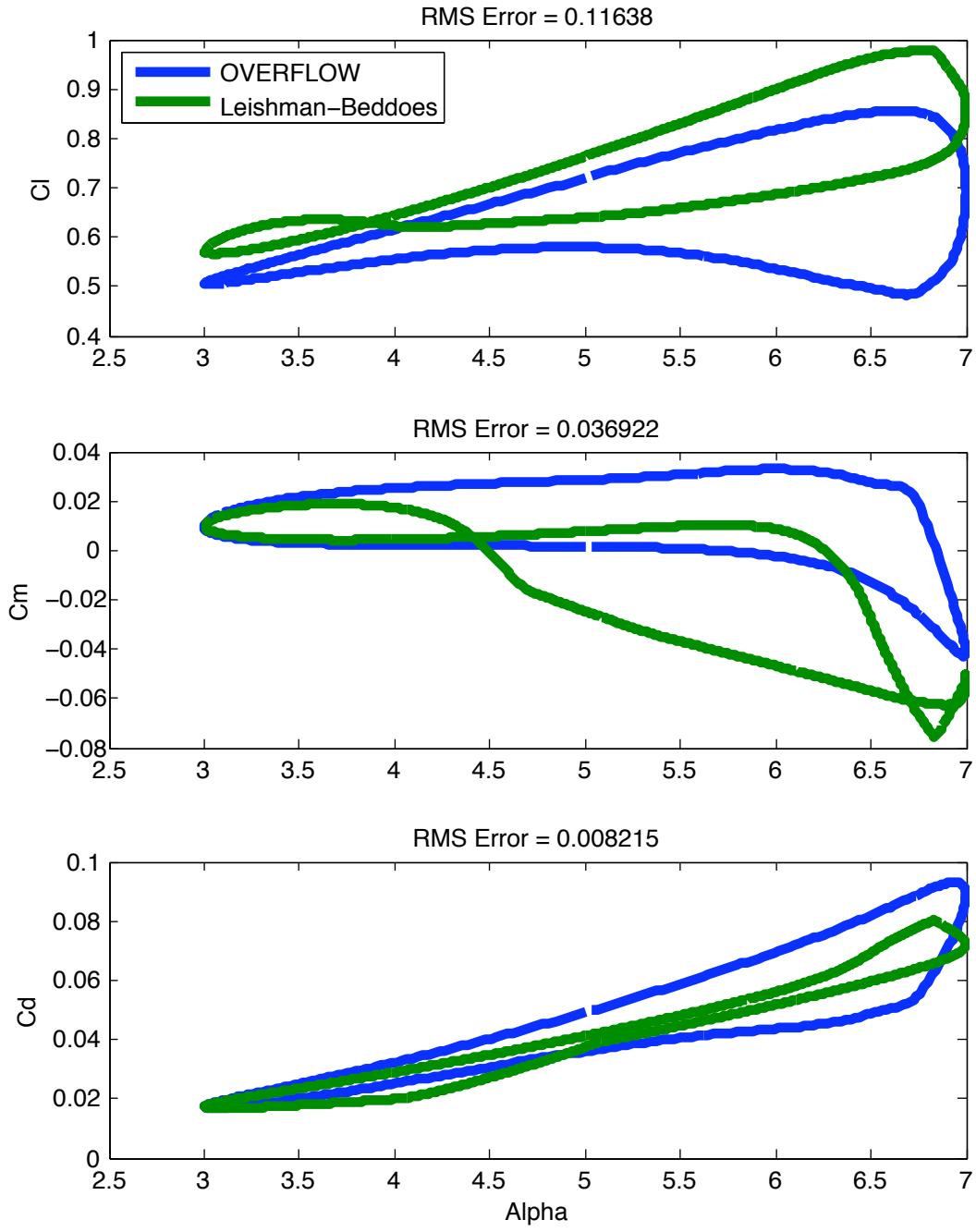

Figure 34: M=0.7, α_m=5, α_c=2, k=0.1

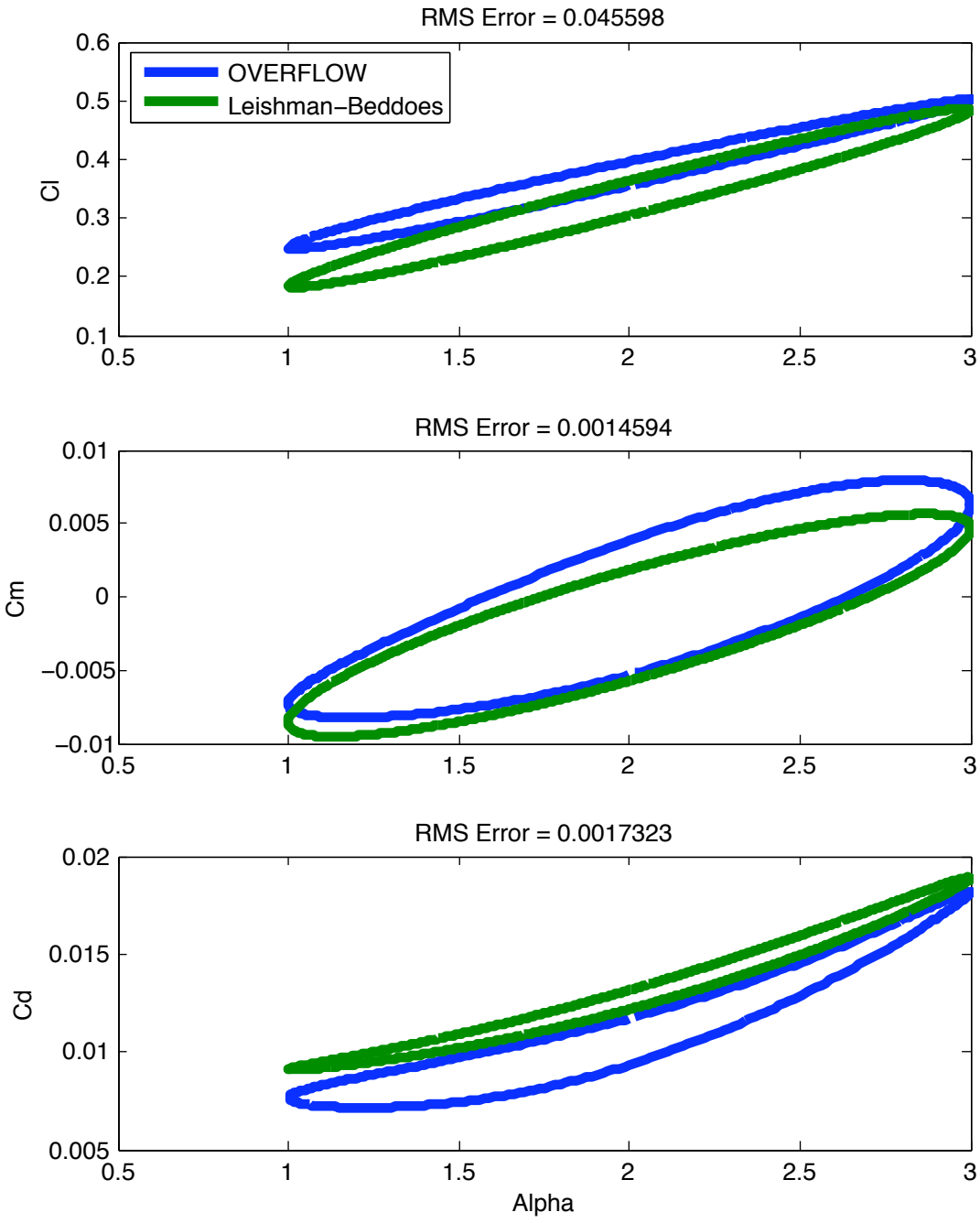

Figure 35: M=0.7, α_m=2, α_c=1, k=0.05

CHAPTER 8: MODIFICATIONS TO THE MODEL AND DISCUSSIONS

Lift Curve Slope and Zero Lift AoA

One readily apparent difference between the Leishman-Beddoes and CFD results is that the lift curve slope and zero lift angle of attack do not perfectly match. The latter should be expected from the formulation given in previous sections; the circulatory component of the normal force coefficient, $Cna*\alpha_{tot}$ does not account for an asymmetrical airfoil where the circulatory component will not be equal to zero at zero angle of attack. Eqns (1) and (41) were modified to include a shift in angle of attack due to zero lift AoA, α_0, to match the Leishman-Beddoes results with the calculated CFD results.

The zero lift angle of attack derived at each Mach number from C-81 data does not correspond very closely to that derived from CFD data. α_0 tends to be greater for the CFD results. Additionally, the lift curve slope derived from C-81 data exceeded that from CFD results and to match up required a small reduction. These changes are outlined in Table 3.

Table 3: Modifications to Cna and Zero Lift AoA

	M=0.3	M=0.4	M=0.5	M=0.6	M=0.7
Cna	0.10	0.105	0.117	0.126	0.138
α_0	0.8	0.8	0.6	0.65	0.7

These modifications affected other aspects of the C_l plot as well; this is as expected, since changing the circulatory component of the normal force will affect when and to what extent separation effects and vortex lift is triggered. One interesting change is that prior to these modifications, the peak C_l from Leishman-Beddoes and OVERFLOW were similar, but the Leishman-Beddoes predictions occurred at a slightly earlier AoA, with this gap greater for lower reduced frequencies. Thus, if the only quantity desired was a peak value of C_l, then this matching would actually be undesirable.

However, matching the zero lift AoA and lift curve slope significantly reduced average error between the two predictions. For example, for the M=0.6, α_m=7, α_c=4, k=0.03 case the RMS error was reduced from 0.14 to 0.10. Improvements for attached flow conditions were even greater. An example of typical results after this modification can be seen in the following figure for the M=0.7, k=0.05, α=5+2sin(wt) case (compare to Figure 33).

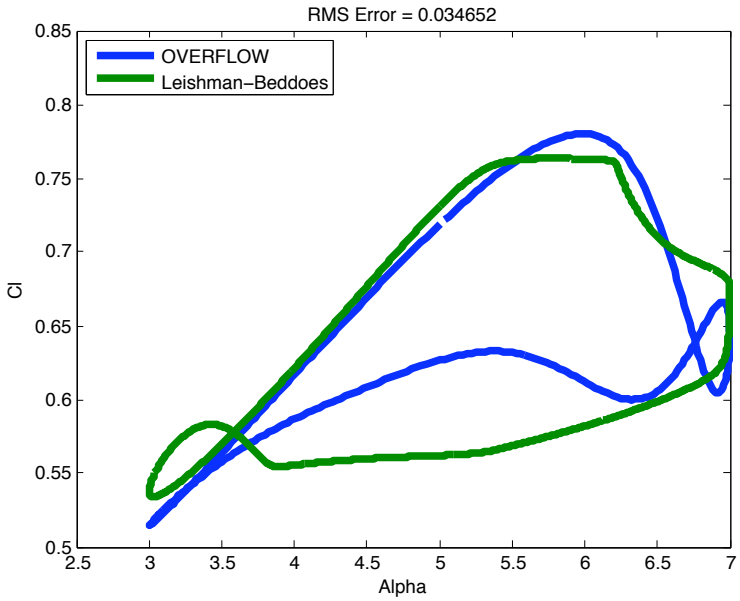

Figure 36: Lift Coefficient After Cna and α_0 Modification

This modification also improved pitching moment; by lining up the peaks of C_l more closely, the peak for the pitching moments become more aligned.

Dynamic Stall Pitching Moment Vortex Convection Time Constant, T_{vl}

With the peak normal force occurring at the approximately the same AoA for both Leishman-Beddoes and CFD results, the difference between the angle at which peak pitching moment occurs for the CFD and Leishman-Beddoes occurs is due to the time constant T_{vl}. The published values[6] for the NACA 0012 airfoil were modified to align the peak pitching moments.

	M=0.3	M=0.4	M=0.5	M=0.6	M=0.7
NACA 0012 T_{vl}	7.0	9.0	9.0	9.0	9.0
Modified T_{vl}	8.0	8.0	8.0	8.0	10.0

Table 4: T_{vl} Values

Trailing Edge Separation Time Constant, T_f

It is observed after these changes that the hysteresis for higher reduced frequencies and peak C_l for many cases undergoing deep stall conditions are smaller for the Leishman-Beddoes method than for the CFD case. Both of these may be improved by increasing the trailing edge separation time constant, T_f. This works by first delaying the lift-reducing flow separation effect by increasing the deficiency function Df, and then slowing the return to attached flow lift values post stall by the same mechanism.

However, the T_f values were not modified here. The reason is that unlike T_{vl} where altering the constant to match peak pitching moment between CFD and Leishman-Beddoes is tied to a physical event (the vortex reaching the airfoil trailing edge), here the value would be altered merely as one mechanism to make the plots appear closer. There would be no physical justification; indeed, just from the results derived in this work it is impossible to know if the lower peak lift and hysteresis found for the Leishman-Beddoes model is due to overpredicting the speed of the response from trailing edge separation and reattachment or a different mechanism.

Effective Separation Point

The ability of the curve fit given by eqn. (35) to model the effective separation point has also been studied across the range of Mach numbers. In the following figures the effective separation point calculated using the C-81 data, f, is compared to the derived curve fit eqn. (35) and plotted against airfoil angle of attack.

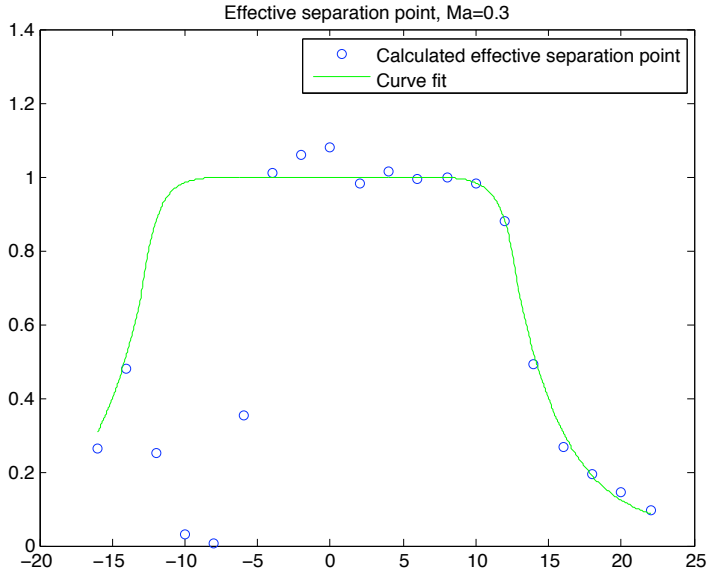

Figure 37: Effective Separation Point, M=0.3

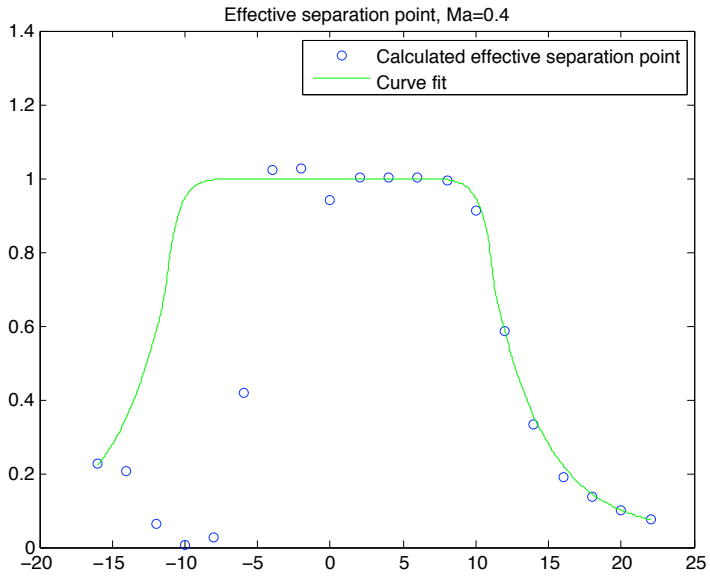

Figure 38: Effective Separation Point, M=0.4

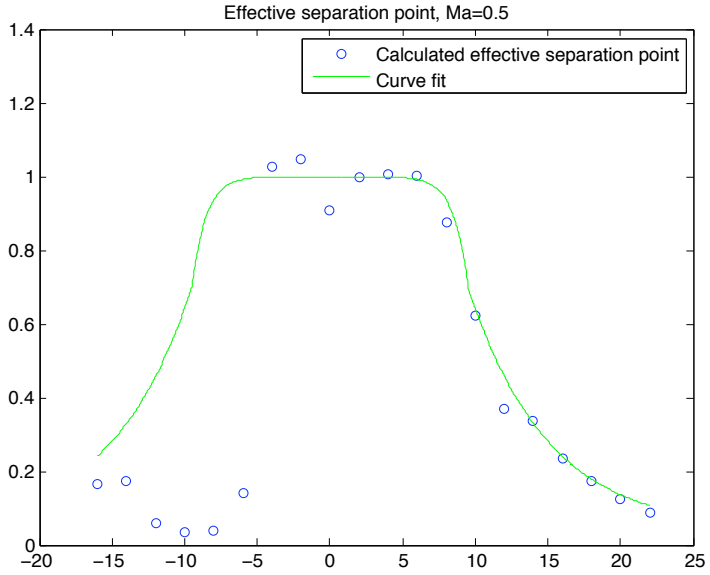

Figure 39: Effective Separation Point, M=0.5

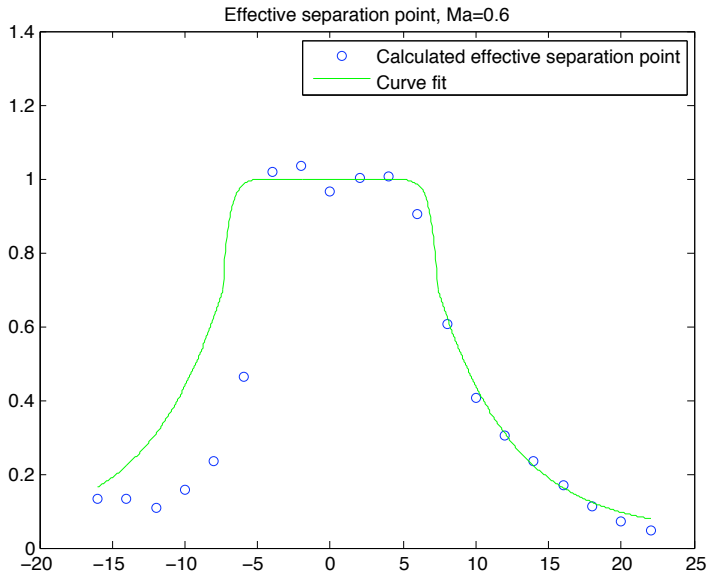

Figure 40: Effective Separation Point, M=0.6

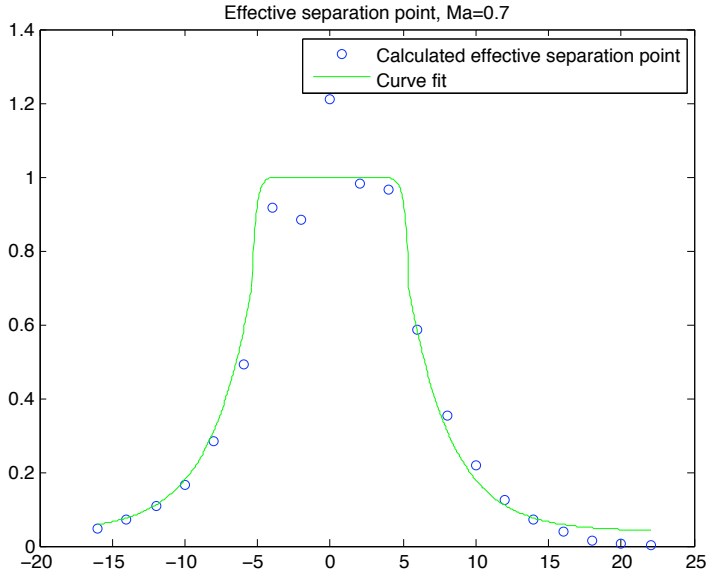

Figure 41: Effective Separation Point, M=0.7

These curve fits were based on data for positive AoA's and from these figures, good correlation between the calculated separation point and the curve fit

for positive angles of attack is evident for all Mach numbers. However, correlation at negative AoA is often poor.

The calculated separation point is very noisy at negative angle of attacks and the curve fit tends to overestimate the extent of flow separation. However, this noise appears to be dampened with increasing Mach number. As such, the error between the calculated and modeled separation point decreases with increasing Mach number, and there is actually very good correlation at both positive and negative angles for the M=0.7 case.

If the model for the separation point differed greatly from the calculated values, one solution would be to use a table lookup and interpolation to calculate f within the program instead of using eqn. (35). This is the method used by the code Aerodyn, with good success. However, since the Leishman-Beddoes method has proved accurate at low Mach numbers, and the error appears to lessen with increasing Mach number, this step appears unnecessary and would only act to increase computational cost. Also, since there does not seem to be a discernable trend at negative angle of attack for some of the cases (particularly the M=0.3 case) there is some question as to whether these results would be reproducible and are physically representative, as opposed to being highly test dependent and noisy. As such, the utility of using an interpolation between two questionable values instead of using a curve fit based on more reliable data in a different region is questionable.

Center of Pressure

In the Leishman-Beddoes method, the center of pressure for calculation of the pitching moment from the normal force is provided by a curve fit, given in eqn (45) and reprinted below.

$$C_m^f = \left(k0 + k1 * (1 - fr') + k2 * \sin(\pi * fr'^m)\right) * C_n^f + C_m^{ai} + C_m^{qi} + C_{m0} - \frac{\pi * c}{8 * U * \beta} * (\dot{\alpha} - X5)$$

f, the separation point, is derived from a curve fit of effective separation point from static data as discussed earlier and described in more detail in Appendix A. k0, k1, and k2 are Mach number dependent parameters derived from applying curve fits to static data and are also discussed in Appendix A. The coefficient m, however tends to be a built in feature of the Leishman-Beddoes program and is usually taken to be equal to 2, although is sometimes taken to be 1 or 0.5.

Since the quantity being multiplied by the normal force is a curve fit attempting to satisfy the relation

$$\frac{C_m - C_{m0}}{C_n} = k0 + k1 * (1 - f) + k2 * \sin(\pi * f^m)$$

where $(C_m - C_{m0})/C_n$ is the center of pressure, the ability of this equation to adequately model the center of pressure is studied here.

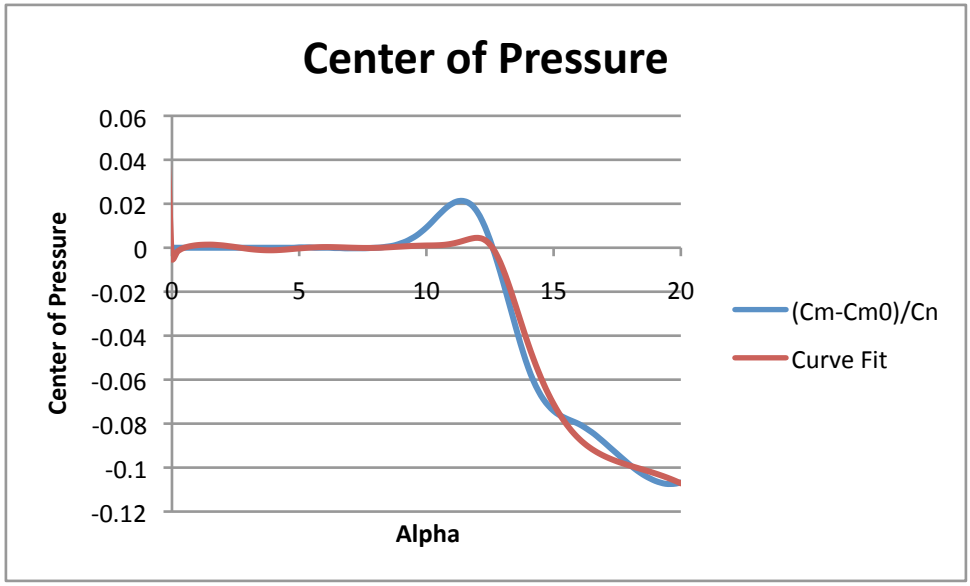

Figure 42: Center of Pressure, M=0.3, m=2

In general, the curve fit with m=2 does a fair job representing the center of pressure derived from the C-81 data. The greatest variation for the M=0.3 case is in the 9-12 degree range. This variation is slightly greater if m is taken to be 1 or 0.5.

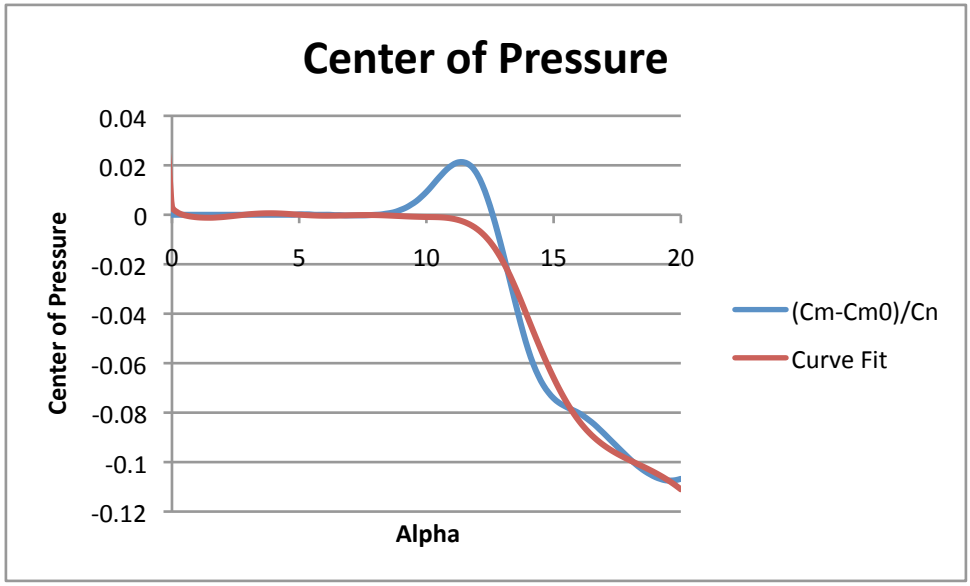

Figure 43: Center of Pressure, M=0.3, m=1

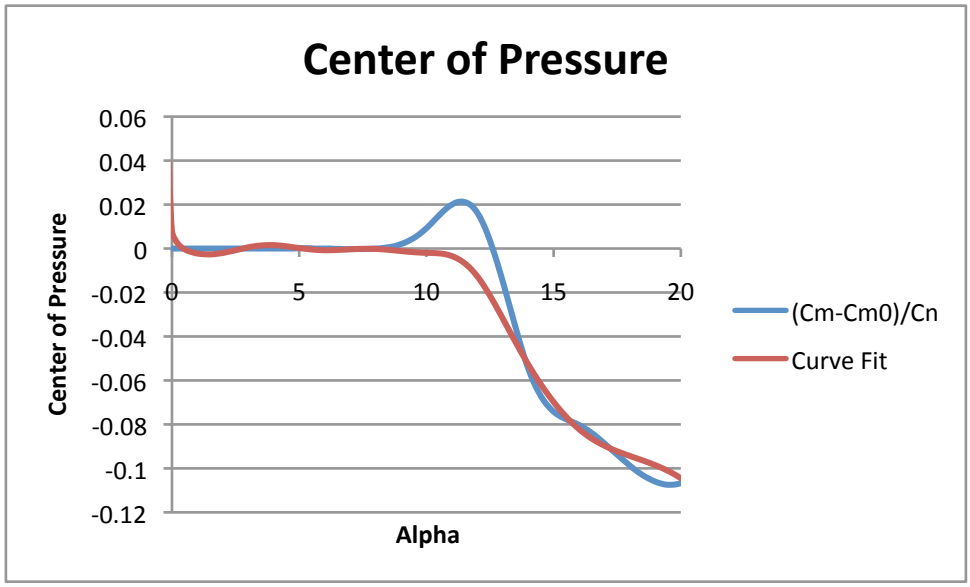

Figure 44: Center of Pressure, M=0.3, m=0.5

The center of pressure in the region around 10 degrees may be better modeled by increasing the value of m, but this causes more oscillations and

subsequent decreased accuracy in other regions, most notably the low angle of attack range.

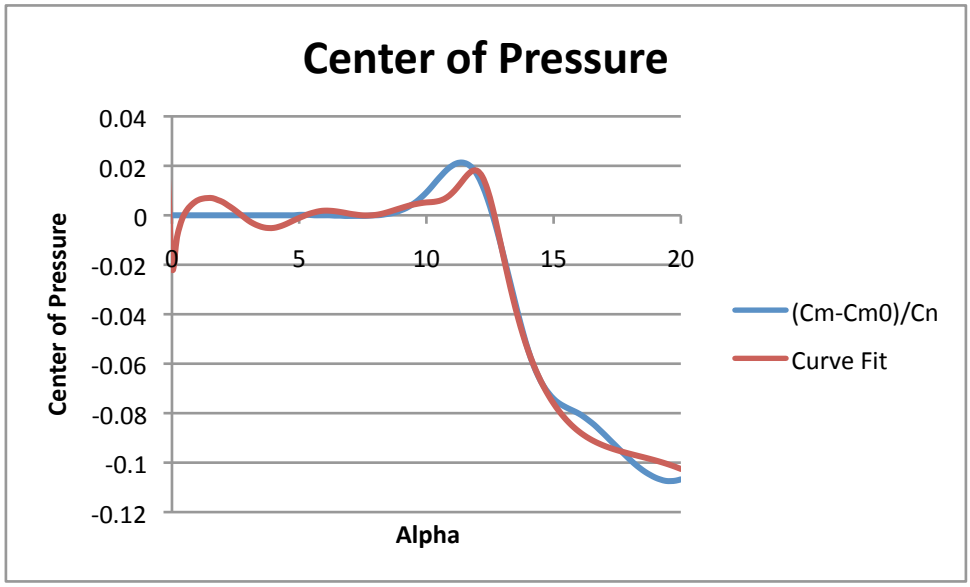

Figure 45: Center of Pressure, M=0.3, m=4

Unless one wants to add yet another Mach dependent parameter to be included in the Leishman-Beddoes method, a value of m must be chosen that accurately models the center of pressure across the range of Mach numbers. m=2 provides a reasonable interpretation of the center of pressure, as shown in the following figures.

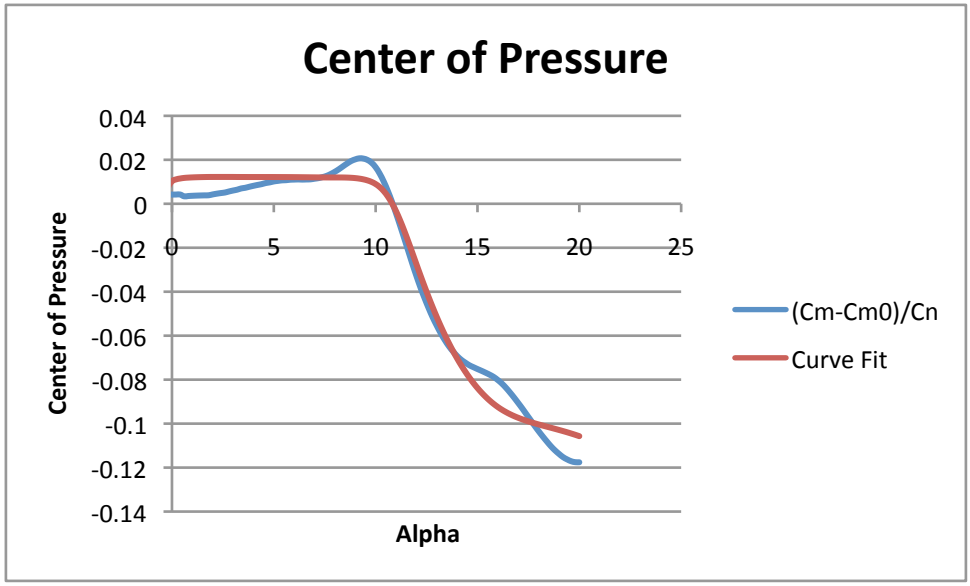

Figure 46: Center of Pressure, M=0.4, m=2

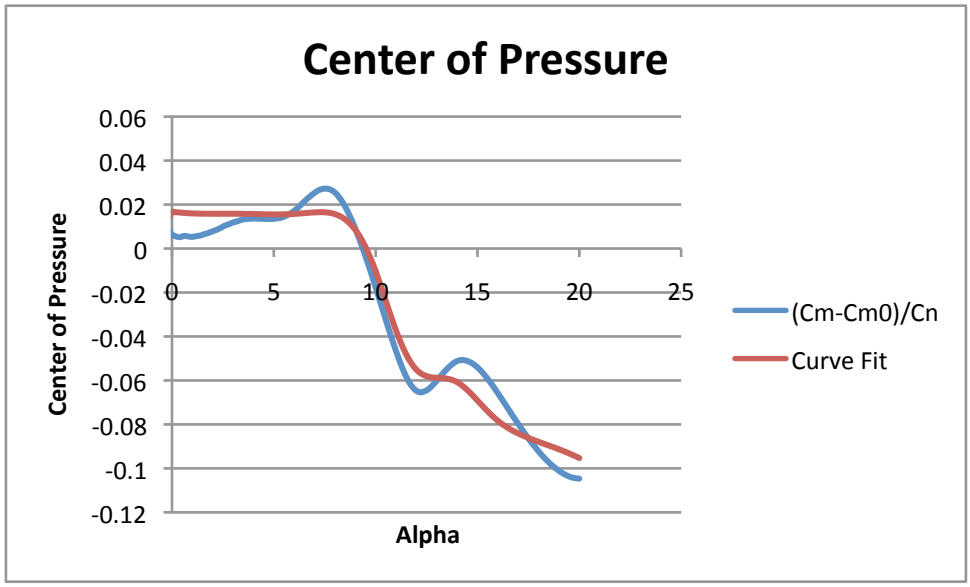

Figure 47: Center of Pressure, M=0.5, m=2

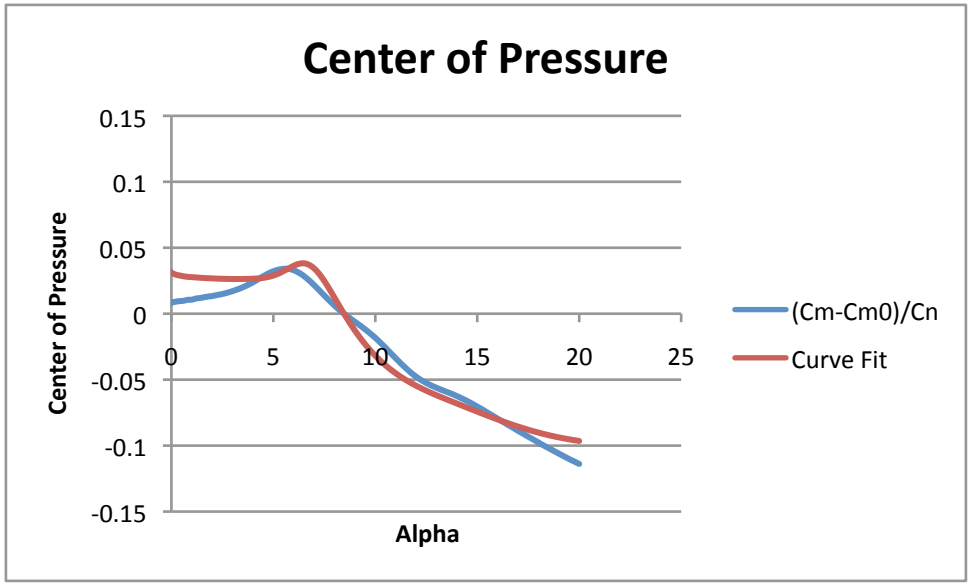

Figure 48: Center of Pressure, M=0.6, m=2

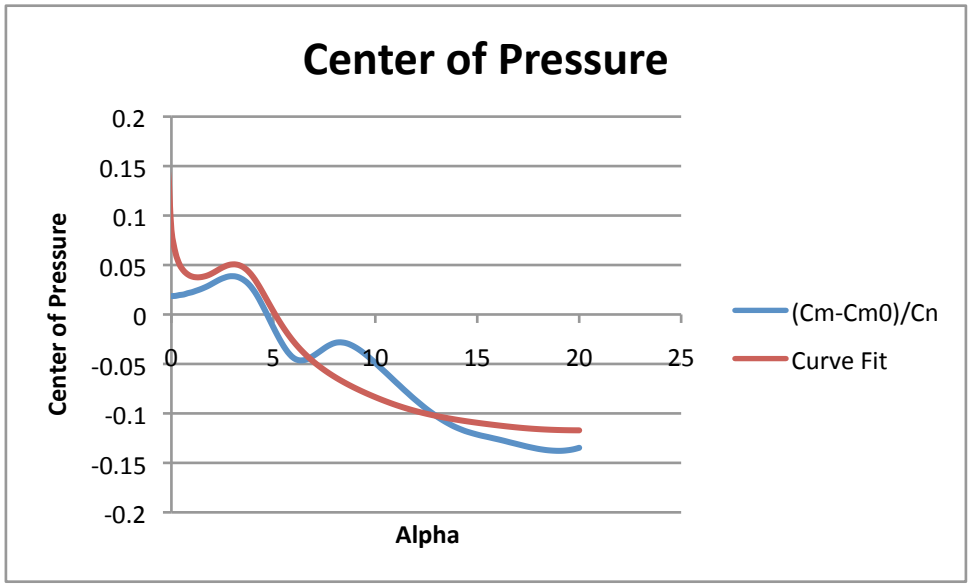

Figure 49: Center of Pressure, M=0.7, m=2

Pitching moment was studied across the range of Mach numbers in regions where flow was not undergoing deep dynamic stall, and it was found that switching m to a value other than 2 could provide some benefit in certain cases,

but no value was found to be better in a general sense and thus in the interest of generality for the model (and the fact that m=2 is used for most other airfoils) it was decided to maintain m=2.

Indicial Constants

There are several constants that scale or are used in the indicial functions on which the Leishman-Beddoes method is built (i.e. A1, A2, b1, b2…). For example, the indicial response function for circulatory loading is given by

$$\phi_{n\alpha}^{C}(S) = 1 - A1 * e^{-b1*\beta^2*S} - A2 * e^{-b2*\beta^2*S} \tag{62}$$

where A1 + A2 = 1 and b1 and b2 are greater than zero. Leishman and Beddoes developed values of A1=0.3, A2=0.7, b1=0.14, and b2=0.53 based on best fit to theoretical indicial functions, and these values have served well in the cases where the Leishman-Beddoes method has been extensively tested. To see if these constants provided ideal results even at a higher Mach number, a case at M=0.7 was studied. Lift for a case at high reduced frequency but attached flow was chosen. These conditions were selected because at high reduced frequency the effect of the deficiency functions will be greater (thus increasing the effect of A1, A2…) and any error involved will not be drowned out by other sources from flow separation and vortex formation. A script was written to automatically provide a search for optimal constants for this test case by cycling through

thousands of combinations of A1, A2, etc. and calculating an RMS error for each combination.

This procedure yielded slightly improved results; RMS error for the C_l hysteresis loop dropped from about 0.006 to 0.0047. Given that the base values provide good results and the optimized values offer only a slight improvement in accuracy, there is no reason to conclude that the indicial coefficients are unsatisfactory in any way, even at the higher Mach numbers.

A sensitivity analysis was also performed for these parameters. For the values A1, A2, A3, and A4, these values were modified by ±0.1 with the constraint that A1+A2=1 and A3+A4=1. For b1, b2, b3, b4, and b5, the base value was tested at ±10%. The resulting rms errors are displayed in Tables 5-7. For Table 5, rms error is based on the coefficient of lift for M=0.7, k=0.1, α_m=2, α_c=1. Table 6 is based on the same test conditions, but utilizes the rms error for pitching moment coefficient. Finally, Table 7 displays results for pitching moment using test conditions M=0.7, k=0.1, α_m=2, α_c=2. These conditions and airload variables were chosen to allow maximum effect from the selected indicial variable with the smallest possible contribution to error from other sources.

As can be seen in the tables, reductions in rms error, where they occur, are typically small. Furthermore, as before it is difficult to assess whether the reductions in rms error are due to an improvement of the fit of the indicial functions at high Mach number, or whether it is inadvertently correcting a different source of error. Since a modified set of indicial coefficients did not

provide better results across the range of different test conditions, the latter is indicated. This provides further credence to maintaining the base values derived by Leishman and Beddoes.

Table 5: Sensitivity of A1, A2, b1, and b2

	base	A1+0.1	A2+0.1	b1+10%	b1-10%	b2+10%	b2-10%
A1	0.3	0.4	0.2	0.3	0.3	0.3	0.3
A2	0.7	0.6	0.8	0.7	0.7	0.7	0.7
b1	0.14	0.14	0.14	0.154	0.126	0.14	0.14
b2	0.53	0.53	0.53	0.53	0.53	0.583	0.477
rms error	0.0061	0.0098	0.0055	0.0061	0.0062	0.0051	0.0077

Table 6: Sensitivity of A3, A4, b3, and b4

	base	A3+0.1	A4+0.1	b3+10%	b3-10%	b4+10%	b4-10%
A3	1.5	1.6	1.4	1.5	1.5	1.5	1.5
A4	-0.5	-0.6	-0.4	-0.5	-0.5	-0.5	-0.5
b3	0.25	0.25	0.25	0.275	0.225	0.25	0.25
b4	0.1	0.1	0.1	0.1	0.1	0.11	0.09
rms error	0.0014	0.0024	0.0012	0.0022	0.0012	0.0012	0.0023

Table 7: Sensitivity of b5

	base	b5+10%	b5-10%
A5	1	1	1
b5	0.5	0.55	0.45
rms error	0.0022	0.0022	0.0023

J.D. Baeder has studied the computation of indicial response functions from CFD data at a range of Mach numbers.[15],[16] This strategy was undertaken because indicial responses cannot be determined through experimentation and analytical solutions do not exist for unsteady compressible flow. Baeder utilized a Navier-Stokes CFD solver and was able to decouple angle of attack time history and pitch rate time history, allowing isolation of the response of a particular step change.

In this way Baeder determined the indicial response and compared to results from analytical methods. He found very strong correlation at lower Mach numbers. At a higher Mach number of 0.8, a modest amount of error was present, which is as expected since the analytical solution was derived for an incompressible flow. The lack of inclusion of compressibility effects in the exact analytical solution should not be a problem in the current analysis, however. Leishman derived the indicial coefficients through a semi-empirical method in which he analyzed data in the frequency domain, which may then be related back to the indicial response.[11]

Post Modification Results and Discussion

Here, the focus will be primarily on deep stall cases; after the modification of Cna and α_0 correlation for attached flow conditions was very good across the range of Mach numbers.

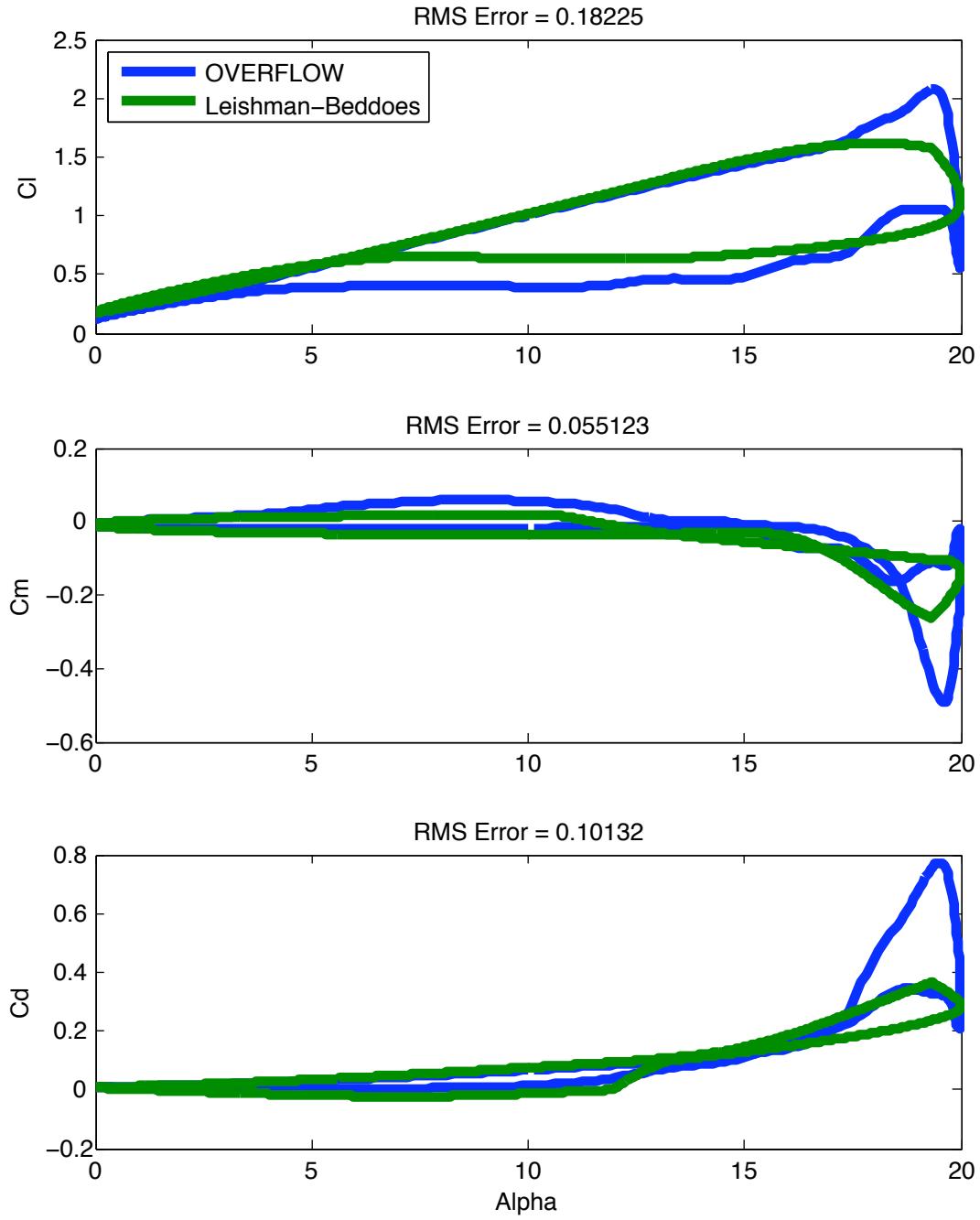

Figure 50: Post Modification, M=0.3, α_m=10, α_c=10, k=0.1

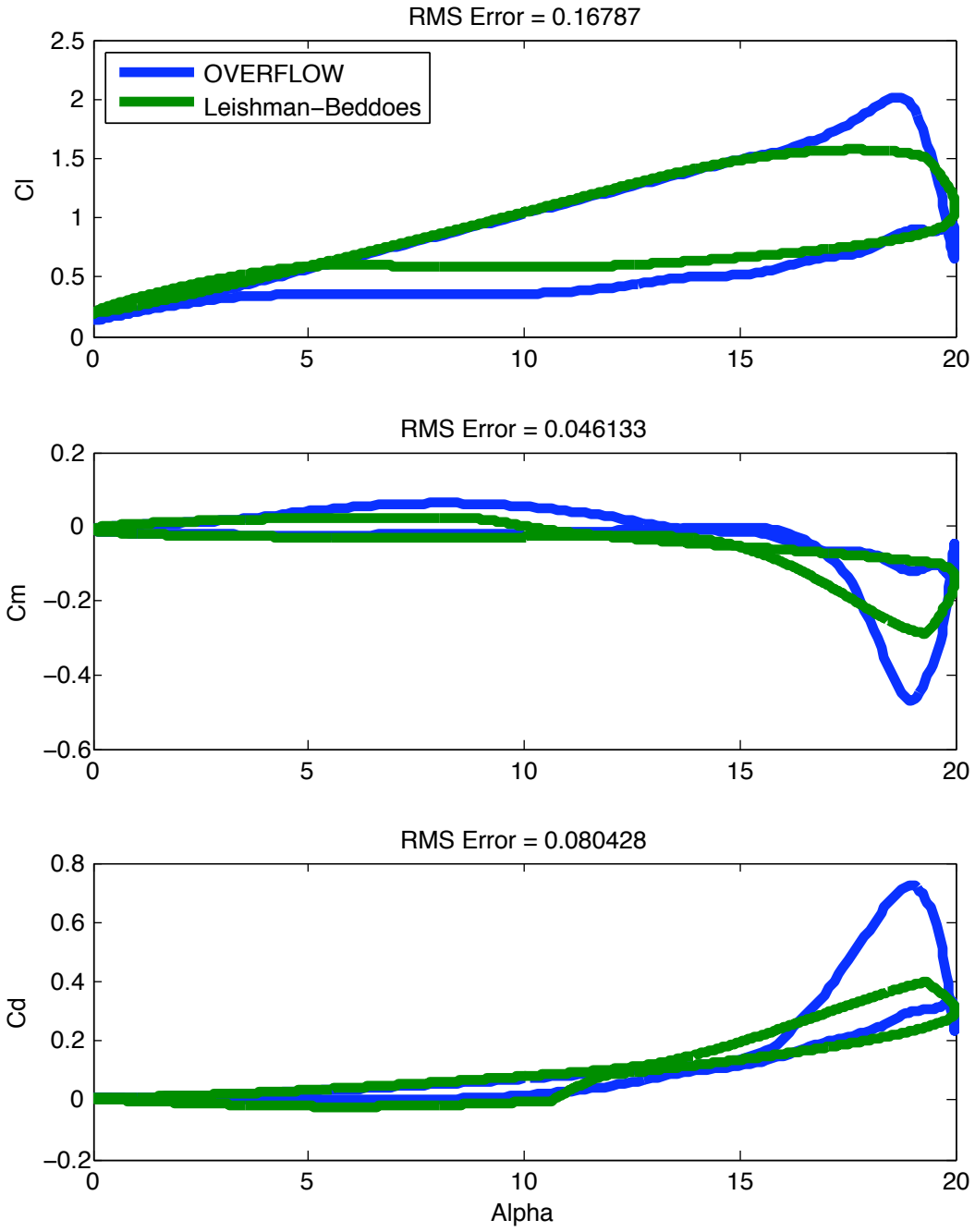

Figure 51: Post Modification, M=0.4, α_m=10, α_c=10, k=0.1

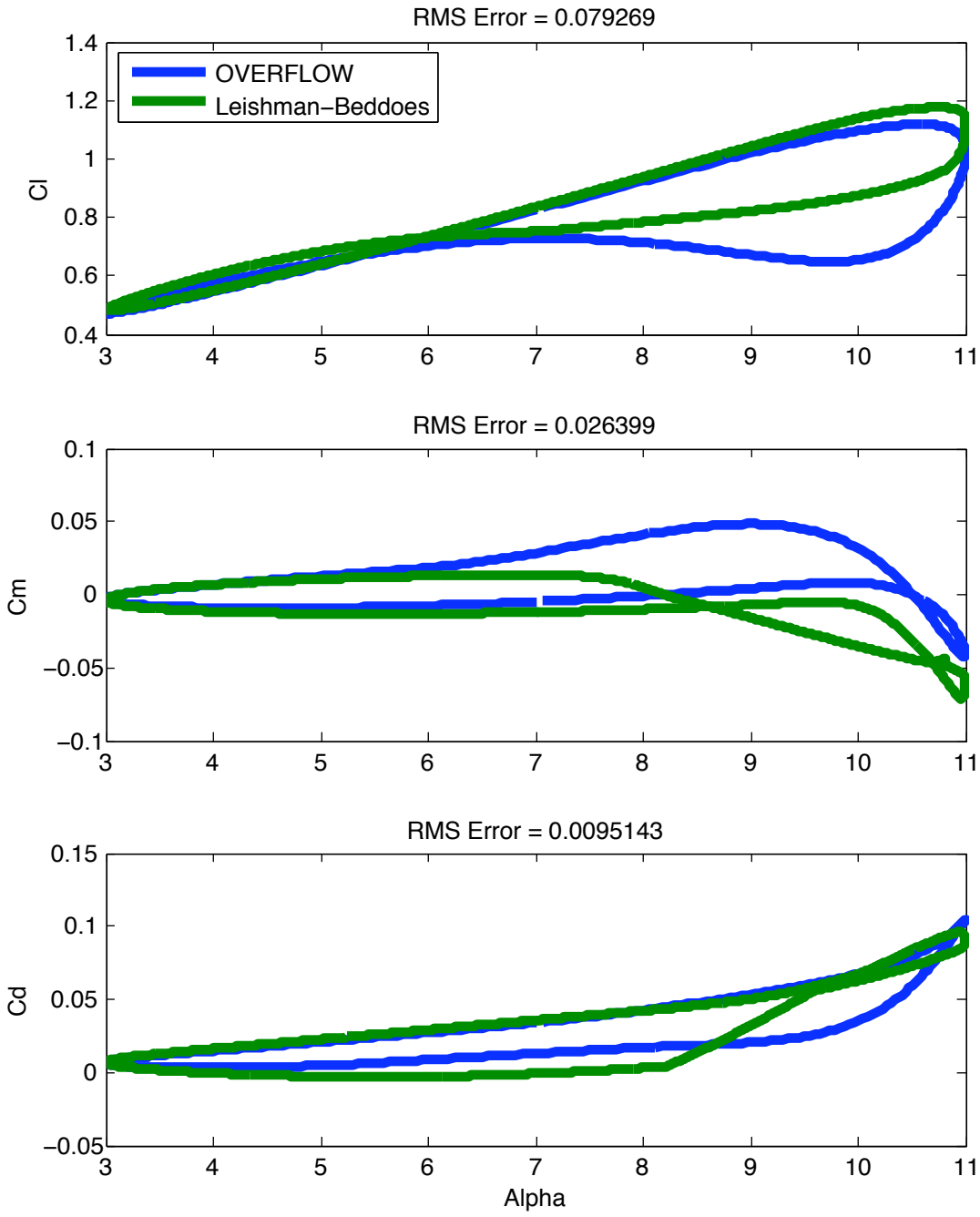

Figure 52: Post Modification, M=0.5, α_m=7, α_c=4, k=0.1

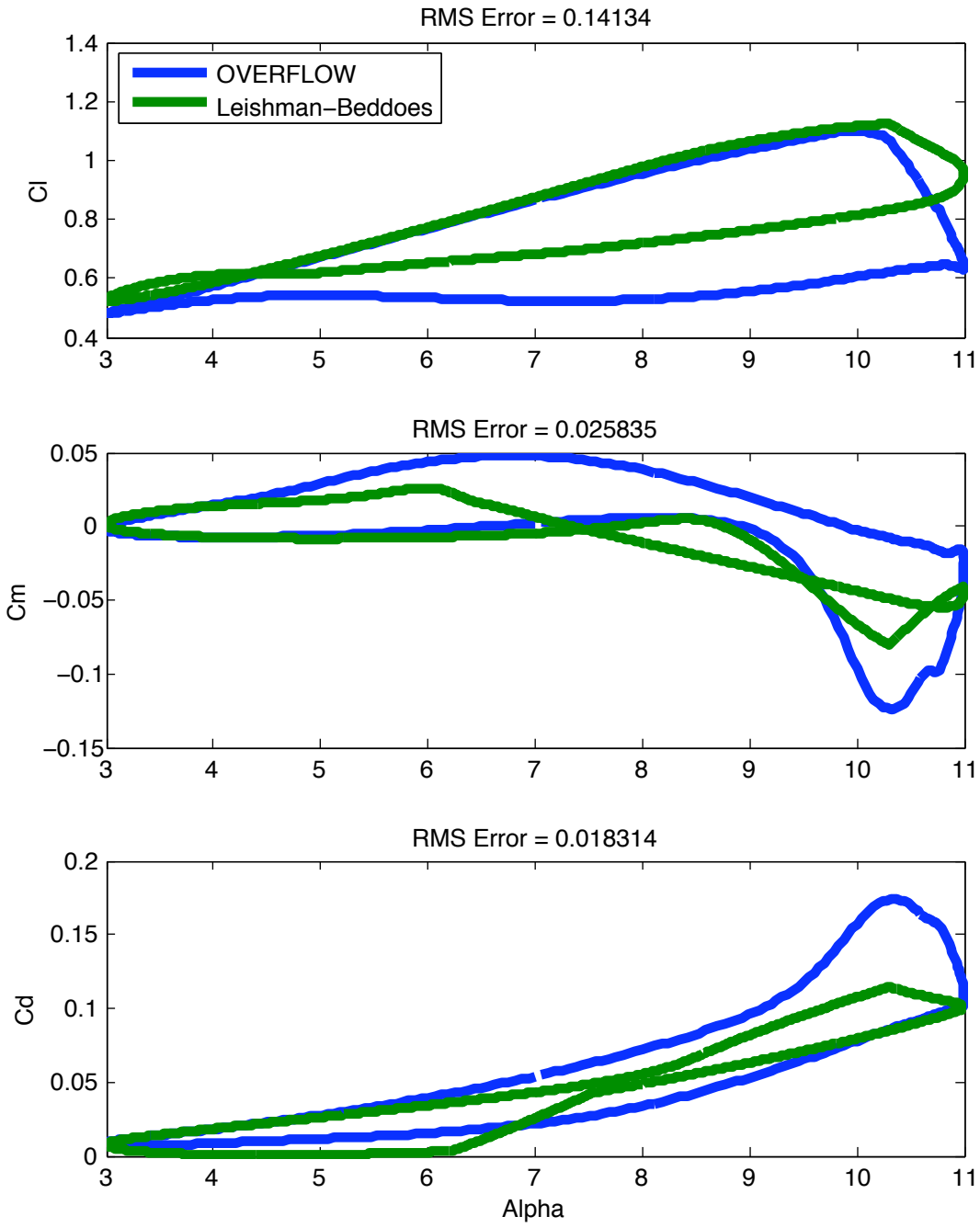

Figure 53: Post Modification, M=0.6, α_m=7, α_c=4, k=0.1

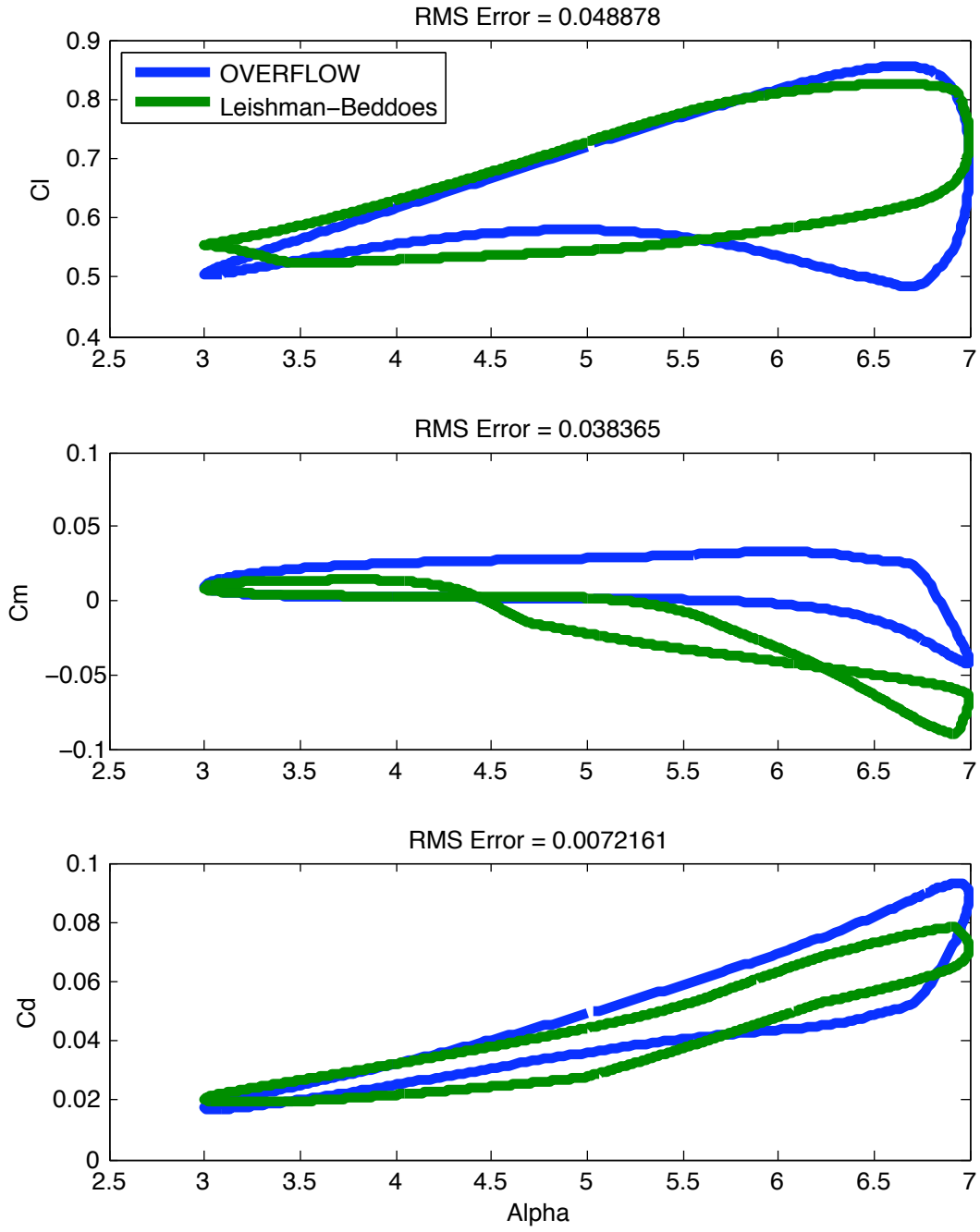

Figure 54: Post Modification, M=0.7, α_m=5, α_c=2, k=0.1

From examining these and other results, it is evident that lift predictions are actually quite good even for high Mach numbers. As discussed previously, the lift on the downstroke is typically too large and occasionally peak lift is not very well modeled, but in general the predictions are good and of value. This is actually a slightly surprising result when flow fields are studied; the scheme by which the Leishman-Beddoes method predicts airloads under dynamic stall conditions is to model a strong shedding vortex moving down the airfoil. This appears to be the correct flow physics for lower Mach numbers, as evidenced in Figure 55. However, at high Mach numbers the existence, shedding, and travel downstream of a strong vortex is not immediately apparent in flow visualizations, as shown in Figure 56. However, the same equations provide valuable results.

In the flow visualizations, the streamlines are colored by vorticity magnitude.

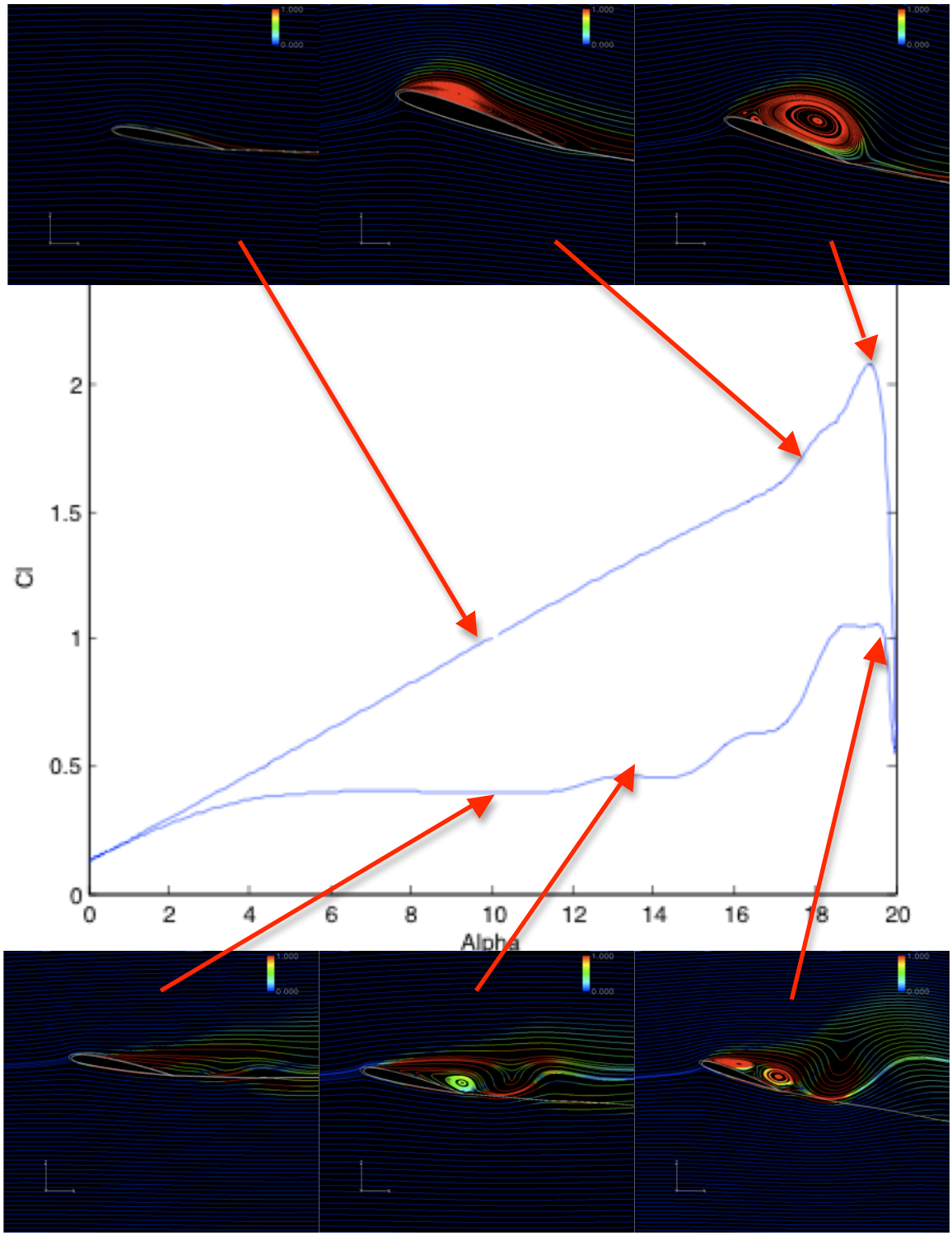

Figure 55: Flow Development, M=0.3, α_m=10, α_c=10, k=0.1

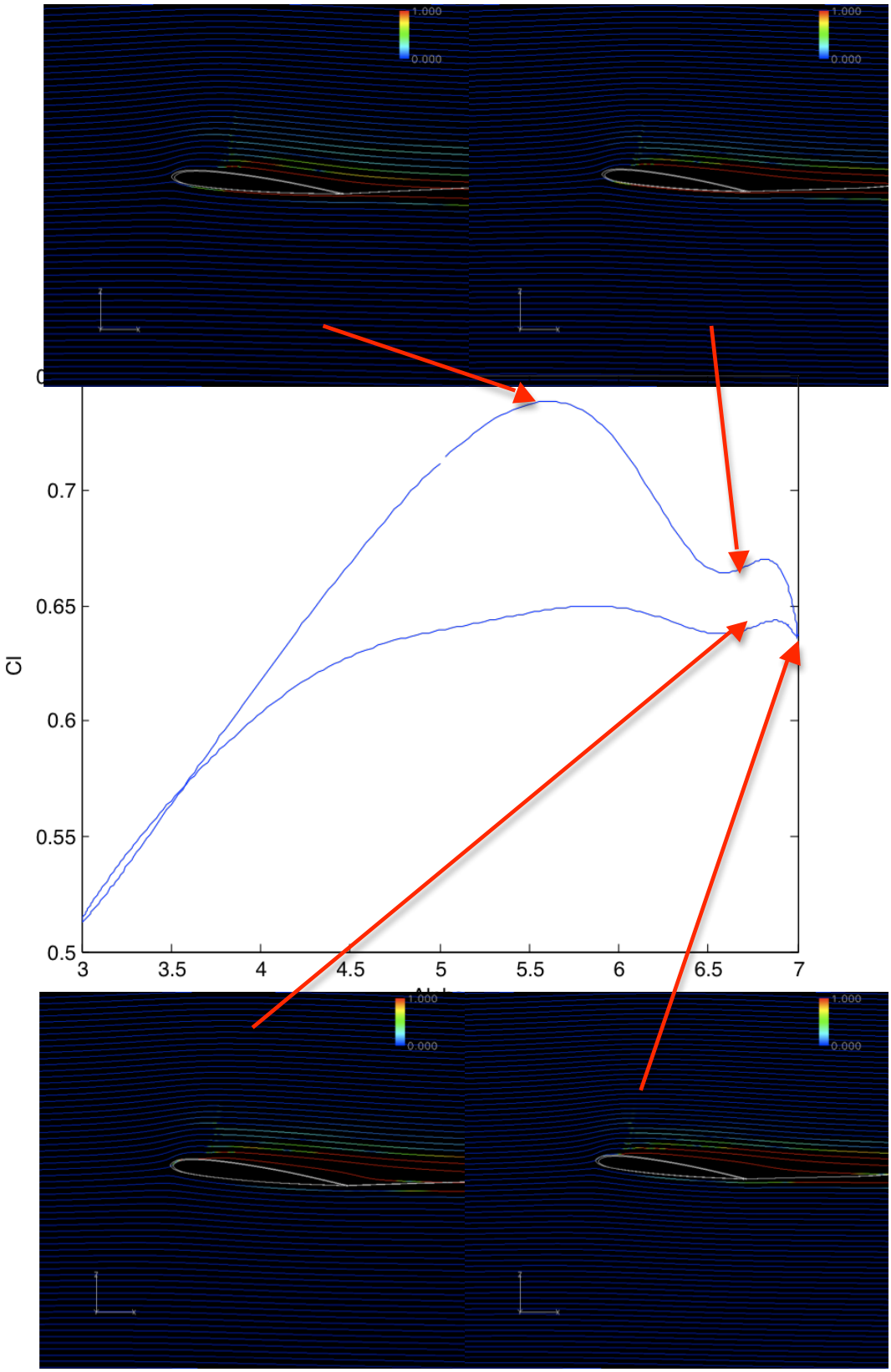

Figure 56: Flow Development, M=0.7, α_m=5, α_c=2, k=0.03

Pitching moment predictions were not quite as good as lift, but still of value. At lower Mach numbers, peak moment predicted by the Leishman-Beddoes method are smaller than those provided by OVERFLOW. However, as discussed in the section on the CFD model, it is unclear how much of this error is due to the Leishman-Beddoes model and how much is from the CFD result.

At higher Mach numbers and higher angle of attack, the Leishman-Beddoes method begins to predict much greater moments than the OVERFLOW results. This has been found to not be the result of the vortex contribution, but rather the center of pressure prediction. In this region, the pitching moment is dominated by the following contribution:

$$C_m = \left(k0 + k1 * (1 - f) + k2 * \sin\left(\pi * f^m\right)\right) * C_n^f$$

Here, the entire quantity in parenthesis is the center of pressure, as discussed earlier. Figures 57-59 illustrate why the pitching moment grows past the CFD prediction.

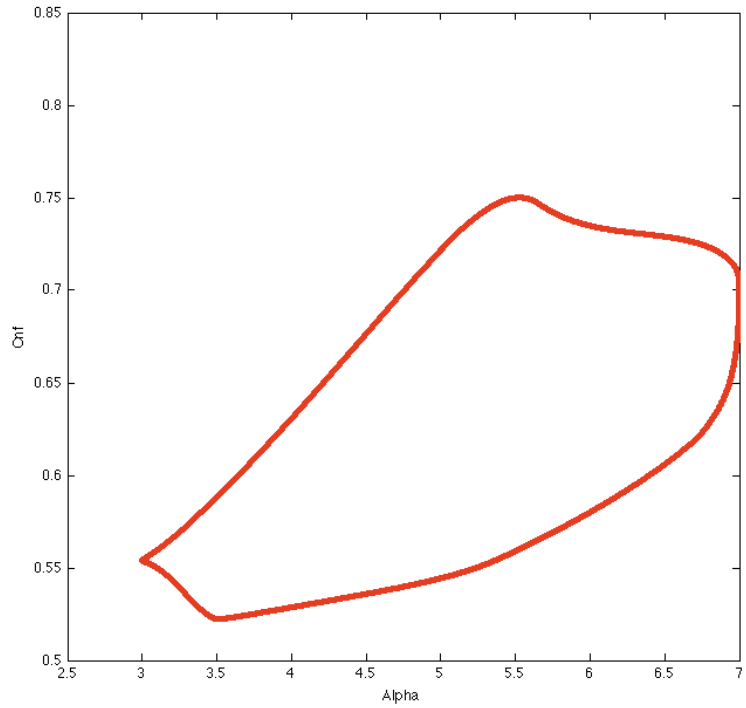

Figure 57: Normal Force including Separation, Cnf, M=0.7, α_m=5, α_c=2, k=0.1

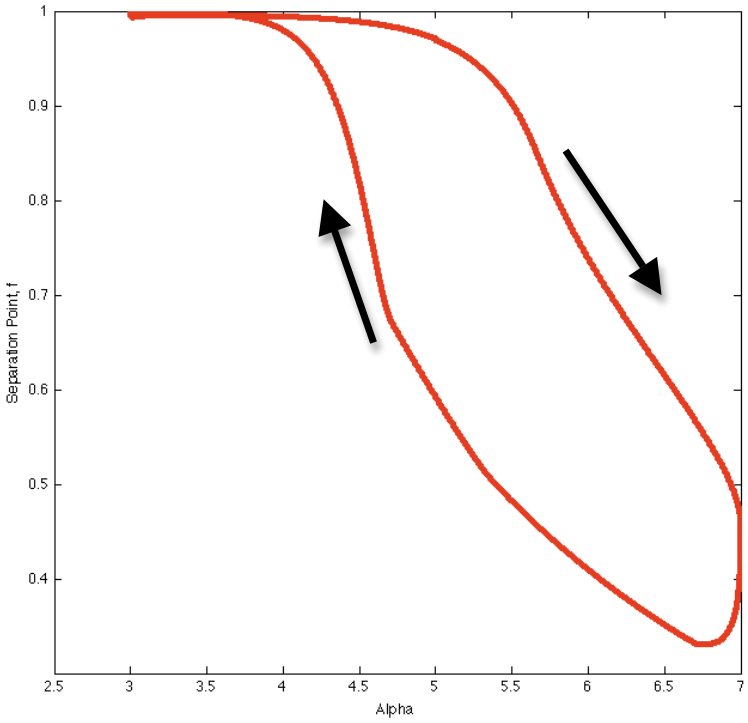

Figure 58: Separation Point, f, M=0.7, α_m=5, α_c=2, k=0.1

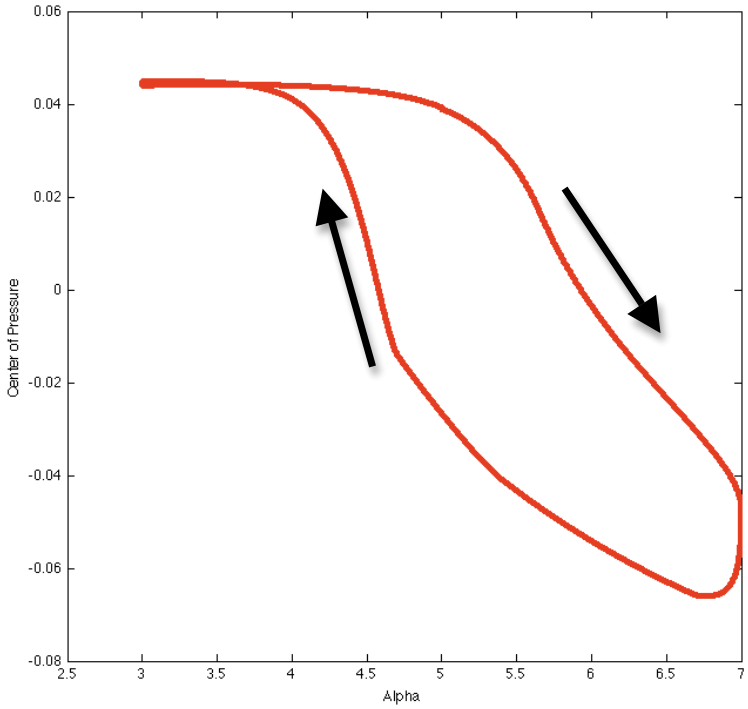

Figure 59: Center of Pressure, M=0.7, α_m=5, α_c=2, k=0.1

From Figures 57-59 we can see that at the higher angle of attack, the large value for Cnf is multiplied by a negative center of pressure growing in magnitude, resulting in a large negative pitching moment. Since the overall prediction for lift is good, we may assume that there likely is not a large error in Cnf. Thus, the center of pressure calculated by Leishman-Beddoes does not correspond well to the CFD results.

The parameters k0, k1, and k2 may be modified to improve pitching moment results. However, Figure 49 indicates that the values of k0, k1, and k2 used cause a good prediction of static center of pressure for varying angle of attack, particularly for the range of angle of attack involved in this particular case. As such, the CFD results point to a possible change in center of pressure from

unsteady loads in high speed flows that is not well modeled by the static center of pressure curve fit.

CHAPTER 9: CONCLUSIONS AND RECOMMENDATIONS

The Leishman-Beddoes method is a robust method able to provide good results even at higher Mach numbers. Lift coefficient has been shown to be accurately modeled across the range of Mach numbers, although under certain conditions there is a small to modest discrepancy in the peak lift and/or angle of attack at which peak lift occurs.

Pitching moment predictions have not been quite as good as lift, but are still of value. However, at high Mach number and high angle of attack the Leishman-Beddoes method begins to overpredict pitching moment contributions from the normal force due to circulatory and separated flow contributions. Since for these conditions the lift predictions appear to be fairly accurate, it is hypothesized that this is due to an inability of the Leishman-Beddoes method to model the center of pressure for high velocity unsteady flows.

It is found that the predictions for the Leishman-Beddoes method are highly sensitive to the input parameters and the experimental data upon which these parameters are derived. As such, when the Leishman-Beddoes method is implemented it is important to compare total airfoil performance across the range of conditions for which the method will be used for analysis to any available test data. If the Leishman-Beddoes method is utilized for predictions for flow conditions where test data is unavailable, a level of uncertainty in the results should be understood. In this work, it is found that the C-81 data disagreed with computational results regarding the lift curve slope and zero lift angle of attack.

These two parameters have a large impact in the subsystems of the Leishman-Beddoes method and affect when and to what extent flow separation and vortex effects take place.

There are several areas where future work may build upon this thesis. The exact cause of the inability of the method to model the center of pressure at high angle of attack and high Mach number is important to understand to improve moment predictions in this region; then, perhaps a physically representative model may be developed to improve predictions. Another area of future work would be to either determine whether there is error in peak drag and moment values in the experimental data or improve the current or develop a new CFD model that reliably reproduces experimental values of moment and drag. Until this step is accomplished, it cannot be said with certainty whether the lower pitching moment predicted by Leishman-Beddoes for many of the cases is due to a failure of the method or error in the CFD code predictions. Finally, this method of analysis may be applied to other airfoils and other test conditions to further validate the Leishman-Beddoes method.

APPENDIX A: DERIVATION OF LEISHMAN BEDDOES PARAMETERS

The C-81 tables for the SC-1095 airfoil were used to derive the constants used in the Leishman-Beddoes model. However, for some of the constants there were not enough data points in the region of interest to get a reliable curve fit. To counteract this, a spline was fit to the data. The splines and related C-81 data are provided in the following figures:

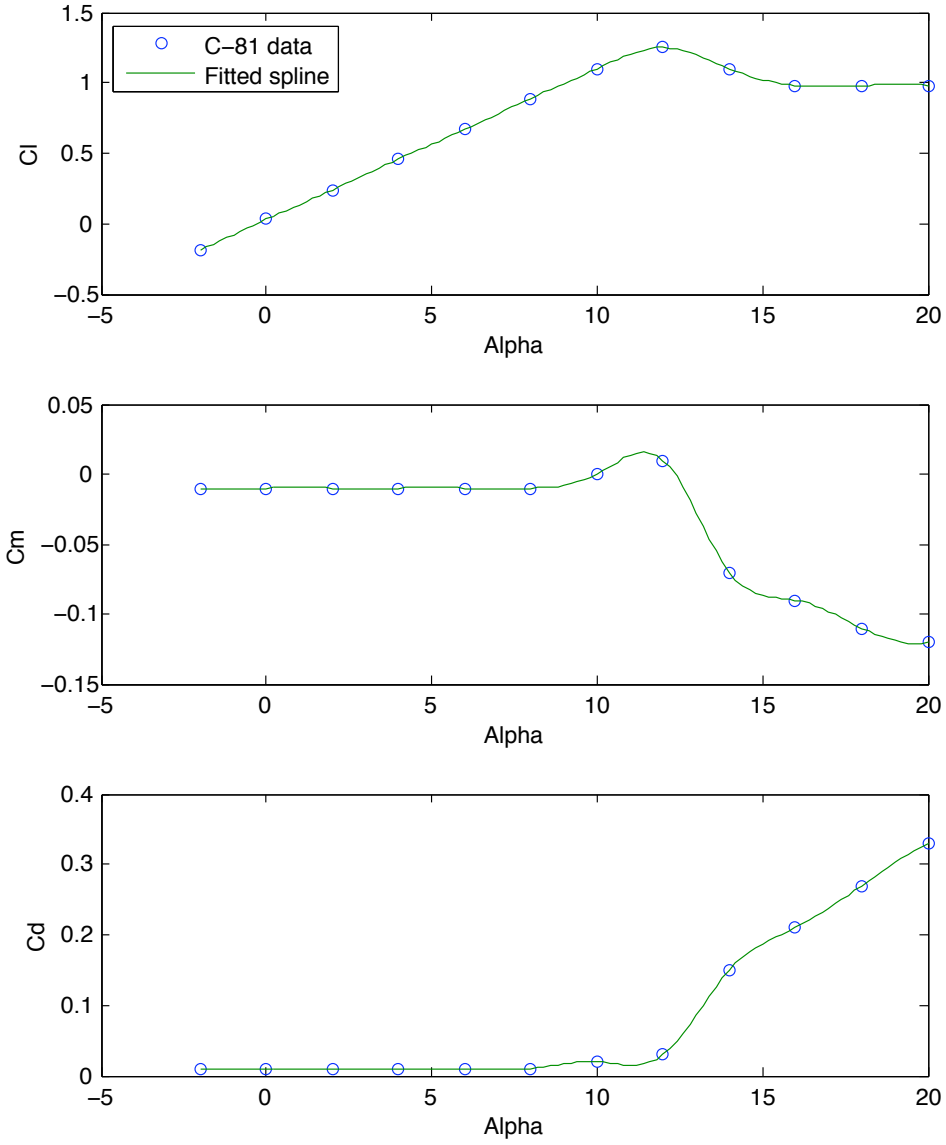

Figure 60: Lift, Moment, and Drag Data at M=0.3

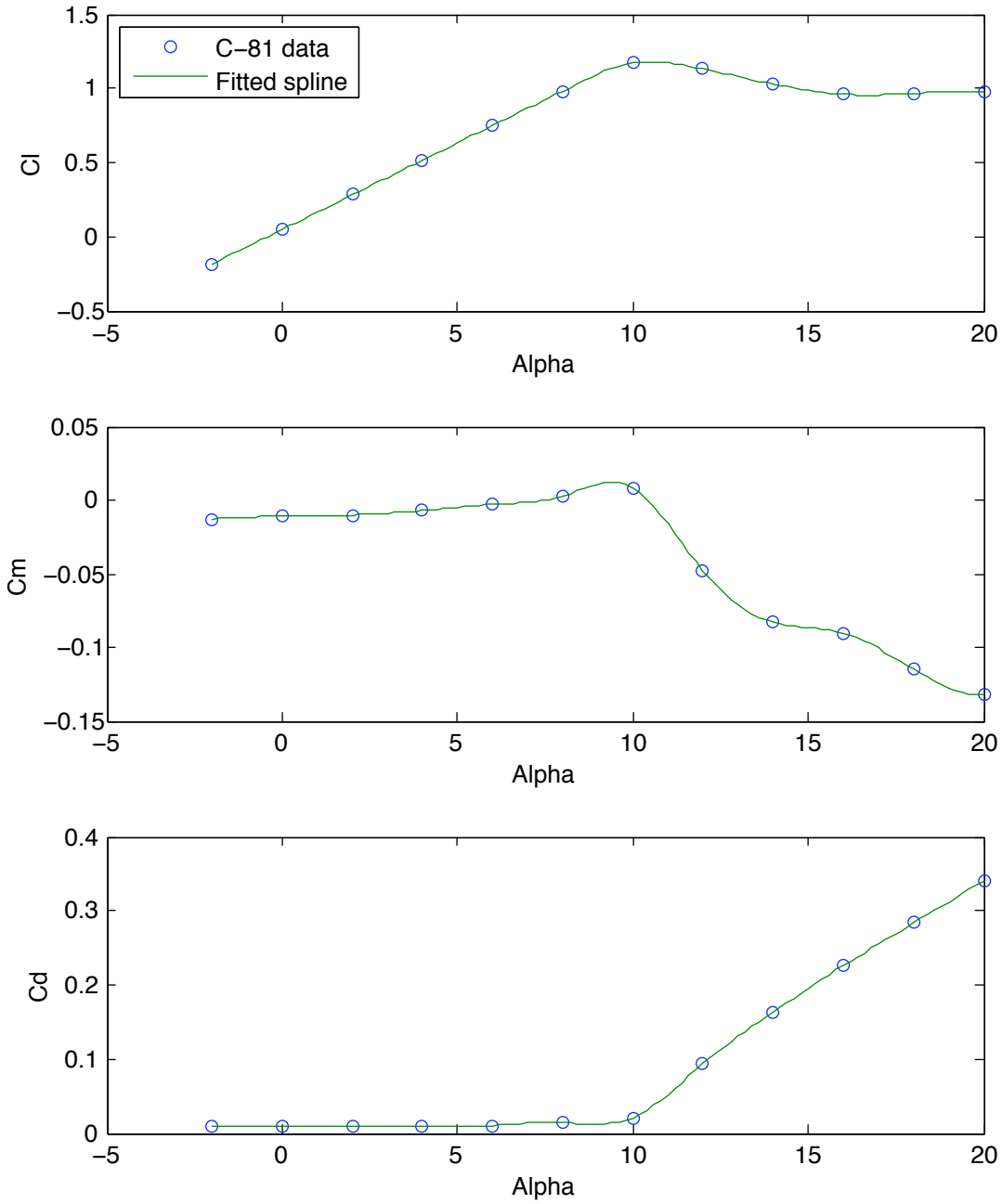

Figure 61: Lift, Moment, and Drag Data at M=0.4

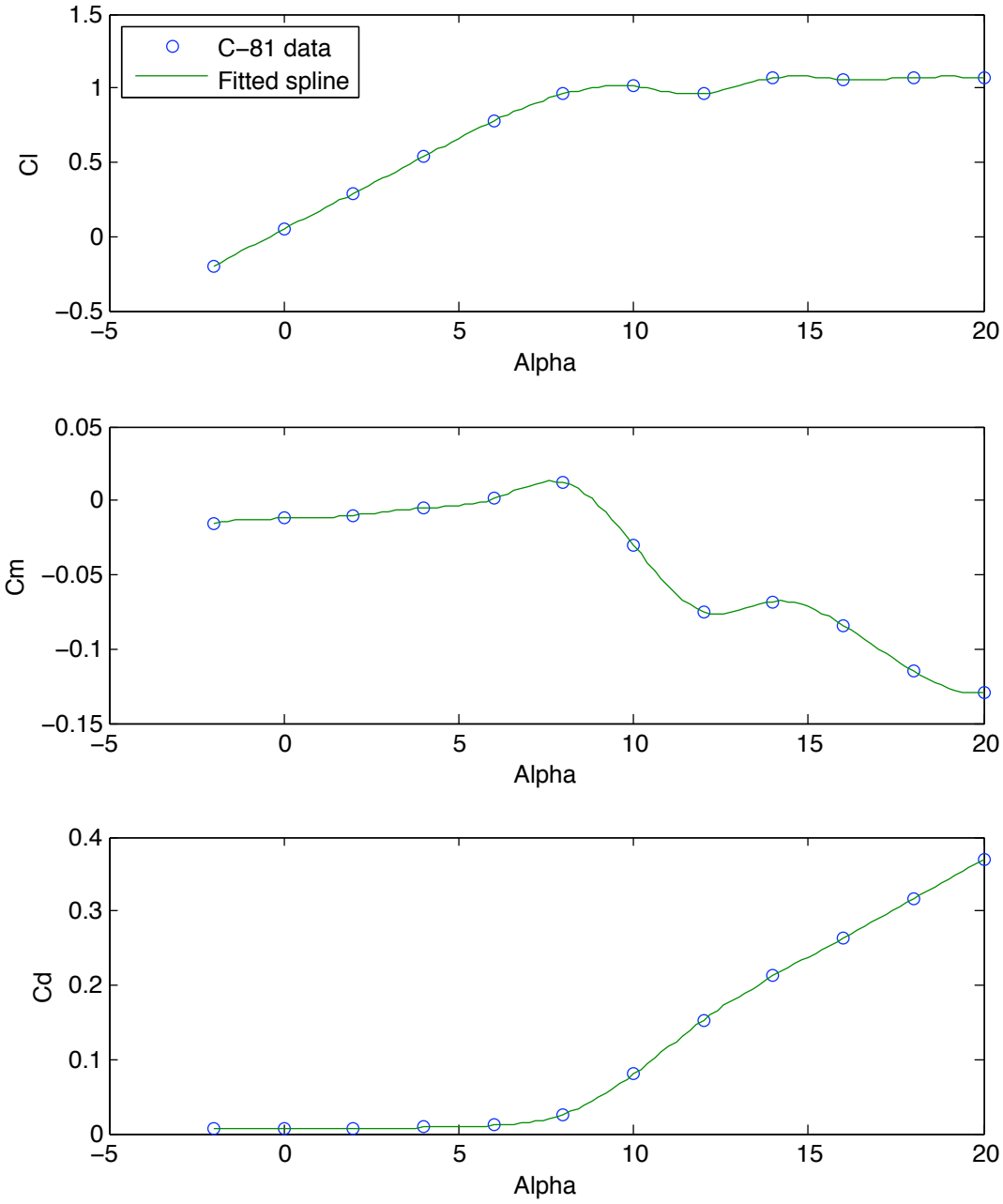

Figure 62: Lift, Moment, and Drag Data at M=0.5

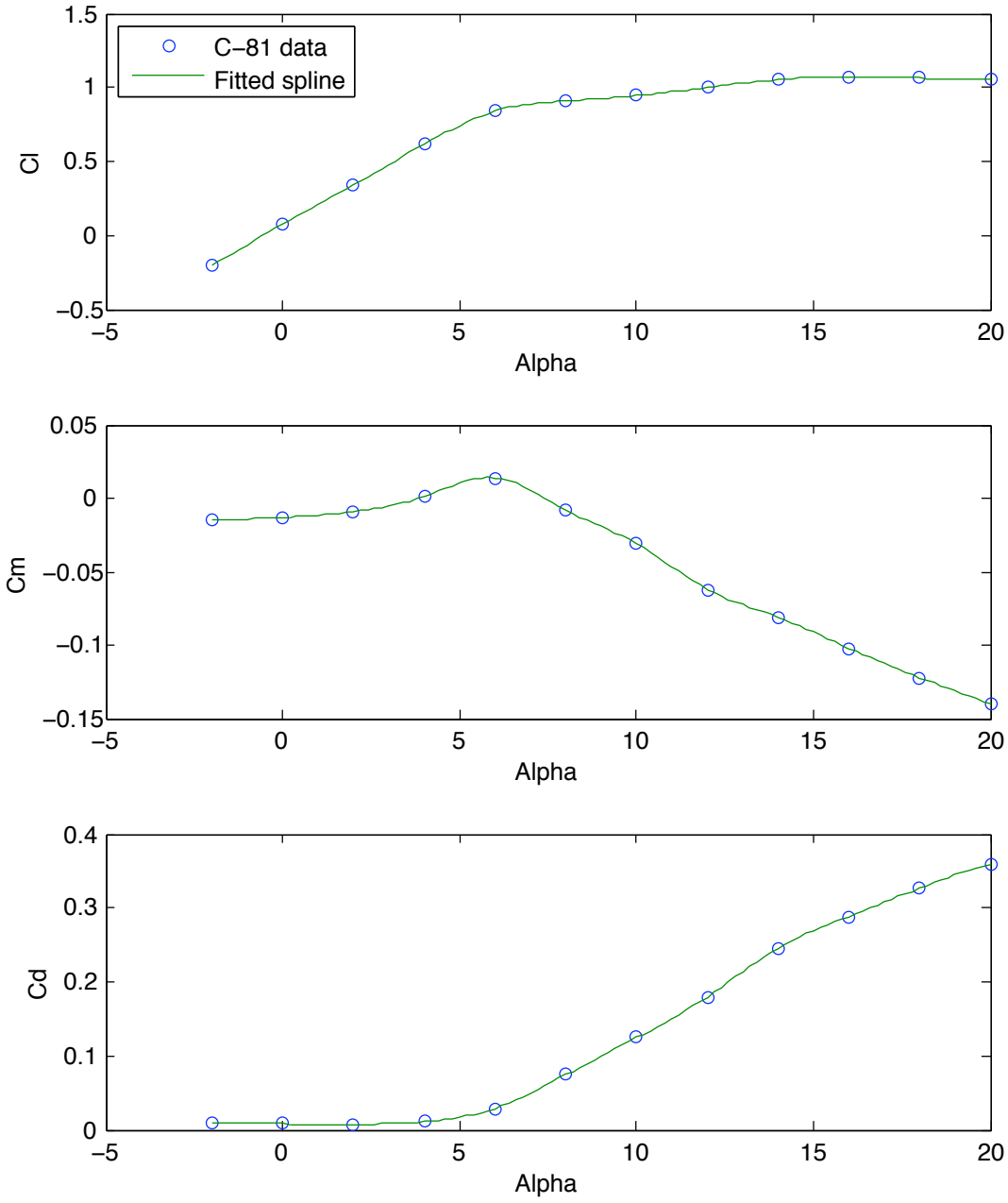

Figure 63: Lift, Moment, and Drag Data at M=0.6

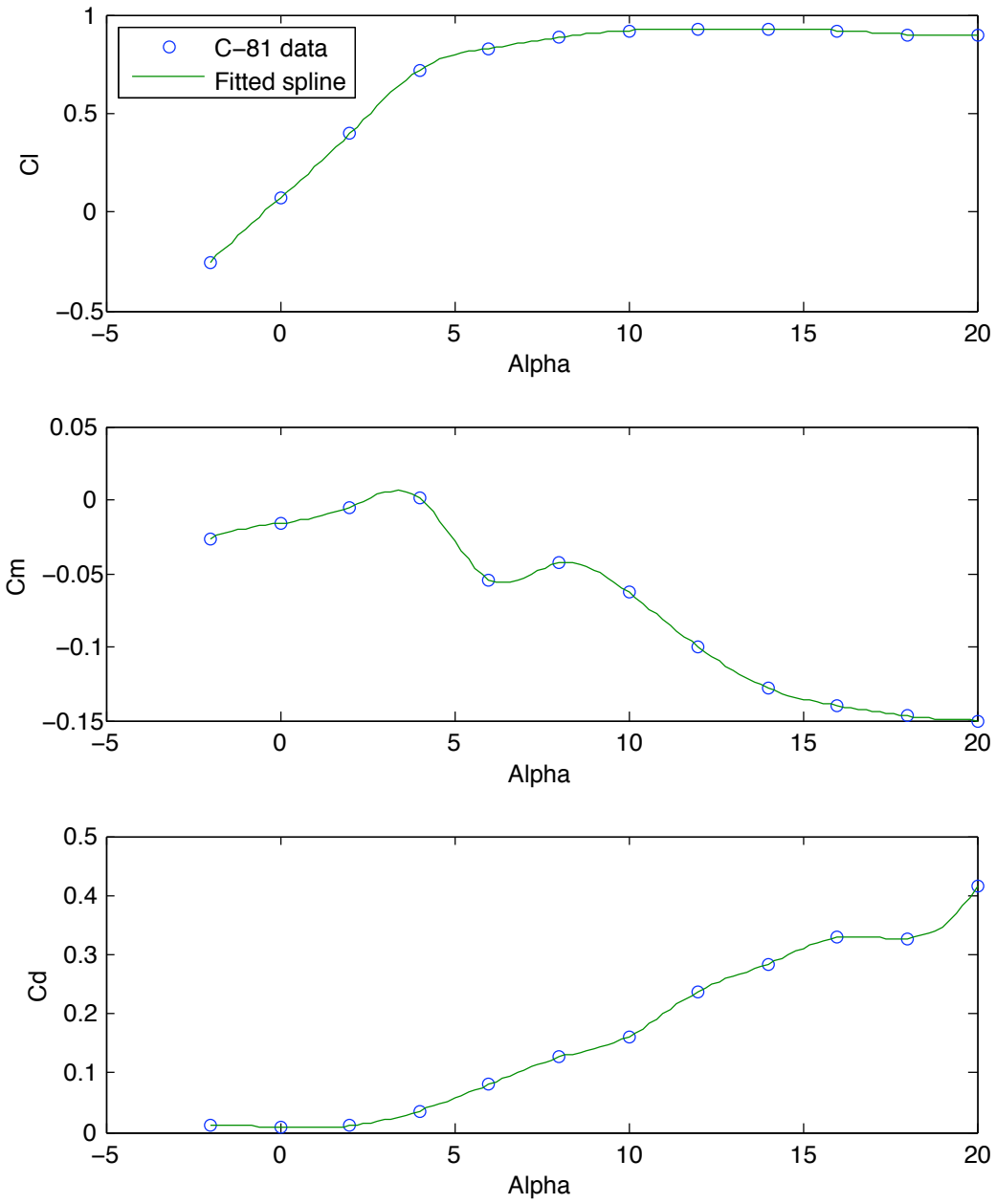

Figure 64: Lift, Moment, and Drag Data at M=0.7

The disadvantage of using splines is that it smoothes out all of the data. Any rapid changes in lift, moment, or drag with variation in angle of attack will not be represented. However, this would be true if a curve fit was done to the C-81 data without using splines as well. The only way to avoid this issue would be to have reliable data at a greater resolution than the two degree increments that the C-81 data was provided, but this was unavailable. However, given the many other approximations, curve fits, etc. used in the Leishman-Beddoes model, this is not expected to be a significant source of error.

The C-81 tables provided lift, moment, and drag data. However, the Leishman-Beddoes method is largely based on normal force, not lift force. These two values are very similar for low angle of attack, but just the same normal force was first computed from C-81 data prior to calculating other parameters. Normal force is given by

$$C_n = C_l \cos(\alpha) + \left(C_d - C_{d0}\right)\sin(\alpha)$$

where C_{d0} is the drag force at zero angle of attack.

Instructions on how the parameters were calculated are now given, using the M=0.3 data as an example.

Normal force curve slope, Cna

Cna is found by performing a linear regression on normal force vs. angle of attack in the linear low angle of attack range and taking the slope of the curve. In this case, Cna=0.1066.

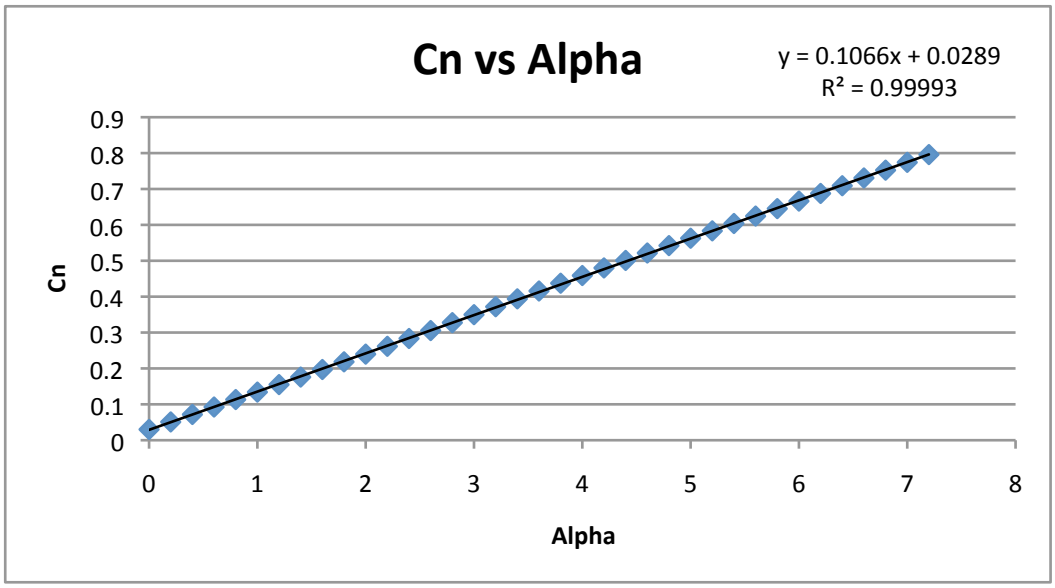

Figure 65: Normal force curve slope, M=0.3

Zero-lift angle, α_0

The zero-lift angle is then easily obtained from the previous regression. It is equivalent to –Cn(0)/Cna where for this case α_0= -.0289/.1066= -.2711. For most helicoper airfoils this value should be between 0 and -2 degrees.

α_1

α_1 corresponds to the angle of attack when the separation point f is equal to 0.7, and is the switching point between the two exponential curve fits of the f vs α

plots. To obtain this value, first the effective separation point must be calculated for all angles of attack using

$$f = \left(2\sqrt{\frac{C_n}{Cna * (\alpha - \alpha_0)}} - 1\right)^2 \tag{63}$$

Then, it is a simple matter of finding for what value of α f=0.7. For the M=0.3 case, this corresponded to an angle of 12.9 degrees.

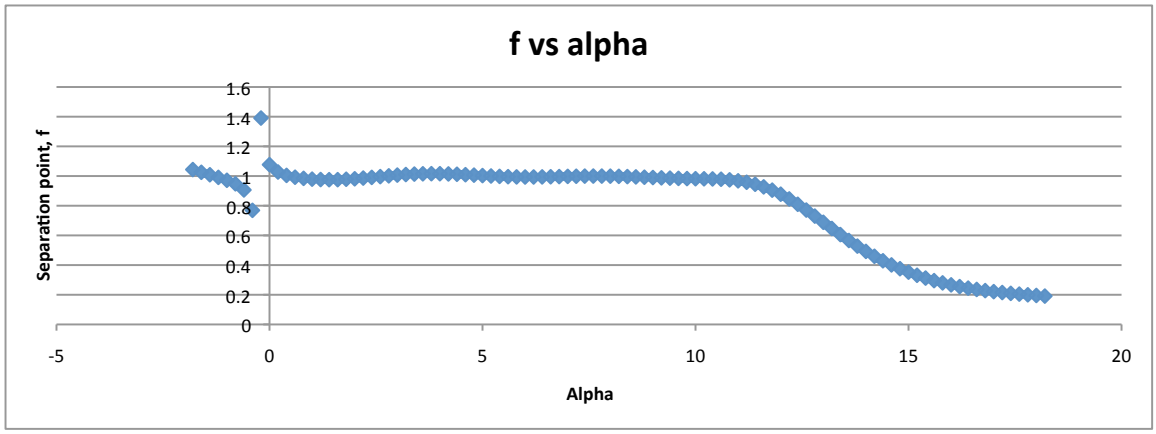

Figure 66: Effective Separation Point vs. Angle of Attack, M=0.3

Kirchoff stall parameter for $\alpha<\alpha_1$, S1

S1 is a parameter used as a curve fit for cases where f>0.7, where

$$f = 1.0 - 0.3 * \exp\left[(\alpha - \alpha_0 - \alpha_1)/S1\right] \tag{64}$$

To find S1, the quantity (α-α_0-α_1) was plotted against (1.0-f)/0.3 for data where f>0.7 and an exponential curve fit was then fit with the constraint that at (α-α_0-α_1)=0, the exponential is equal to one (i.e., that it is not scaled by a constant, meaning that the regression will reduce error through adjustment of S1 only).

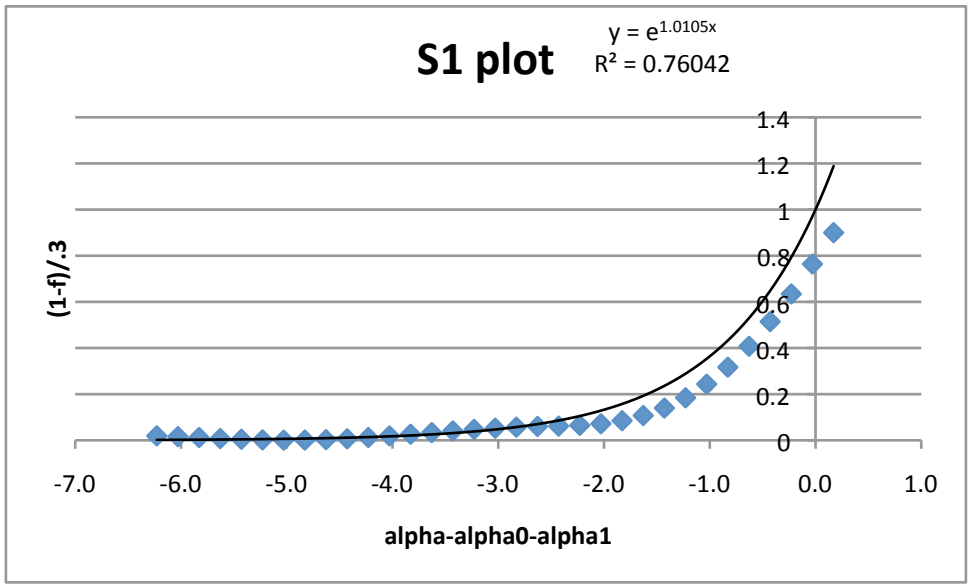

Figure 67: Derivation of S1 Parameter, M=0.3

S1 for this example is then given by 1/1.0105=.9896.

Kirchoff stall parameter for $\alpha>\alpha_1$, S2

The process is the same for S2, but here the separation point curve fit is given by

$$f = 0.04 + 0.66 * \exp\left[\left(\alpha_1 - \alpha + \alpha_0\right)/S2\right] \quad (65)$$

As such, the quantity (α_1-α+α_0) is plotted against (f-0.04)/0.66 for all values where f<0.7. It is again constrained such that the exponential is scaled by one.

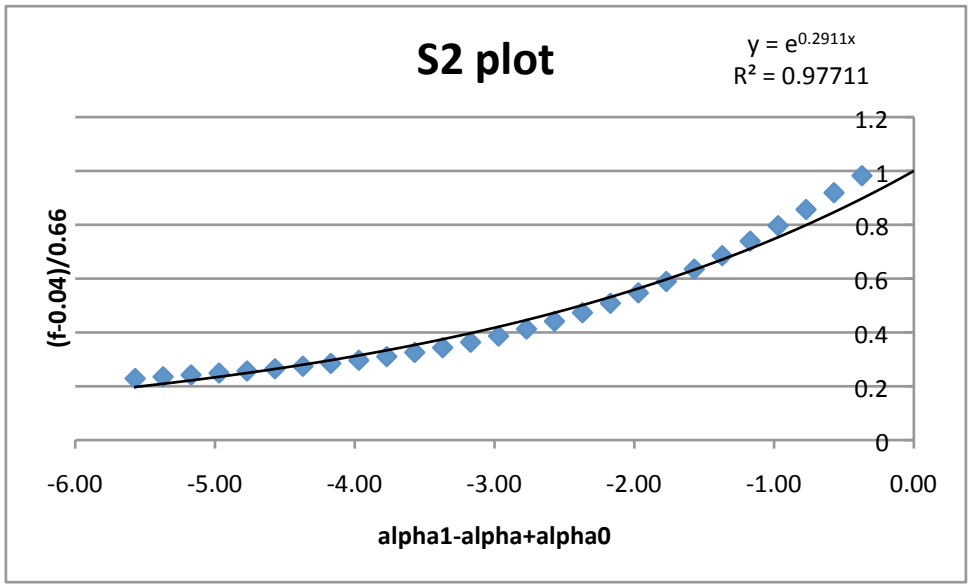

Figure 68: Derivation of S2 Parameter, M=0.3

Here, S2=1/0.2911=3.435

Zero lift pitching moment, C_{m0}

C_{m0} is easily obtained by plotting C_m against C_n and taking the y-intercept. In this case, it was found to be -.01.

Center of pressure offset, k_0

The pitching moment is modeled using the polynomial

$$\frac{C_m - C_{m0}}{C_n} = k_0 + k_1(1-f) + k_2 * \sin\left(\pi * f^m\right)$$

k_0 is found by performing a linear regression of C_m against C_n for $C_n > 0$.

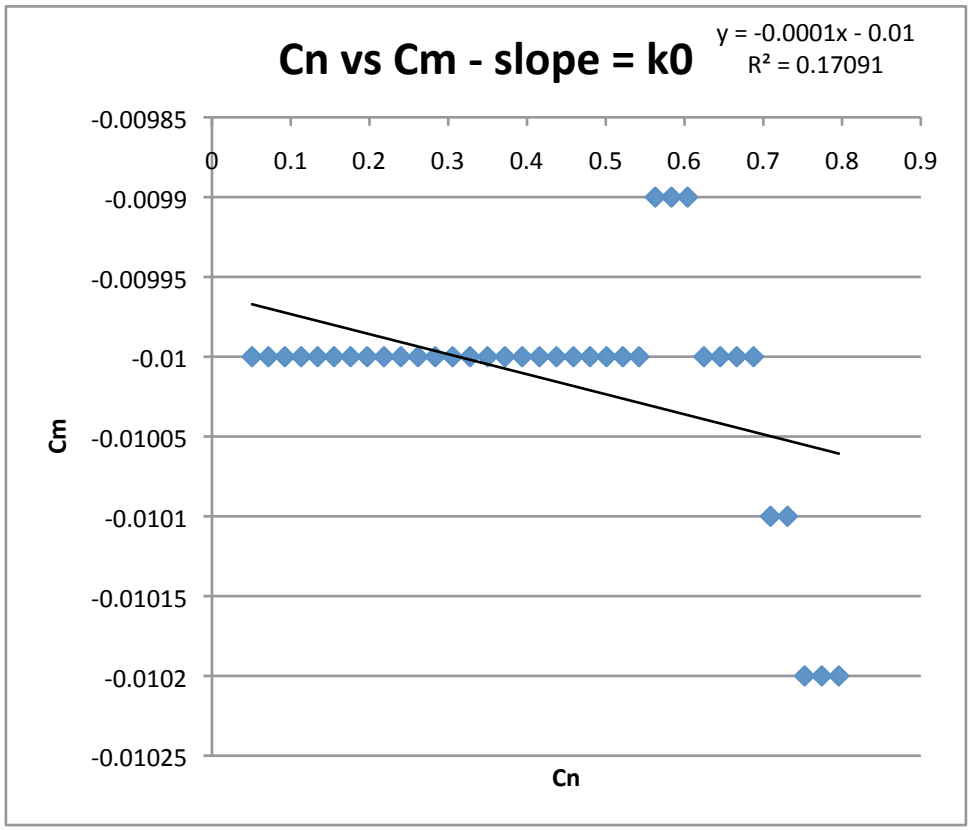

Figure 69: Derivation of k_0, M=0.3

Here, k_0 is -0.0001.

Static pitching moment parameters, k_1 and k_2

To obtain k_1 and k_2, first two plots were created. In one, the quantity (1-f) was plotted against the following:

$$\frac{C_m - C_{m0}}{C_n} - k_0 - k_2 * \sin\left(\pi * f^m\right) \tag{66}$$

A linear regression then gives a value of k_1. To find a value for k_2, $\sin(\pi * f^m)$ was plotted against

$$\frac{C_m - C_{m0}}{C_n} - k_0 - k_1(1 - f) \tag{67}$$

and again a linear regression was performed. Since the relation for k_1 contains k_2 and vice versa, error had to be reduced by changing these two values in tandem, using the result for one as an input in the other iteratively until convergence.

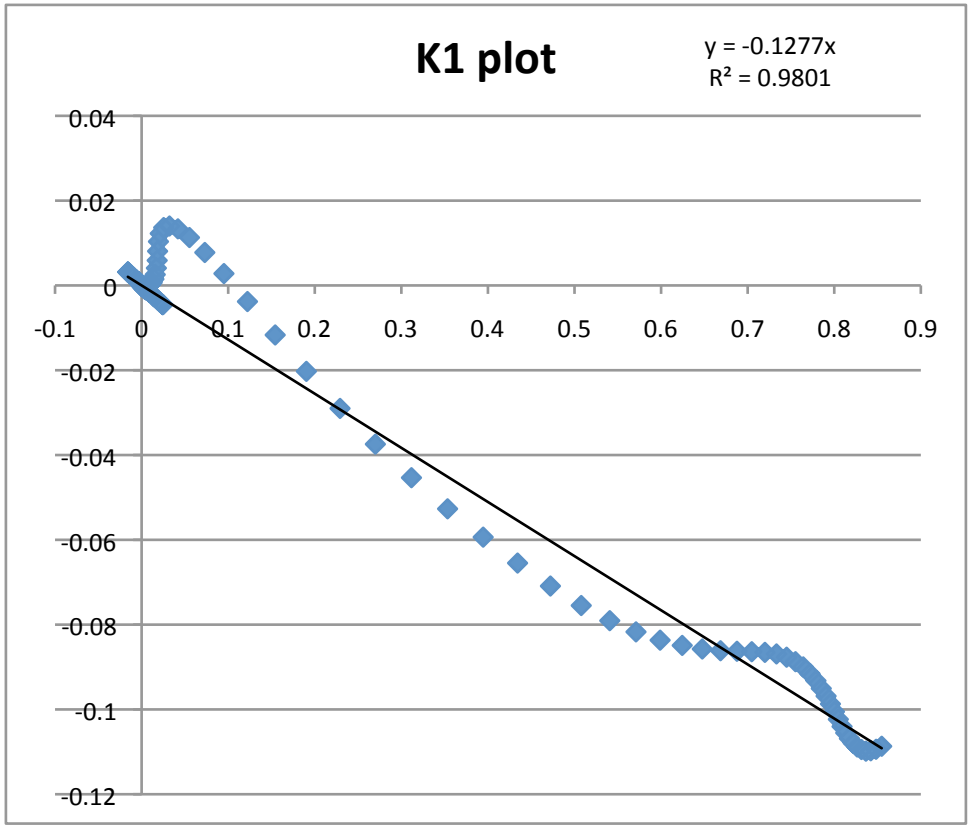

Figure 70: Derivation of k_1 constant, M=0.3

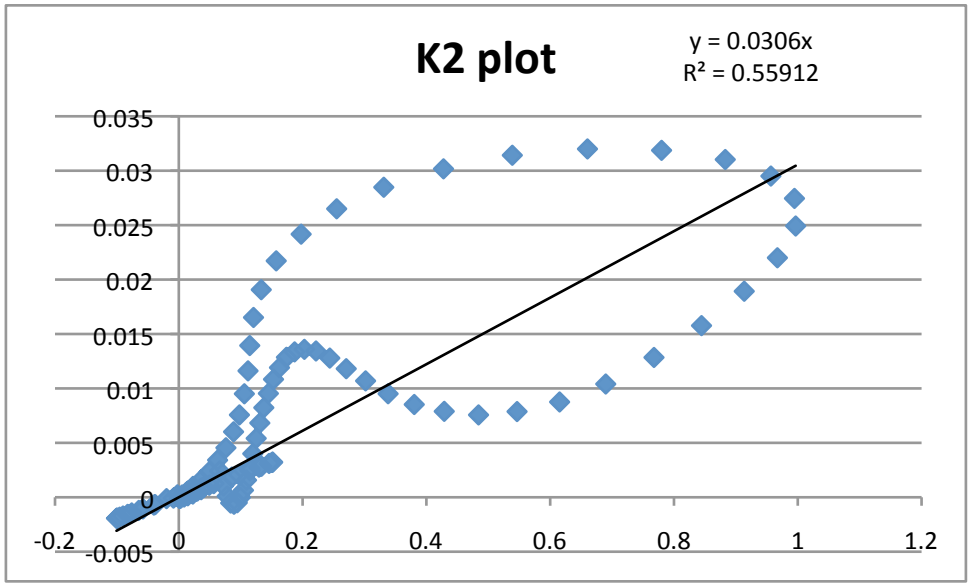

Figure 71: Derivation of k_2 constant, M=0.3

From the previous plots we see that k_1=-0.1277 and k_2=0.0306. It was common to have low correlation coefficients, particularly for the k_2 plot, but the correlation between the resulting pitching moment curve fit and static moment data was good. To provide the closest curve fits, these regressions were performed over a range of angle of attack that corresponded tightly to the range of angles reflected in the test matrix.

Critical normal force coefficient, C_{n1}

The critical normal force coefficient is related to the break in chord force. As such, first a chord force was calculated from the spline-interpolated C-81 data using

$$C_C = \frac{C_n * \sin(\alpha - \alpha_0) - (C_d - C_{d0})}{\cos(\alpha - \alpha_0)} \tag{68}$$

Then, the chord force coefficient was plotted against normal force coefficient to find the point at which the chord force breaks, providing C_{n1}.

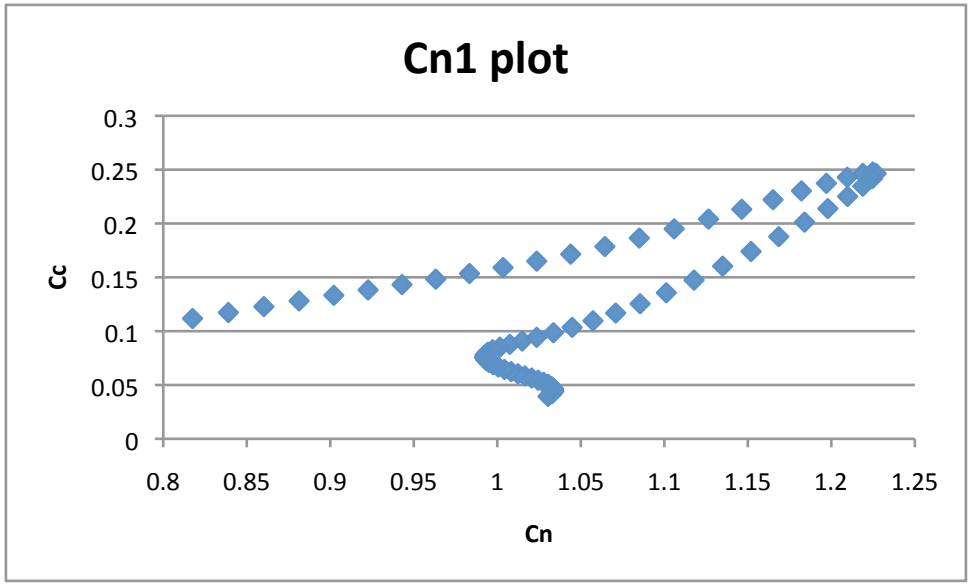

Figure 72: Derivation of C_{n1} Coefficient, M=0.3

In this case, C_{n1} was determined to be roughly 1.22.

Skin friction drag coefficient, C_{d0}

As mentioned previously, C_{d0} is the drag force coefficient correlating to a zero angle of attack. Here, it is 0.01.

Chord force recovery factor, η

η represents the failure of the airfoil to achieve the leading edge suction it would achieve in potential flow. To obtain this correction factor, the chord force coefficient calculated from interpolated C-81 data previously is compared to the theoretical curve

$$C_C = \eta * Cna * (\alpha - \alpha_0)^2 \quad (69)$$

η is found easily through linear regression. Here, we find a value of 1.00.

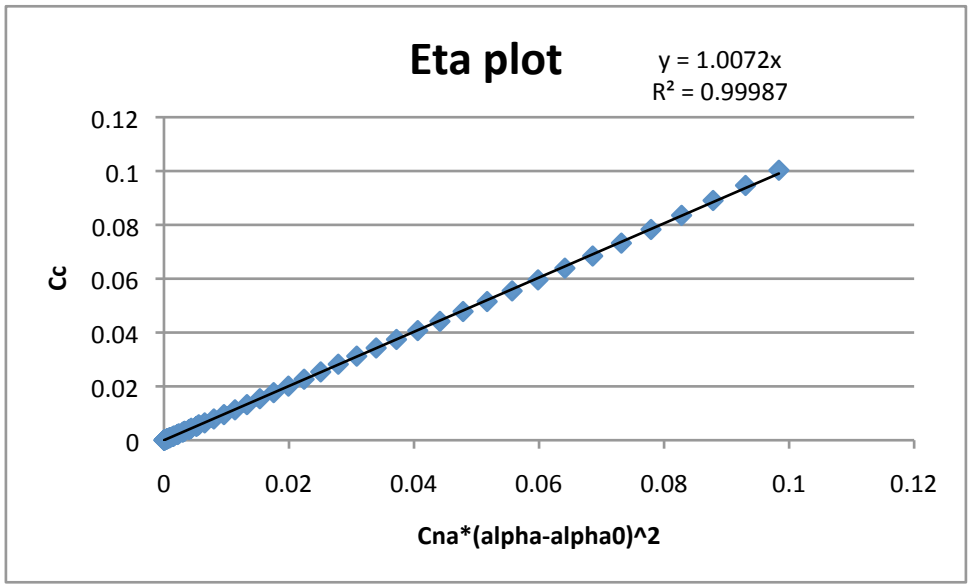

Figure 73: Derivation of η Coefficient, M=0.3

Chord force smoothing parameter, DFD

From the following equation,

$$C_C = \eta * Cna * \alpha_{tot}^2 * \sqrt{f''} * \left(f''\right)^{0.5*DFD*(C_n'-Cn1)} \quad (70)$$

the power for the second effective separation point is constrained to be between 0 and 0.5. Thus,

$$0 < DFD * \left(\text{Cna} * (\alpha - \alpha_0) - C_{n1}\right) < 1 \quad (71)$$

DFD may be determined through trial and error.

Time constants T_f, T_p, T_v, and T_{vl}

These four time constants have been theorized to be Mach number dependent but fairly insensitive to airfoil shape, with only small variations. In this project, published values for the NACA 0012 airfoil were used.

REFERENCES

[1] Johnson W. 1969. “The Effect of Dynamic Stall on the Response and Airloading of Helicopter Rotor Blades,” *Journal of the American Helicopter Society* 14 (2), pp. 68-79.

[2] Carr L.W., McAlister K.W., and McCroskey W.J. 1977. “Analysis of the Development of Dynamic Stall Based on Oscillating Airfoil Measurements,” NASA TN D-8382.

[3] Beddoes T.S. 1979. “A Qualitative Discussion of Dynamic Stall,” AGARD Report 679.

[4] McCroskey W.J. 1981. “The Phenomenon of Dynamic Stall,” NASA TM-81264.

[5] McCroskey W.J., McAlister K.W., Carr L.W., and Pucci S.L. 1982. “An Experimental Study of Dynamic Stall on Advanced Airfoil Sections,” Vols. 1, 2, &3 NASA TM-84245.

[6] Leishman J.G. and Beddoes T.S. 1986. “A Generalized Method for Unsteady Airfoil Behavior and Dynamic Stall Using the Indicial Method,” *42nd Annual Forum of the American Helicopter Society, Washington D.C., June 2-5.*

[7] Leishman J.G. 1987. “Validation of Approximate Indicial Aerodynamic Functions for Two-Dimensional Subsonic Flow,” *Journal of Aircraft* 25 (10) pp. 914-922.

[8] Leishman J.G. and Nguyen K.Q. 1988. “State Space Representation of Unsteady Airfoil Behavior,” *AIAA Journal* 28 (5) pp. 836-844.

[9] Leishman J.G. and Beddoes T.S. 1989. “A Semi-Empirical Model for Dynamic Stall,” *Journal of the American Helicopter Society*, 34 (3), pp.3-17.

[10] Leishman J.G. 1989. “Modeling Sweep Effects on Dynamic Stall,” *Journal of the American Helicopter Society* 34 (18), pp. 18-29.

[11] Leishman J.G. 1993. “Indicial Lift Approximations for Two-Dimensional Subsonic Flow as Obtained from Oscillatory Measurements,” *Journal of Aircraft* 30 (3), pp. 340-351.

[12] Johnson W. 1994. Helicopter Theory. New York: Dover Publications.

[13] Hariharan N. and Leishman J.G. 1996. “Unsteady Aerodynamics of a Flapped Airfoil in Subsonic Flow by Indicial Concepts,” *Journal of Aircraft* 33 (5) pp. 855-868.

[14] Pierce K. 1996. “Wind Turbine Load Prediction Using the Beddoes-Leishman Model for Unsteady Aerodynamics and Dynamic Stall,” Masters of Science Thesis, Department of Mechanical Engineering, University of Utah, Salt Lake City, UT.

[15] Singh R. and Baeder J.D., 1996. “The Direct Calculation of Indicial Lift Response of a Wing Using Computational Fluid Dynamics,” AIAA-96-2508-CP.

[16] Parameswaran V. and Baeder J.D., 1997. “Indicial Aerodynamics in Compressible Flow – Direct Computational Fluid Dynamic Calculations,” *Journal of Aircraft* 34 (1), pp. 131-133.

[17] Nguyen K.Q. and Johnson W. 1998. “Evaluation of Dynamic Stall Models with UH-60 Airloads Flight Test Data,” *54th Annual Forum of the American Helicopter Society, Washington D.C., May 20-22*.

[18] Johnson W. 1998. “Rotorcraft Aerodynamics Models for a Comprehensive Analysis,” *54th Annual Forum of the American Helicopter Society, Washington D.C., May 20-22*.

[19] Minnema J.E. 1998. “Pitching Moment Predicitions on Wind Turbine Blades Using the Beddoes-Leishman Model for Unsteady Aerodynamics and Dynamic Stall,” Masters of Science Thesis, Department of Mechanical Engineering, University of Utah, Salt Lake City, UT.

[20] *RCAS Theory Manual, Version 2.0*, United States Army Aviation and Missile COMmand/AeroFlightDynamics Directorate (USAAMCOM/AFDD) Technical Report 02-A-005, US Army Aviation and Missile Command, Moffett Field, CA, June 2002.

[21] Bousman W.G. 2003. “Aerodynamic Characteristics of SC1095 and SC1094 R8 Airfoils,” NASA/TP-2003-212265, AFDD/TR-04-003.

[22] Hansen M.H., Gaunaa M., and Madsen H.A. 2004. “A Beddoes-Leishman Type Dynamic Stall Model in State-space and Indicial Formulations,” Riso National Laboratory, Roskilde, Denmark Riso-R-1354(EN).

[23] Leishman J.G. 2006. Principles of Helicopter Aerodynamics 2nd Edition. New York: Cambridge University Press.

[24] Bain J.J., Mishra S.S., Sankar L.N., and Menon S. 2008. “Assessment of a Kinetic-Eddy Simulation Turbulence Model for 3D Unsteady Transonic Flows,” *26th AIAA Applied Aerodynamics Conference, Honolulu, Hawaii, August 18-21*.

[25] Nichols R.H. and Buning P.G. *User’s Manual for OVERFLOW 2.1 version 2.1t*, August 2008.

[26] He C., Zhao J., Bain J.J., Sankar L.N., and Prasad J.V.R. 2009. “Development of a Reduced Order Modeling Framework for Flight Mechanics Oriented Modeling of On-Blade Control Concepts,” *35th European Rotorcraft Forum, Hamburg, Germany, September 2009*.

[27] Liu L., Padthe A.K., Friedmann P.P., Quon E., Smith M.J., 2009. “Unsteady Aerodynamics of Flapped Airfoils and Rotors Using CFD and Approximate Methods,” *65th Annual Forum of the American Helicopter Society, Grapevine, TX, May 27-29.*

[28] Bain J.J. E-mail to the author. 7 December 2009.